AEROMECHANICAL CONTROL OF HIGH-SPEED AXIAL COMPRESSOR STALL

An Undergraduate Honors Thesis

Presented in Partial Fulfillment of the Requirements for the

Bachelor of Science of Civil Engineering with Distinction in the

College of Engineering at The Ohio State University

By

Keith LaMar Coleman

* * * * *

The Ohio State University
2006

Examination Committee:

Dr. Oliver G. McGee III, Advisor

Dr. Patrick J. Fox

Approved By

Advisor
Department of Civil & Environmental Engineering & Geodetic Science

First and foremost, I would like to dedicate this work to my Lord and Savior Jesus Christ. With Him all things are possible. This is also for my family for their continual support. Thanks Mom and Jess.

ABSTRACT

General methodologies will be developed in this work for the evaluation of passive high-speed compressor stabilization strategies using tailored structural design and aeromechanical feedback control. These passive stabilization strategies will be compared in their performance of several aeromechanical stabilization approaches which could potentially be implemented in high-speed axial compressors used by industry. The stability of aeromechanically-compensated high-speed compressors will be determined from linearized, compressible structural-hydrodynamic equations of stall inception developed in this study. This work offers a systematic study of the influence of ten aeromechanical feedback controller schemes to increase the range of stable operation of two high-speed laboratory compressors, using static pressure sensing and local structural actuation to postpone modal (long wave) stall inception. The maximum operating range for each scheme is determined for optimized structural parameters, and the various schemes are compared. Ten passive stabilization schemes that could potentially be used by industry were discussed and examined in a high-speed compressible flow environment. The concept of elasticity was introduced and implemented to examine the effects of flow non-uniformity, entropic loss, and unsteadiness on thermodynamic state changes within the compression system. Finally, pumping and aeroelastic characteristics of these laboratory compressors both with and without feedback were analyzed.

ACKNOWLEDGEMENTS

I would like to first thank my advisor and friend, Dr. Oliver G. McGee III, for inspiring me and also believing in my potential. I appreciate you for spending those longs nights in your office with me to make sure that I understood the material. Thanks for 'hurtin' my head' so that I may become a better thinker. I truly believe that you have prepared me to be successful in the next stage of my academic career. I look forward to the times ahead. Here's to a long lasting friendship.

Secondly, I thank Dr. Chih Fang, for his advice and support. I wish you and your family well.

I am grateful for the support of The Ohio State University Summer Research Opportunities Program, The OSU Civil and Environment Engineering & Geodetic Science Department, and The OSU Engineering Experiment Station for deeming my work as "worthy of research".

Last and certainly not least, I must thank my lab partners and friends, Celeste Chavis and Dan Work, for making my undergraduate research experience worthwhile. You two will truly be missed. Best wishes in your future endeavors. Maybe someday we may work together as colleagues. Only time will tell.

Thank you all!

TABLE OF CONTENTS

List of Figures

List of Figures (cont'd)

List of Tables

CHAPTER 1: Introduction

1.1 Introduction

The operating range of aeroengine compression systems is limited by two classes of aerodynamic instabilities known as *rotating stall* and *surge* (Emmons et al, 1955). *Rotating stall* is a multi-dimensional instability in which regions of low or reversed mass flow (i.e., stall cells) propagate around the compressor annulus due to incidence variations on adjacent airfoils (Greitzer, 1976, 1980, 1981). *Surge* is primarily a one-dimensional instability of the entire pumping system (compressor, ducts, combustion chamber, and turbine). It is characterized by axial pulsations in annulus-averaged mass flow, including periods of flow reversal through the machine. In high-speed compressor hydrodynamics (Fréchette, 1997), rotating stall is generally encountered first, which then (loosely) "triggers" surge (often after a few rotor revolutions, Greitzer, 1976). Therefore, the focus of this work will be on rotating stall. With either instability, the compression system experiences a substantial loss in performance and operability, which sometimes result in mechanical failure.

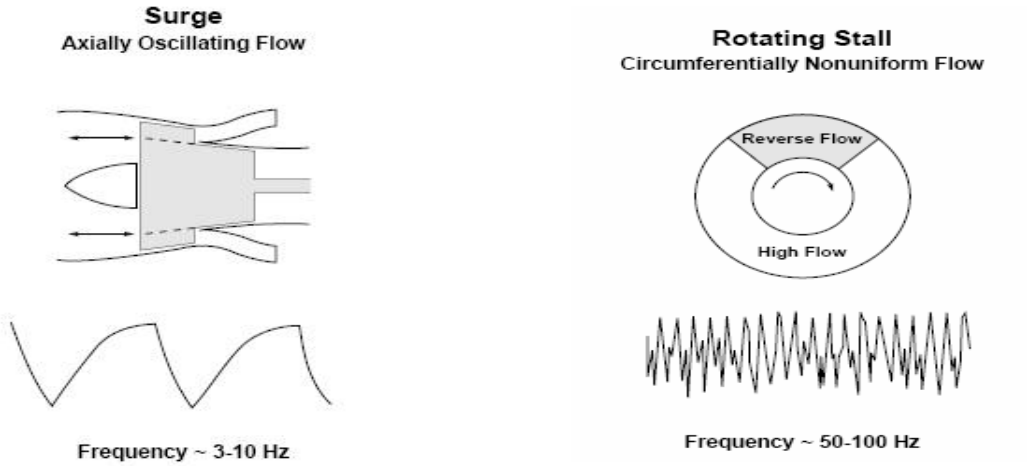

Fig. 1.1a Illustration of rotating stall and surge. A sketch of the transient signatures that would be given by high response pressure probes in the compressor (for rotating stall) or in the combustor, or other volume downstream of the compressor (for surge). (Fréchette 1997)

An experience-based approach for avoiding such performance loss is to operate the compressor at a safe range from the point of instability onset (i.e., with *stall margin*). The stall margin ensures that the engine can endure momentary off-design operation. The margin also reduces the available pressure rise and efficiency of the machine (see Fig 1.1b). It is proposed here that addition of tailored structural dynamic components or aeromechanical feedback controllers, locally sensed by unstable perturbations in annulus pressure and actuated by non-uniformities in the high-speed flow distribution around the annulus, can be shown to inhibit the inception of rotating stall of high-speed compressor devices. As a result, the stable operating range will be effectively extended, allowing higher performance operating conditions.

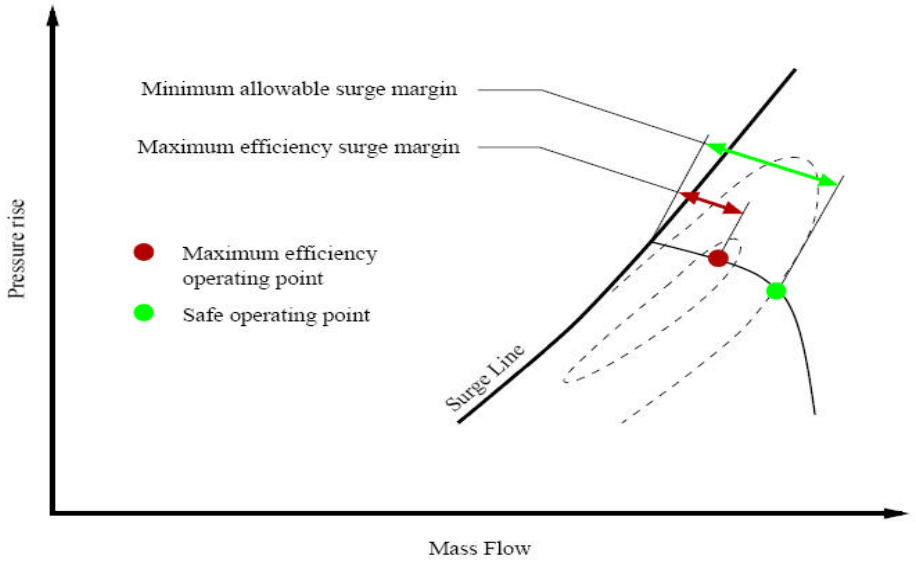

Fig. 1.1b Compressor map illustrating the surge margin (from Fréchette 1997).

Aeromechanical feedback can be loosely defined as the dynamic interaction between flexible structures and fluid dynamics of the compression system, without external electromechanical input. When approaching the stall line, flow disturbances induce local pressures on the structures. When tailored with the appropriate dynamic characteristics, the structure deforms to counteract flow disturbances, either directly or by modifying the local unsteady pressure rise of the compressor. High-speed compressor stabilization using aeromechanical feedback control is investigated here as a passive means of improving stability so that the compressor can operate safely at lower mass flows. This approach incorporates tailored structural feedback control within the machine that can alter the fluid dynamic behavior, so that the performance of the compressor can be extrapolated to operating ranges outside the empirical database generated by years of experience. Passive approaches to high-speed compressor stability have received no previous attention in the open literature. However, some important fundamentals in aeromechanical control of low-speed devices have been achieved (Gysling and Greitzer, 1995; McGee et al, 2004; Fréchette et al, 2004).

1.2 Objectives and Scope of Study

This work presents a systematic development and evaluation of tailored structural design and aeromechanical feedback stabilization of rotating stall in high-speed axial compressors. The focus of this research is to evaluate aeromechanical feedback stabilization strategies of long wave-length, high-speed compressible, modal stall (Fréchette, 1997) that employ static pressure sensing and structural actuation for dynamic compensation. Ten aeromechanical feedback stabilization strategies are considered, which generally include: (1) aeromechanically incorporating variable duct geometries for dynamic impedance control, (2) dynamically restaggered inlet guide vanes and rotor blades for diffusing or contracting blade passage control, (3) movable casing walls for dynamic tip clearance flow control, and (4) dynamic fluid injection for unsteady circumferential flow and pressure rise control across the compressor. To quantify the effectiveness of the various schemes, the analysis is applied to two laboratory compressors (ideally modified for high speeds) for which the empirical modeling inputs have been previously determined: (i) the MIT single-stage compressor (Gsyling and Greitzer, 1995) and (ii) the MIT three-stage compressor (Haynes et al, 1994).

The proof-of-concept studies of Gysling and Greitzer (1995), McGee et al (2004), and Fréchette et al (2004) demonstrated the feasibility of aeromechanical control of low-speed stalled compressors. However, some additional questions remain for high-speed devices. The motivation of the present modeling development and evaluation is to address three overarching questions: (1) What is the high-speed stall control capability of other aeromechanical feedback stabilization strategies, and how do they compare to that modeled and demonstrated by Gysling and Greitzer (1995), McGee et al (2004), and Frechette et al (2004)? (2) Are there destabilizing high-speed, compressible fluid-structural interactions which should be avoided through tailored structural design? (3) How do the aeromechanical

feedback dynamics couple with the pre-stall compressible fluid dynamics (Fréchette, 1997) to postpone or induce the inception of high-speed rotating stall?

The significance of the problem posed here is extremely unique and timely. Fluid-structural interaction effects are not only essential in devising high-speed compressor stabilization strategies, but also useful in establishing constraints on the structural design of compressors used by industry. As lightweight, less rigid structures are incorporated into new high-speed compressor designs, the level of fluid-structure interactions is likely to increase and result in reduced stall margin if the structures are not properly tailored. The practical insight and motivation here is to achieve light-weight, more efficient compressor builds using tailored, less rigid structures, while preventing potential stall margin reductions. There is therefore a need for broader study evaluating the potential of various passive control schemes to better assess the effect of aeromechanical interaction on high-speed compressor stability.

The overarching goals of this study are to evaluate the role of flexible structures on compressor stability, and to elucidate that a proper choice of local structural dynamic compensation close-coupled to the compressor affects (either beneficially or detrimentally) the stability of the system. The paper presented here re-introduces the ten aeromechanical feedback schemes developed by McGee et al (2004) and the nonlinear measured high-speed compression system dynamics calculated from a MIT single-stage and a MIT three-stage compressor characteristics employed therein (Fréchette et al, 2004; Gysling and Greitzer, 1995 (MIT single-stage); Haynes et al, 1994 (MIT three-stage)).

1.3 Methodology

An extensive literature review of low-speed and high-speed compressor system hydrodynamic stability models and aeromechanical feedback approaches for passive control of such devices was conducted. Specifically, a state-of-the-art high-speed, compressible

hydrodynamic model (Fréchette 1997) was examined and extending to a *linearized*, compressible structural-hydrodynamic model of stall inception examined herein.

Subsequently, proof-of-concept schemes of aeromechanical control technologies were developed in order to describe how such feedback can be utilized to stabilize high-speed compressor stall of axial compressors, and how different tailored structural designs impact high-speed compression system stability. Optimal structural parameters for aeromechanical compensators were determined to maximize the stable operating range of the high-speed compression system. The use of optimized aeromechanical feedback control to stabilize the system and extend the operating range will be discussed later. The theoretical basis of ten aeromechanical control schemes examined here was evaluated under a compressible flow environment. These schemes are broadly classified as: (1) dynamic fluid injection upstream of the compressor for control of inlet flow non-uniformities, (2) variable compressor inlet and exit duct geometries for impedance control inside the ducts, (3) flexible compressor casing wall providing control of tip clearance flow processes, and (4) dynamically re-staggered inlet guide vanes and rotor blades for control of deviation and dissipation loss mechanisms.

Completing the evaluation of the aforementioned aeromechanical control methodologies developed, the low-speed computer codes of McGee et al (2004) was modified and extended to high-speed, compressible flow regimes. Off-design operation of an aeromechanically-controlled (or dynamically-compensated) high-speed compressor can dramatically affect the performance characteristic curve shape of the device. Any change in inlet conditions can change the discharge pressure and gas horsepower. Besides changing the characteristic pressure and horsepower curves, the characteristic head curve and the head curve sensitivity (associated with the stability of the high-speed compressor) also changes. This phenomenon is due to specific volume or gas density ratio effects and equivalent speed

effects on the compressor. Since the performance map curves change with speed (higher losses at higher speeds), the overall shape of these curves change, which can be compounded by compressibility (specific volume or gas density ratio) effects closely-coupled with dynamic compensation associated with aeromechanical feedback controls.

The modified computer codes were utilized in order to construct the essential performance maps, discharge pressure vs. flow (bringing forth a measure of gas density and speed changes affecting a dynamically-compensated compressor's stability).

CHAPTER 2: Thermodynamics and the Compressible Rotating Stall Inception Model

2.1 Compressor Characteristic

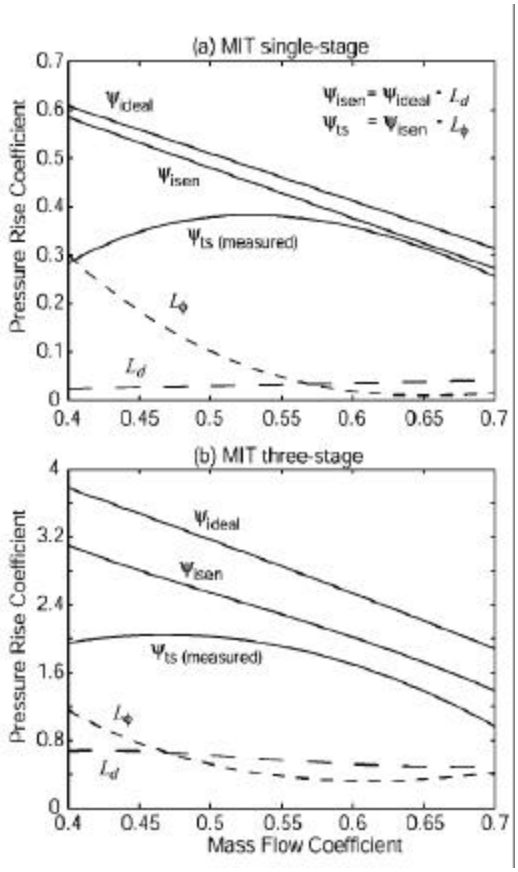

As previously mentioned, empirical compressor characteristics associated two low-speed laboratory compressors were used in this study by way of simplicity and illustrative purpose of the concepts proposed herein. Characteristic curves and pressure loss buckets for the MIT single-stage compressor (Gysling and Greitzer, 1995) and the MIT three-stage compressor (Haynes et al, 1994) are shown in Figure 2.1a. The polynomial expressions for the MIT single-stage compressor are as follows:

$$\Psi_{ts} = 5.75f^3 - 14.4f^2 + 10.4f - 1.94 \qquad (2\text{-}1)$$

$$\Psi_{isen} = -1.039\ f + 1 \qquad (2\text{-}2)$$

$$\Psi_{ideal} = -0.98\,f + 1 \qquad (2\text{-}3)$$

The MIT three-stage compressor expressions are:

$$\Psi_{ts} = -10.4f^2 + 9.430f - 1.85 \qquad (2\text{-}4)$$

g. 2.1a Compressor characteristics ed in this study: (a) MIT single stage ysling and Greitzer 1995), (b) MIT ree-stage (Haynes et al, 1994)

$$\Psi_{isen} = -7.499f^2 + 8.995f - 3.374 + \frac{1.011}{f} \quad (2\text{-}5) \qquad \Psi_{ideal} = -0.547f^2 - 2.559f + 3 \quad (2\text{-}6)$$

$$\frac{\partial \Psi_{ideal}}{\partial g} = -1.02f \quad (2\text{-}7)$$

Where, Ψ, f, and g are the pressure rise coefficient, flow coefficient, and stagger angle respectively.

The thermal loss due to *viscous dissipation* is estimated by:

$$L_f = \Psi_{isen} - \Psi_{ts} \quad (2\text{-}8)$$

and the propulsive loss due to *blade flow incidence deviation changes* was estimated by :

$$L_d = \Psi_{ideal} - \Psi_{isen} \quad (2\text{-}9)$$

These compressor characteristics were used to create critical performance maps, which will be discussed in the proceeding sections. The compressor input parameters are assumed as follows:

- design shaft speed - 10,000 rpm
- axial velocity ratio - 0.5
- density of atmospheric air - 1.229 kg/m^3
- specific heat ratio - 1.4
- atmospheric pressure - 101.3 kPa

Through manipulation of the total-to-static pressure rise coefficient equation shown above and assuming the given inlet pressure, P_1, inlet density, $?_o$ and wheel speed, U, the performance map for a MIT single-stage and MIT three-stage compressor can be developed. This map can then be used to evaluate essential thermodynamic properties (Gresh 2001). First, the exit to inlet pressure ratio must be obtained for the compressor. The total-to-static pressure rise coefficient equation can be defined as:

$$\Psi_{ts} = \frac{P_2 - P_1}{\frac{1}{2} r_o U^2} \qquad \text{(2-10a)}$$

Solving for P_2,

$$P_2 = P_1 + \Psi_{ts}\left(\frac{1}{2} r_o U^2\right) \qquad \text{(2-10b)}$$

Finally, dividing by the inlet pressure, yields the pressure ratio

$$\frac{P_2}{P_1} = 1 + \frac{\Psi_{ts}\left(\frac{1}{2} r_o U^2\right)}{P_1} \qquad \textit{where } P_2 = \text{pressure at the compressor exit} \qquad \text{(2-10c)}$$

Now that we have attained the exit-to-inlet pressure ratio, we can now develop the exit-to-inlet temperature ratio using the laws of thermodynamics for a polytropic process using the following relation (Gresh 2001):

$$\frac{T_2}{T_1} = \left(\frac{P_2}{P_1}\right)^{(n-1)/n} \qquad \textit{where } n = \textit{polytropic exponent} \qquad \text{(2-11)}$$

Finally, the exit-to-inlet density ratio can be found by dividing the pressure ratio by the temperature ratio (Gresh 2001):

$$\frac{r_2}{r_1} = \frac{\left(P_2 / P_1\right)}{\left(T_2 / T_1\right)} \qquad \text{(2-12)}$$

2.2 Losses and Efficiency

The propulsive pressure loss due to deviation (L_d) was estimated by taking the difference between the ideal pressure rise characteristic ($?_{ideal}$) and the isentropic characteristic ($?_{isen}$). Similarly, the thermal pressure loss due to viscous dissipation (L_f) was estimated from the difference between the isentropic pressure characteristic ($?_{isen}$) and the measured total-to-static characteristic ($?_{ts}$). To obtain a reasonable measure of loss at each

speed, both deviation and viscous loss were proportioned appropriately. For example, if the engine operates at 70 percent design speed, loss is then reduced by 30 percent. Accordingly, if the engine is sped up to 110 percent design, loss is then increased by 10 percent.

Propulsive, thermal, and overall efficiency can be found by considering the losses.

Thermal efficiency is:

$$h_t = 1 - L_j \tag{2-13}$$

Propulsive efficiency is defined as:

$$h_p = 1 - L_d \tag{2-14}$$

The total loss experienced by the compressor is:

$$L_{tot} = L_d + L_j \tag{2-15}$$

Therefore, the overall efficiency of the compressor can now be simply described as follows:

$$h_{tot} = 1 - L_{tot} \tag{2-16}$$

Now that all efficiencies of the machine have been defined, the work and head can now be considered (Gresh, 2001). Specifically, propulsive head, thermal head, propulsive work, and thermal work will be evaluated.

Propulsive head is:

$$H_p = \left(\frac{n}{n-1}\right)\left(\frac{P_1}{r_1}\right)\left[\left(\frac{P_2}{P_1}\right)^{(n-1)/n} - 1\right] \tag{2-17}$$

Thermal head is:

$$H_t = \left(\frac{k}{k-1}\right)\left(\frac{P_1}{r_1}\right)\left[\left(\frac{P_2}{P_1}\right)^{(k-1)/k} - 1\right] \tag{2-18}$$

where k=specific heat ratio

Propulsive work is:

$$W_p = \left(\frac{H}{h} \right)_p \tag{2-19}$$

Thermal work is:

$$W_t = \left(\frac{H}{h} \right)_t \tag{2-20}$$

2 .3 Compressible Rotating Stall Inception Model

The stability model of McGee et al (2004) was similar to the model of Moore and Greitzer (1986), which was an extension of Emmons' original work on stall inception in 1955. Emmons theorized that the stall cell starts as a flow separation in a single blade passage, which causes blockage in the passage. As a result, approaching flow is diverted to the adjacent blade passage causing the stalled cell to propagate. Circumferentially, the length of this type of disturbance was short scale, meaning that it was limited to a small number of blade passages. The more inclusive model of Moore and Greitzer (1986) idealized a multi-stage compressor mathematically as a two-dimensional, incompressible flow machine of large hub-to-tip ratio, with three-dimensional unsteady effects at the casing walls. Their model assumes that the flow and its perturbations are radially uniform. This model also assumes that the initial harmonic wave-like disturbance is circumferentially longer than that of the Emmons-type disturbance. As the point of instability is approached, this disturbance grows in intensity until it becomes a fully developed stall cell. The low-speed model of McGee et al (2004) captures the same essential physics and mathematics as that of Moore and Greitzer (1986) with the addition of several aeromechanical feedback stabilization schemes. McGee's low-speed stability model, however, made a few simplifying assumptions such as, constant shaft speed, constant axial velocity, constant density ratio, and constant

temperature ratio suggesting that the fluid is incompressible. This notion is fairly valid at relatively low speeds. However, as the compressor approaches higher speeds this theory collapses and the fluid is, in fact, compressible. Since the current study involves high-speed compressible fluid, the low-speed stability model of McGee et al (2004) and Frechette et al (2004) had to be modified to account for variable shaft speed, variable axial velocity, variable density ratio, and variable temperature ratio to incorporate compressibility affects. To achieve this, Fréchette's (1997) fluidic compressibility parameters were integrated into the model. These parameters are (Fréchette, 1997):

- *axial velocity-density ratio,*

$$AVDR = \frac{r_2 V_{x,2}}{r_1 V_{x,1}} \tag{2-21}$$

- *blade row continuity parameter,*

$$I_{br} = \frac{1+c}{2} \qquad where\ c = \frac{V_{x,2}}{V_{x,1}} \tag{2-23}$$

These two compressibility parameters modify the fluidic blade row inertias of McGee et al (2004) in the rotors, ?, and also in the rotors + stators, µ. The blade row inertia parameters are now defined as:

$$l = \left(\sum_{rotors} \frac{c_x / r_o}{\cos^2 g} \right) I_{br} AVDR \tag{2-24}$$

$$m = \left(\sum_{rotors+stators} \frac{c_x / r_o}{\cos^2 g} \right) I_{br} AVDR \tag{2-25}$$

with c_x , r_o , and g representing the axial chord, mean radius, and blade row stagger angle, respectively.

For low-speed incompressible flow assumptions, the velocity and density are held constant, thus, the AVDR and I_{br} is unity. In addition, the fluidic blade row inertia parameters (equations 2-24 and 2-25) are identical to the low-speed model of McGee et al (2004) and

held constant. In the present study, the I_{br} is constant at 0.75 and AVDR is variable due to the changes in the density ratio.

CHAPTER 3: Aeromechanical Feedback Control

3.1 Static Pressure Sensing, H(s)

The structural feedback responds to fluctuations in static pressure in the ducts either upstream, downstream, or within the compressor depending on the scheme. These unsteady pressure disturbances are then used to serve as input parameters to the structural controller. A transfer function for the sensor was developed by McGee et al. (2004) relating the upstream or downstream velocity with the pressure disturbance. The transfer function is defined as follows:

$$H(s) = -2\left(\frac{s}{m} + \Phi_u\right) \quad where\ s = iw \qquad (3\text{-}1)$$

with m and F_u representing the m^{th} spatial harmonic mode and steady sate upstream axial flow, respectively. In the present analysis m was set to unity, assuming the instability of the first harmonic as the initial inception of stalling condition, and F_u was variable. By definition, the disturbance rotational frequency is:

$$w = \frac{-ml}{m_n} \qquad where\ m_n = \frac{4}{m} + m \qquad (3\text{-}2)$$

3.2 Structural Controller, C(s)

McGee et al (2004) also developed a transfer function for the structural controller. This structural controller provides the feedback to the compression system. This controller is defined as:

$$C(s) = \frac{\overline{W}}{s^2 + 2Qxs + Q^2} \qquad (3\text{-}3)$$

with $\overline{W}$, Q, and x as the mass ratio, frequency ratio, and critical damping ratio, respectively. In McGee et al (2004) these parameters were restricted to constructible sizes for low-speed compressor builds using materials that were readily obtainable. In the current high-speed compressor study, these parameters carry the same restrictions. The constraints restricted the mass ratio to $\overline{W} = 0.583$, the frequency ratio within $0.3 \le Q \le 2.9$, and the critical damping ratio within $0.3 \le Q \le 2.9$ (Gysling & Greitzer, 1995). These ranges of values for the frequency and critical damping ratio were chosen to maximize stability in the compression system and are shown in Figure 3.2a below (McGee et al, 2004; Frechette et al, 2004).

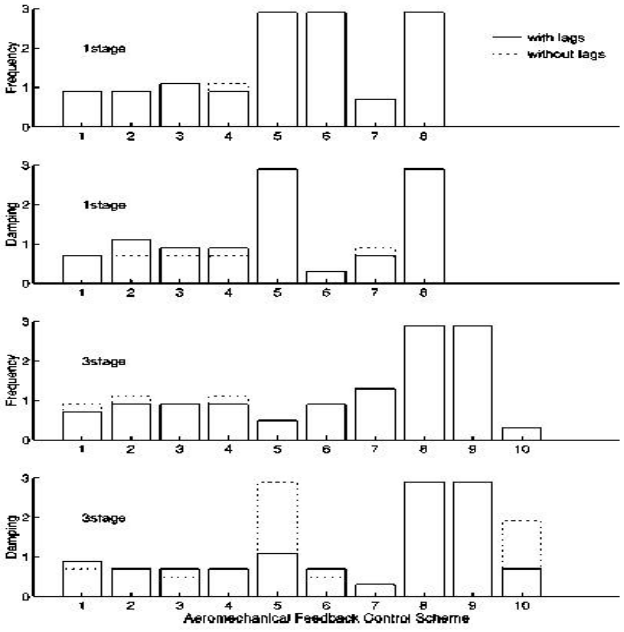

Fig. 3.2a Structural control parameters for maximum stable extension. Optimal structural frequency, Q, and damping ratio, x are shown for the various aeromechanical schemes. (McGee et al, 2004)

Note: Time lags are not considered in the present study and the frequency* needed to *be increased from 0.3 to 1.1 for the 3-stage scheme # 10 in order to achieve reasonable stability.

3.3 Effective Slope

In order to delay the inception of stall in the machine, the compression system was aeromechanically dampened instantly. To achieve this, McGee et al (2004) defined the "ideal" effective growth rate of the compression system at neutral stability as:

$$\left(\frac{\Psi_{ts}}{\partial f}\right)_{eff} = \frac{\partial \Psi_{ts}}{\partial f} + b_r \left|HC\right| \cos b \qquad (3\text{-}4a)$$

with $\frac{\partial \Psi_{ts}}{\partial f}$ representing the slope of the steady-state compressor characteristic and b_r denoting the essential feedback control parameter for this study. The b term measures the degree to which the fluid is in phase with the structural response of the controller. In this study we ideally assume that the fluid is 180 degrees out of phase with the structural response thus reducing the equation to:

$$\left(\frac{\Psi_{ts}}{\partial f}\right)_{eff} = \frac{\partial \Psi_{ts}}{\partial f} - b_r \left|HC\right| \qquad (3\text{-}4b)$$

with the term $b_r \left|HC\right|$ defined as the ideal control authority. The b_r parameter is defined differently for each scheme. These definitions are presented in Table 2 of the next section. The equation of the best fit line through the points that create the effective slope versus corrected flow scatter plot is integrated with a certain initial condition to produce an effective total-to-static characteristic curve $\left(\Psi_{ts}\right)_{eff}$. The initial condition simply implies that $\left(\Psi_{ts}\right)_{eff}$ must initially equal $\left(\Psi_{ts}\right)$ at stall.

3.4 Description of Aeromechanical Feedback Stabilization Schemes

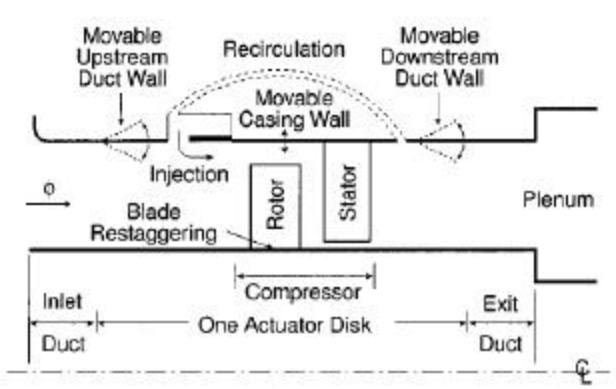

Fig. 3.4a Illustration of the ten aeromechanical feedback schemes (McGee et al, 2004)

The aeromechanical feedback strategies studied are shown in Fig. 3.4a and listed in Table 1. They are categorized as (i) dynamic fluid injection (with and without exit flow recirculation) to supplement the axial momentum entering the compressor, implemented with a circumferential array of reed valve injectors that react to local static pressure (Gysling and Greitzer, 1995) (Schemes #1-#4); (ii) movable compressor inlet and exit duct walls for flow field impedance control, potentially implemented as flexible wall liners or as a structurally tuned case that resonates with the pre-stall, local static pressure fluctuations (Schemes #5-#7); (iii) flexible compressor casing wall to provide dynamic control of rotor tip clearance flow processes, implemented through structurally-tuned casing or flexible casing treatment (Scheme #8); and (iv) dynamically restaggered inlet guide vanes and rotor blades, possibly implemented through flexible root attachments or structurally tuned blades (Schemes #9 & #10). (McGee et al, 2004)

Table 1 Aeromechanical feedback schemes

Scheme	Description
#1	Radially mixed-out injection at the compressor face
#2	Tip injection at the rotor leading edge
#3	Radially mixed-out injection at the compressor face with exit flow recirculation
#4	Tip injection at the rotor leading edge with exit flow recirculation
#5	Movable inlet duct wall with inlet static pressure sensing
#6	Movable exit duct wall with inlet static pressure sensing
#7	Movable exit duct wall with exit static pressure sensing
#8	Movable casing wall with front-to-back average static pressure sensing
#9	Dynamically restaggered inlet guide vanes with inlet static pressure sensing
#10	Dynamically restaggered rotor blades with front-to-back average static pressure sensing

The broad range of control schemes are considered without limiting the study to the most feasible schemes to implement. This provides further insight on the impact of the interactions between the fluid and structure during the inception of stall. It also indicates which phenomena are most beneficial or detrimental in stabilizing the compression system. Different combinations of actuation principles and sensing locations (upstream, downstream, and average) are investigated. Further design work would be necessary to construct a practical configuration that implements the most promising approaches.

A schematic of the system considered is shown in Fig. 3.4a. Flow enters through an inlet duct, a compressor then pumps the flow through an exit duct to a plenum, which then exhausts through a throttle (not shown) and an exit nozzle (not shown). The aeromechanical components are integrated at one of the various locations shown. The table shown below defines the essential feedback control parameter for the current study, b_r. As mentioned in the previous section, this b_r factor is an essential component of the ideal control authority of McGee et al (2004).

Table 2 Essential Feedback Control Parameter, b_r*	
# 1	$\Phi_i\left[\frac{\partial \Psi_{ts}}{\partial f} + 2(\Phi_i - \Phi_u)\right]$
#2	$\left(\frac{\partial \Psi_{ideal}}{\partial a_i}\right)(\Phi_i / \Phi_u)^2$
#3	$\Phi_i\left[\frac{\partial \Psi_{ideal}}{\partial f} + 2\Phi_i)\right]$
#4	$\left(\frac{\partial \Psi_{ideal}}{\partial a_i}\right)(\Phi_i / \Phi_u)^2 + 2\Phi_i\Phi_u$
#5	$\Phi_u\left[\frac{\partial \Psi_{ideal}}{\partial f} - 2\Phi_u)\right]$
#6	$\Psi_{ts} - 2\Phi_u^2$
#7	$\Psi_{ts} - 2\Phi_u^2 - \left(\frac{\partial \Psi_{ts}}{\partial f}\right)\Phi_u$
#8	$\frac{\Psi_{ideal}}{\partial e}$
#9	$\frac{\Psi_{ideal}}{\partial g} - ln^2\ \Phi_u m_{igv}$
#10	$\frac{\Psi_{ideal}}{\partial g}$

**Note that b_r is divided by μ_n for all schemes. For schemes #2 and #4 $\frac{\partial \Psi_{ideal}}{\partial a_i} = 0.64$, for scheme #8 $\frac{\Psi_{ideal}}{\partial e} = 0.8$, and for scheme #10 $\frac{\partial \Psi_{ideal}}{\partial g} = -1.02j$ (McGee et al, 2004).*

CHAPTER 4: Nonlinear Measured High-Speed Compression System Dynamics

4.1 Introduction

The following data has been produced for the MIT single-stage compressor using the compressor characteristic of Gysling and Greitzer (1995). Subsequent data was produced for the MIT three-stage compressor using the characteristic of Haynes et al (1994). The curves were then manipulated to include aeromechanical feedback for each scheme. A detailed explanation of findings will be presented using scheme #1 (radially mixed-out injection at the compressor face) as the basis for discussion. The results for the remaining schemes can be found in the Appendix section. A new metric called elasticity, which is a non-dimensional measure of relativeness, will be discussed in the next chapter.

4.2 Corrected Pressure Ratio (Density Ratio)

Figure 4.2a depicts the Corrected Pressure Ratio vs. the Corrected Flow at variable speed. In order to obtain these "corrected" quantities the pressure was divided by the temperature ratio (T_2/T_1) and the flow was divided by the pressure ratio (P_2/P_1). The corrected pressure ratio can now be defined as the density ratio. See *Section 2.1 Compressor Characteristic* for the development of these quantities. The corrected T_2/T_1 values on the opposite side of the y-axis depict lines of constant temperature ratios between the compressor inlet (T_1) and the compressor exit/combustor inlet (T_2). Figure 4.2b also represents the

Corrected Pressure Ratio vs. the Corrected Flow; however, the values on the opposite side of the y-axis depict lines of constant corrected T_3/T_1 ratios between the compressor inlet (T_1) and the combustor exit/turbine inlet (T_3). The critical T_3/T_1 ratio was found to be 1.126 for the MIT single-stage, as shown in the diagram, because it is the highest T_3/T_1 temperature ratio that can be achieved at 70 percent design before the machine begins to stall. This value was estimated by obtaining the slope from the highest point on the 70 percent corrected pressure ratio curve to the origin at one. The remaining T_3/T_1 lines were then proportioned accordingly. Notice that the safe operating line is not located along the maximum efficiency line; instead, it is located a safe distance away from the surge line called the *stall margin* (recall the discussion in Chapter 1).

The effective surge line with scheme #1 aeromechanical feedback is found in Figure 4.2c and Figure 4.2d. With the new surge line in place, the compressor will now be capable of operating closer to the original maximum efficiency line. Also, notice how the T_2/T_1 (compressor exit to compressor inlet) temperature ratio lines shift as a result of the increased corrected pressure due to the feedback scheme. The T_3/T_1 (combustor exit to compressor inlet), however, remains unchanged; but, Figure 4.2d gives a new critical T_3/T_1 ratio of 1.24, which is about a 10% increase in temperature.

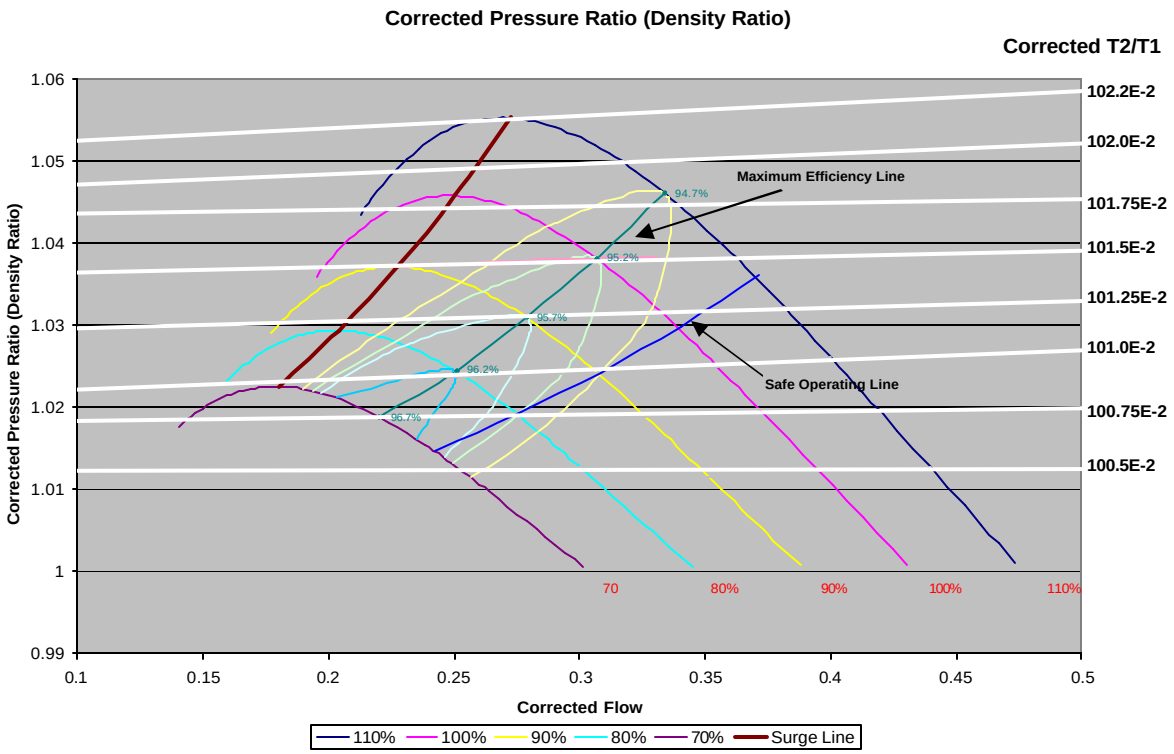

Fig. 4.2a Corrected Pressure Ratio & Density ratio versus Corrected Flow of a MIT single stage compressor with lines of constant T_2/T_1 temperature ratio.

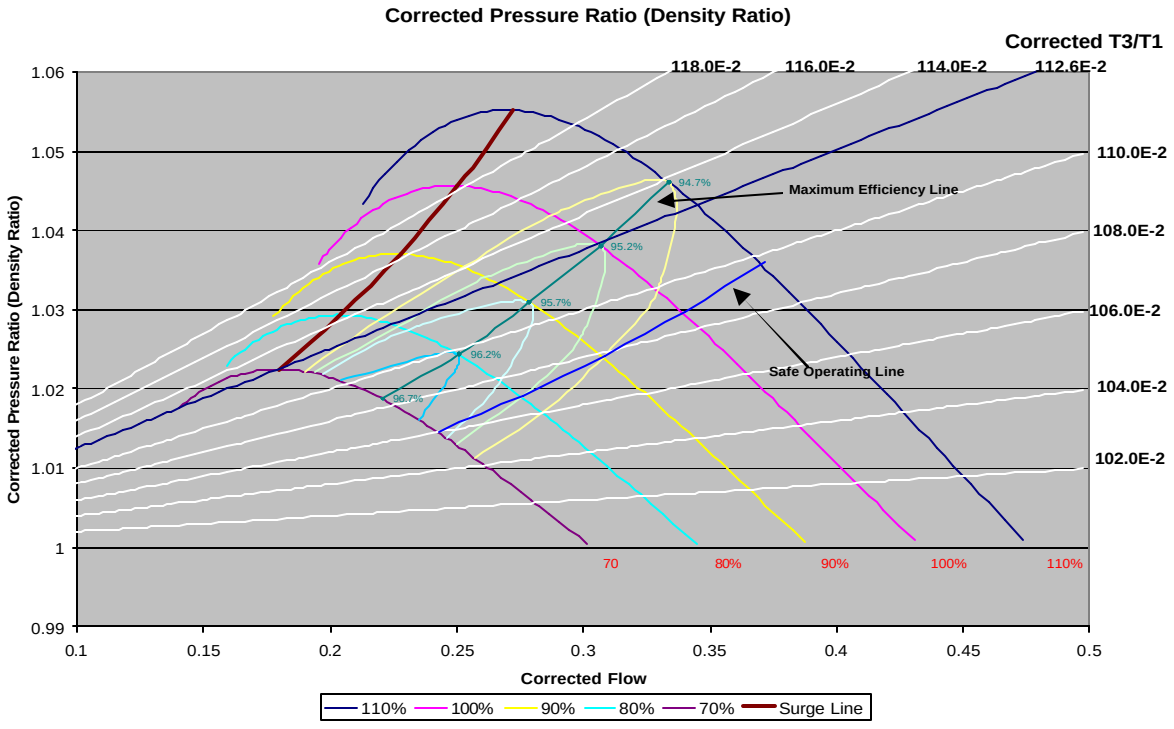

Fig. 4.2b Corrected Pressure Ratio & Density ratio versus Corrected Flow of a MIT single stage compressor with lines of constant T_3/T_1 temperature ratio.

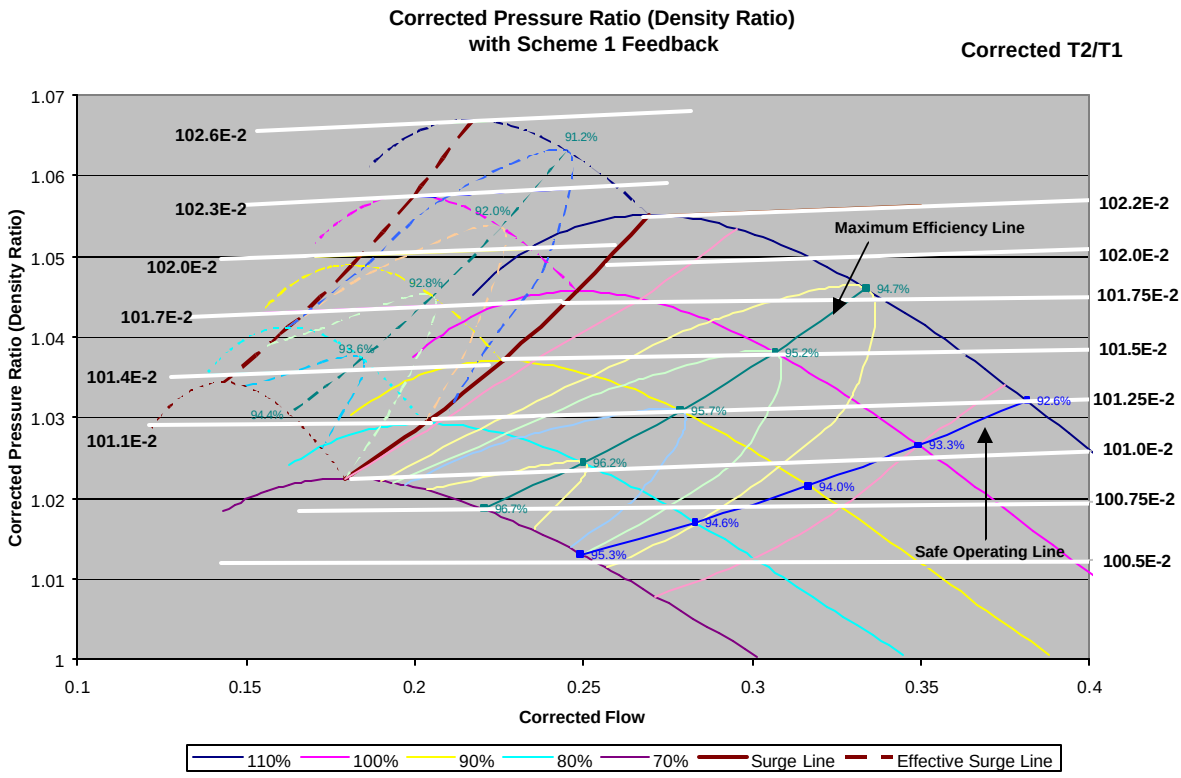

Fig. 4.2c Corrected Pressure Ratio & Density ratio versus Corrected Flow of a MIT single stage compressor with lines of constant T_2/T_1 temperature ratio and aeromechanical feedback.

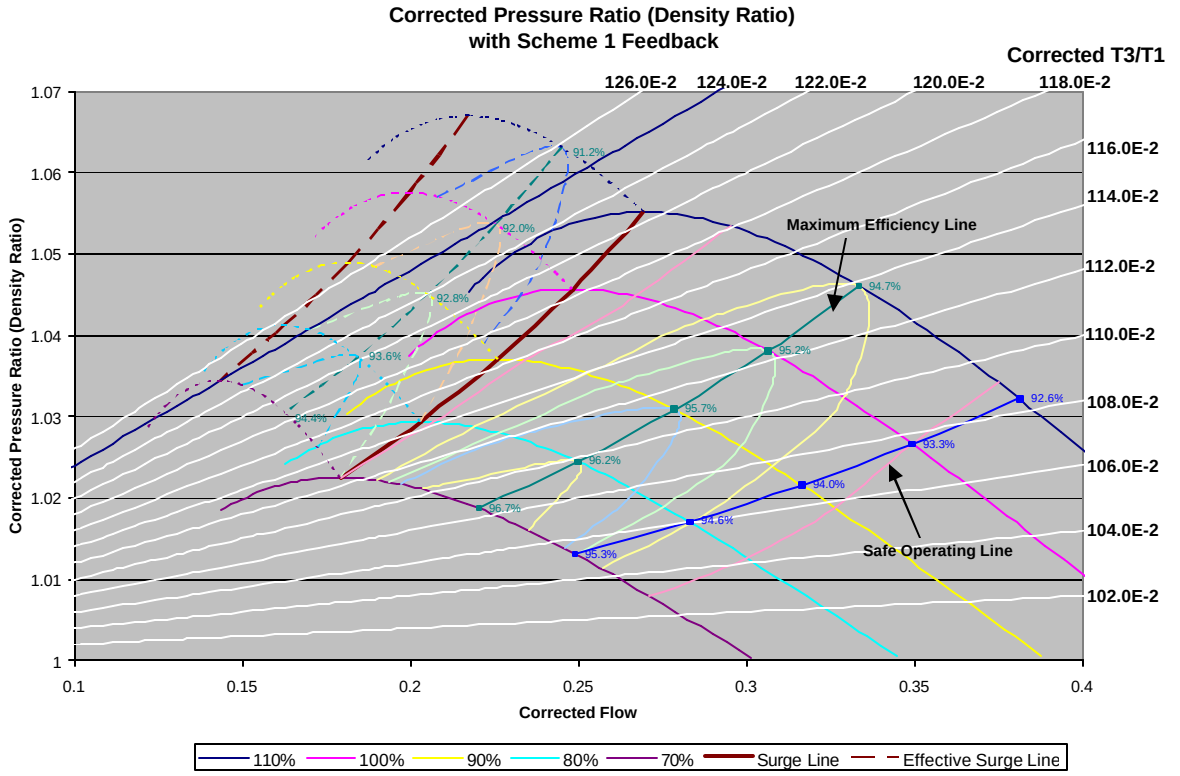

Fig. 4.2d Corrected Pressure Ratio & Density ratio versus Corrected Flow of a MIT single stage compressor with lines of constant T_3/T_1 temperature ratio and aeromechanical feedback.

4.3 Compressor Stability

Shown below is the stability of the compression system. It measures the slope of the MIT single-stage compressor at various speeds. The surge line extends across the horizontal axis at a value equal to zero. A negative slope means that the compression system is stable and corresponds to the values below the surge line on Figure 4.3a. Note that the effective surge line extends to the left of the original surge, thus enabling a dynamically-compensated compressor using Scheme #1 aeromechanical feedback to reach stability at lower flow as shown in Figure 4.3b.

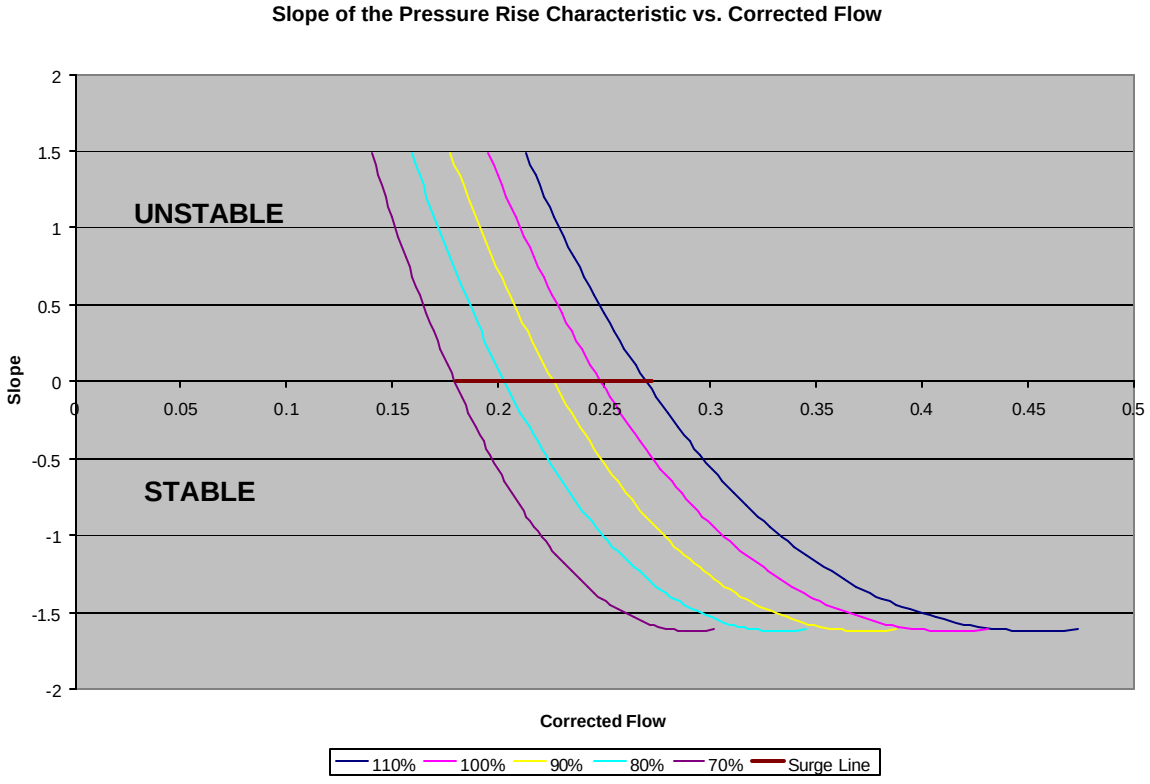

Fig. 4.3 a Corrected Compressor Stability versus Corrected Flow of a MIT single-stage compressor.

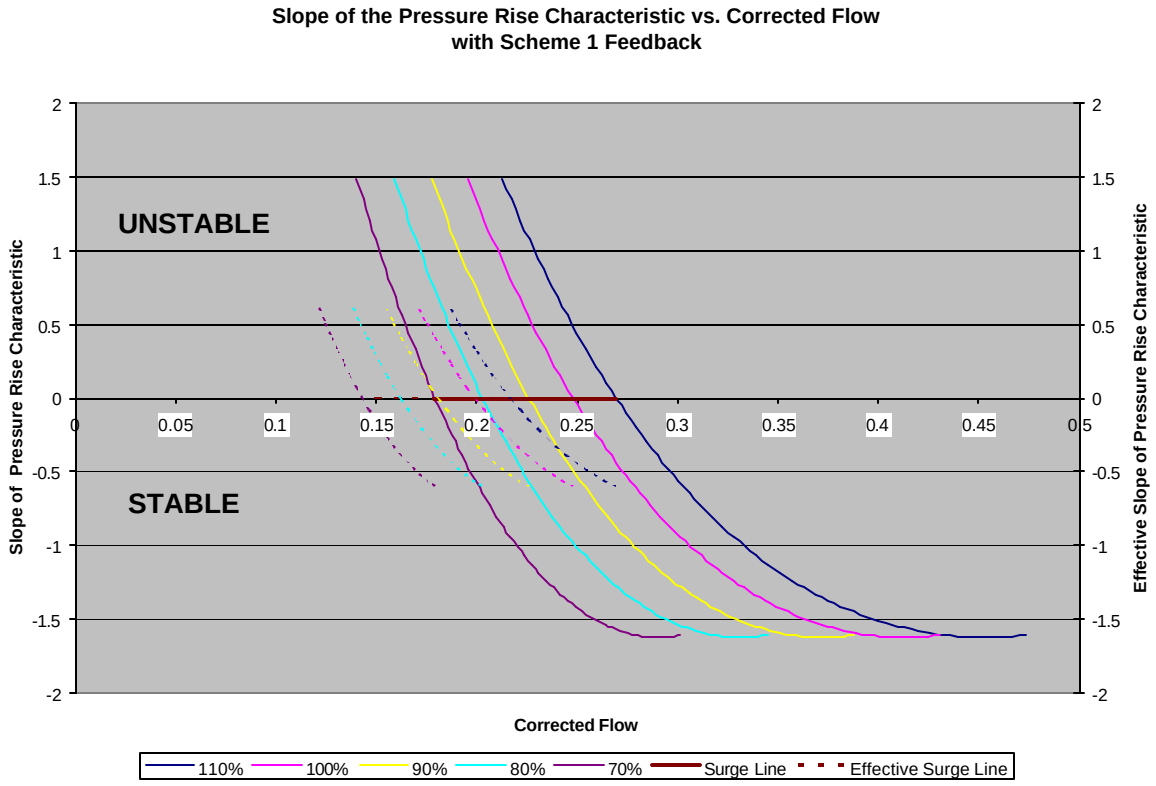

Fig. 4.3 b Corrected Compressor Stability versus Corrected Flow of a MIT single-stage compressor with aeromechanical feedback.

4.4 Compressor Efficiency

The efficiency of the compression system can be divided into three categories- *thermal efficiency, propulsive efficiency, and overall efficiency.* It should be duly noted, however, that thermal efficiency is a more useful measure in analyzing high-speed compressor performance. The efficiency was calculated and plotted using the compressor characteristic equations. See the *Section* 2.2 *Losses and Efficiency* for a description of the efficiencies. Aeromechanical feedback causes maximum thermal and overall efficiency at design speed to be regained by 95.794% and 96.660%, respectively (see Figs. 4.4.1b and 4.4.3b). The propulsive efficiency, however, is shown in Figure 4.4.2 exhibit negligibly small change with shaft speed. This is because we are assuming the propulsive efficiency is not affected by changes in the total-to-static pressure rise characteristic, although propulsive efficiency is assumed to be affected by empirically-measured affected aerodynamic flow losses due to blade flow incidence deviation changes, whose overall aggregated effects are considerably smaller by comparison to viscous dissipation losses attributing to the

considerably larger thermal efficiency of the Scheme #1 dynamically-compensated compression system.

4.4.1 Thermal Efficiency *(refer to equation 2-13)*

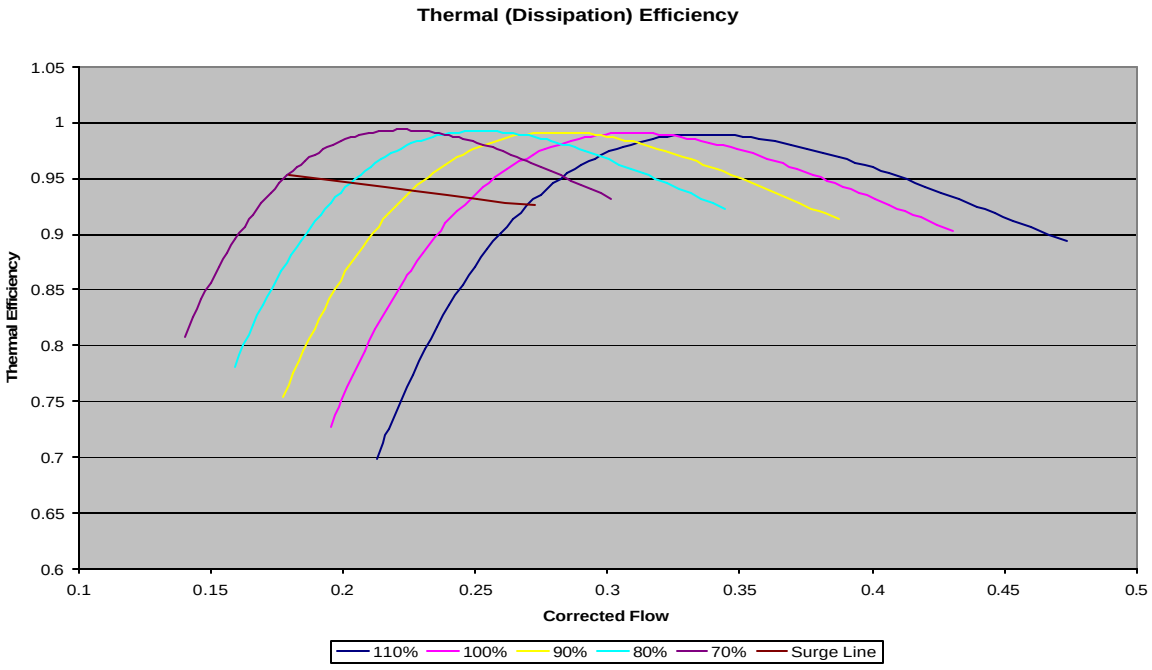

Fig. 4.4.1a Thermal Efficiency versus Corrected Flow of a MIT single-stage compressor at various speeds.

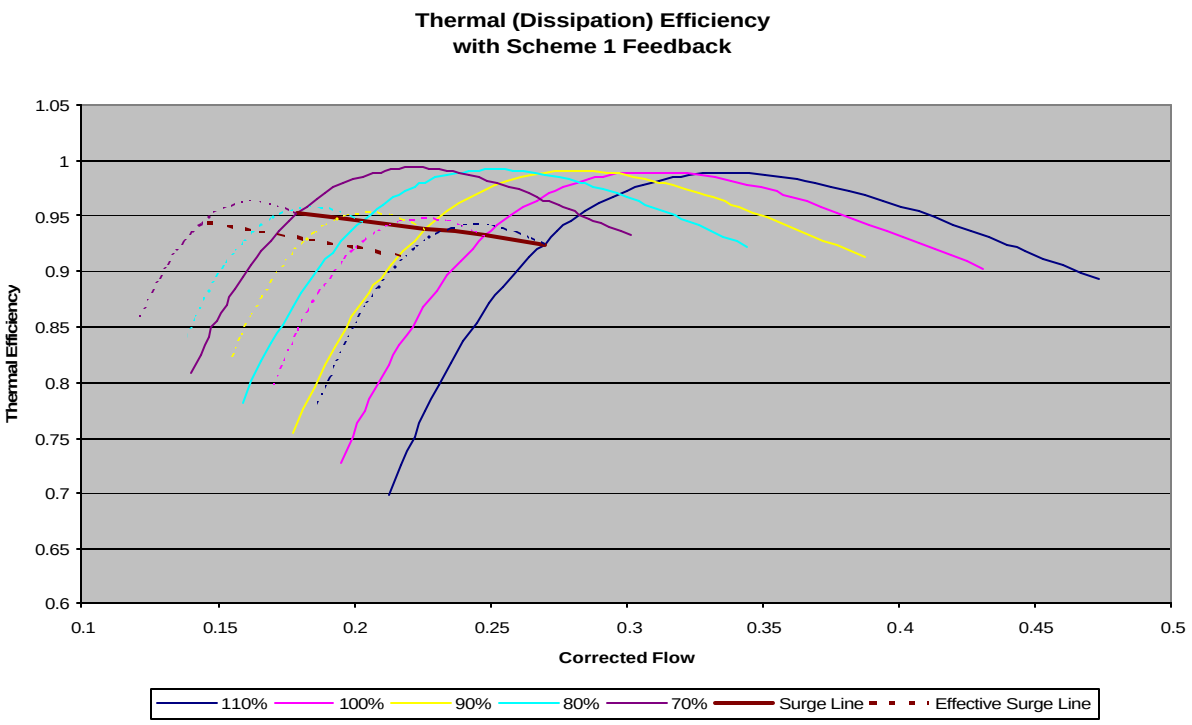

Fig. 4.4.1b Thermal Efficiency versus Corrected Flow of a MIT single-stage compressor with aeromechanical feedback at various speeds.

4.4.2 Propulsive Efficiency *(refer to equation 2-14)*

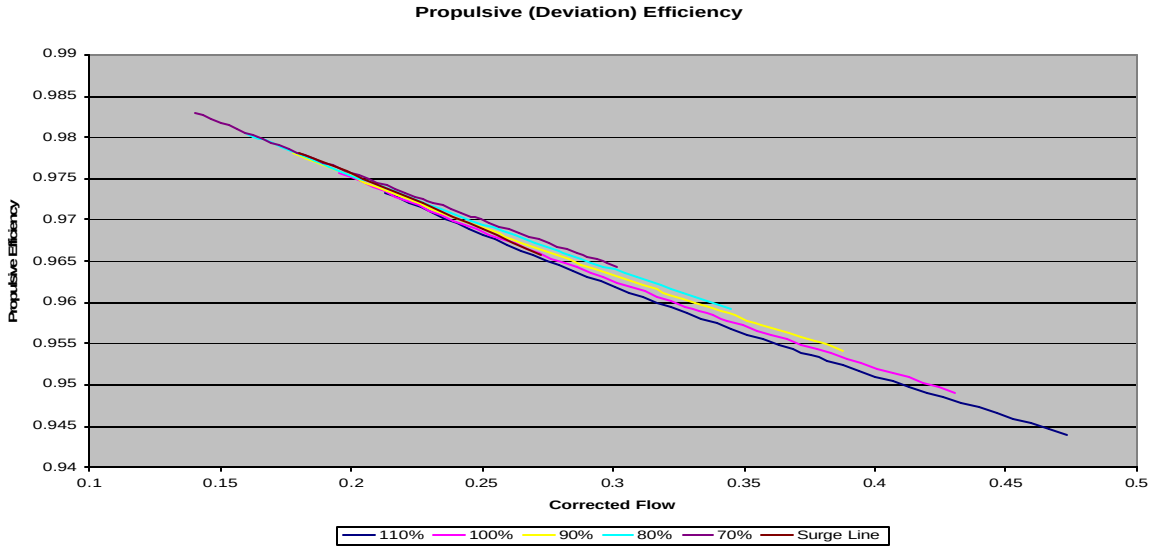

Fig. 4.4.2a Propulsive efficiency versus Corrected Flow of a MIT single-stage compressor at various speeds. ***Note: Propulsive efficiency is not affected by changes in the total-to-static characteristic according to its definition. Hence, aeromechanical feedback will not affect the propulsive efficiency of the machine. Refer to section on Losses and Efficiency.***

4.4.3 Overall Efficiency *(refer to equation 2-16)*

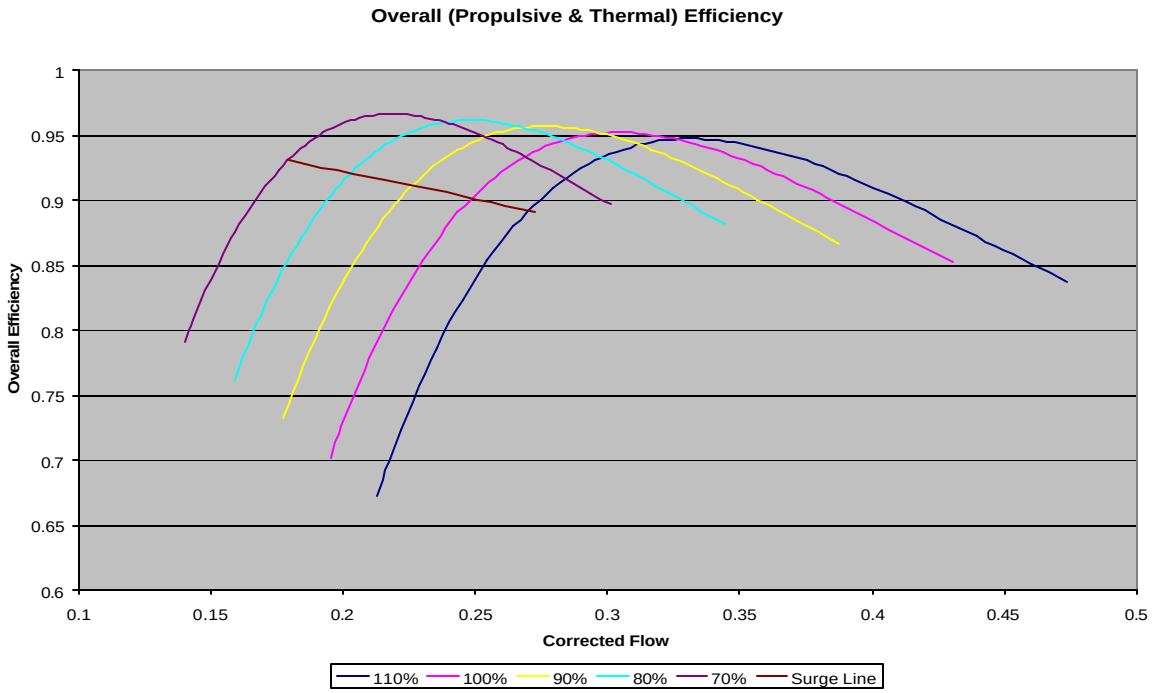

Fig.4.4.3a Overall efficiency versus Corrected Flow of a MIT single-stage compressor at various speeds.

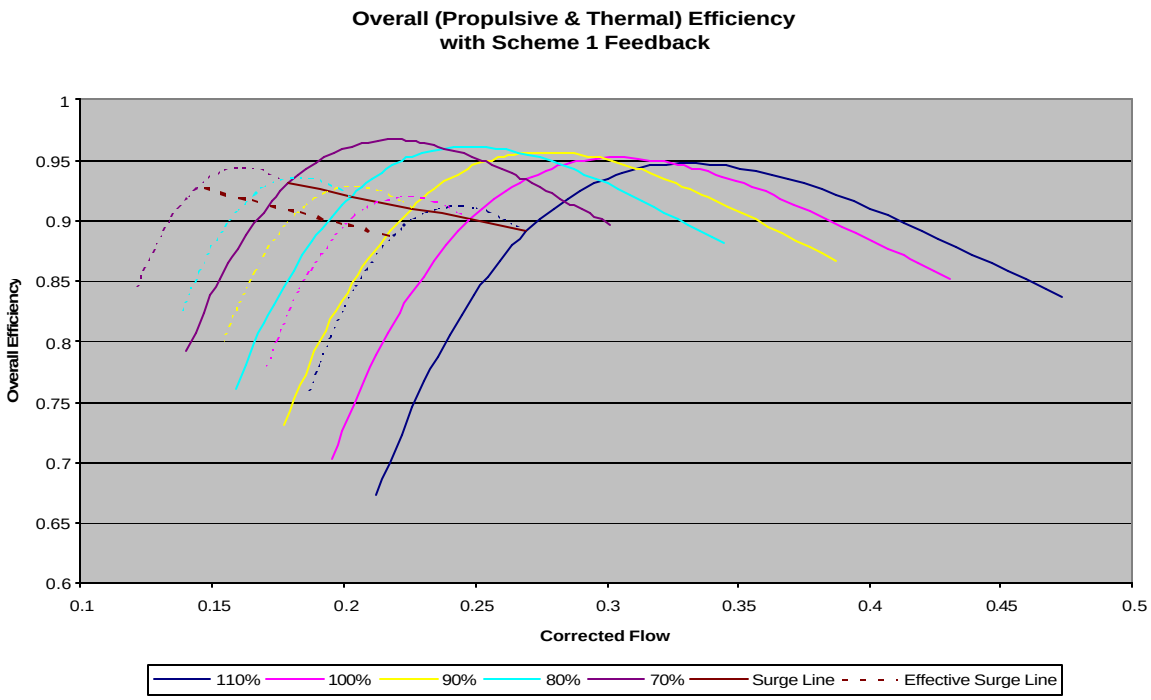

Fig.4.4.3 b Overall efficiency versus Corrected Flow of a MIT single-stage compressor with aeromechanical feedback at various speeds.

4.4.4 Efficiency Ratio (Propulsive/Thermal)

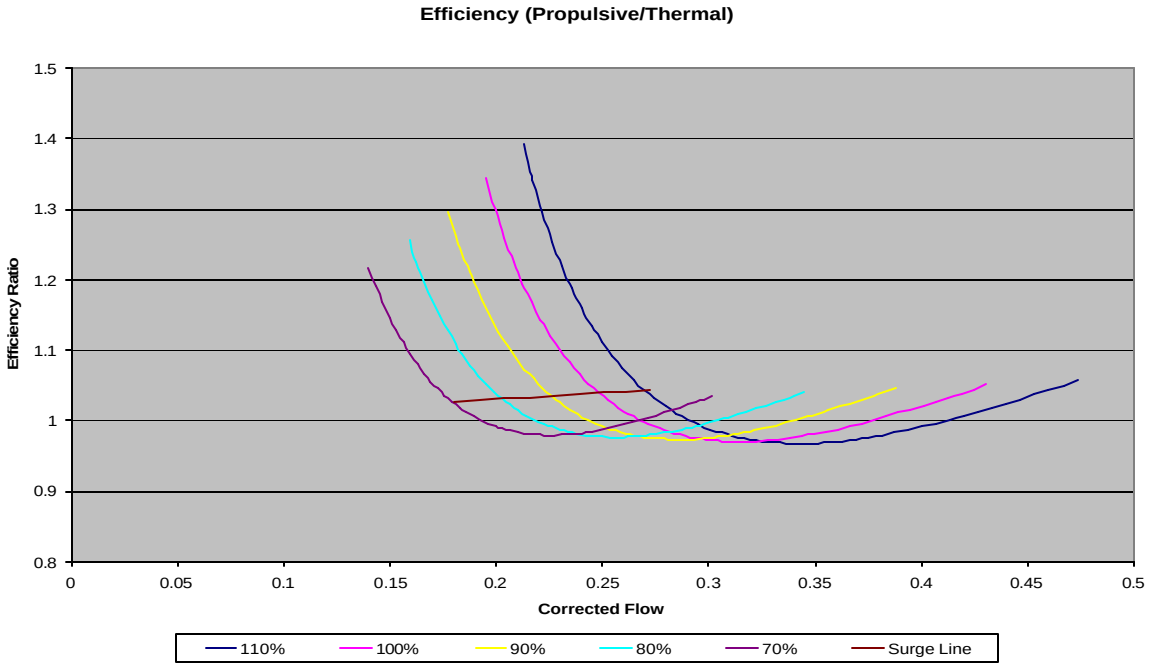

Fig. 4.4.4a Efficiency Ratio (Propulsive/Thermal) versus Corrected Flow of a MIT single-stage compressor at various speeds.

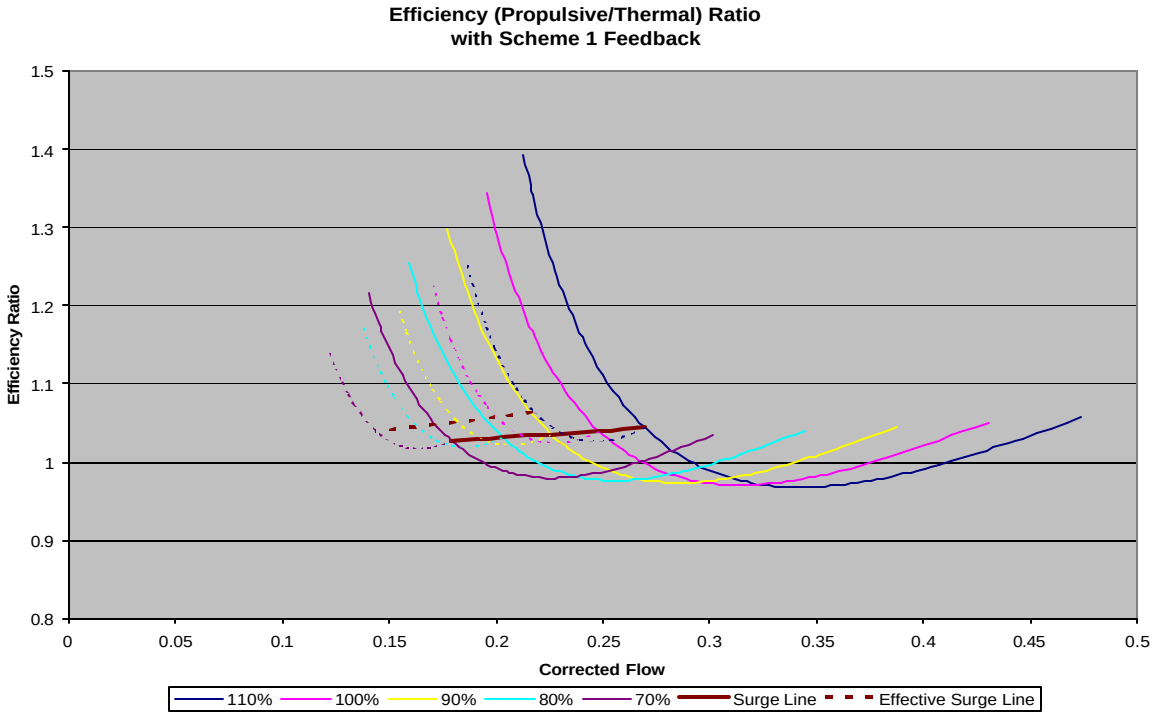

Fig.4.4.4b Efficiency Ratio (Propulsive/Thermal) versus Corrected Flow of a MIT single-stage compressor with aeromechanical feedback at various speeds.

4.5 Compressor Losses

The loss of the compression system can be divided into the same three categories as efficiency- *thermal loss, propulsive loss, and overall loss.* The loss was calculated and plotted using the compressor characteristic equations. See the *Section 2.2 Losses and Efficiency* for a description of the losses. In accordance with compressor efficiency, notice that aeromechanical feedback causes loss at design speed to be reduced to 95.794% and 96.660%, respectively (see Figs. 4.5.1b and 4.5.3b). The propulsive loss, however, remains unchanged because of how it was defined in *Section 2.2 Losses and Efficiency*. We are assuming the propulsive loss is not affected by changes in the total-to-static pressure rise characteristic.

4.5.1 Thermal Loss *(refer to equation 2-8)*

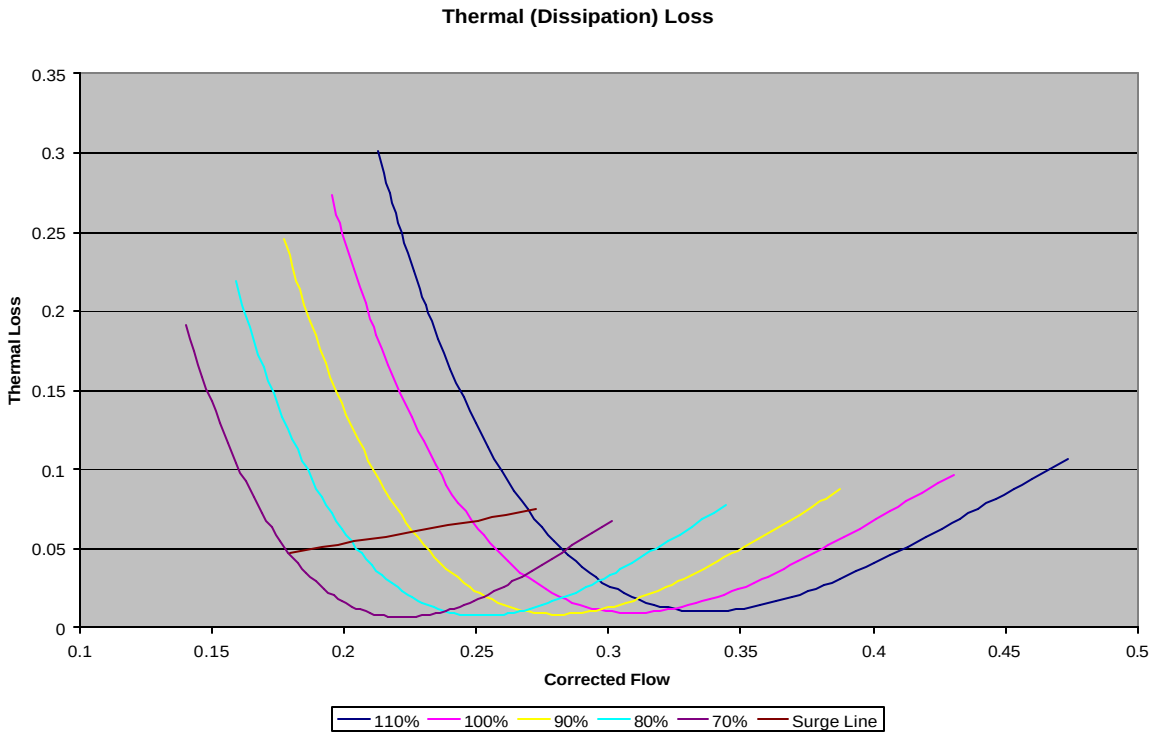

Fig. 4.5.1a Thermal Loss versus Corrected Flow of a MIT single-stage compressor at various speeds.

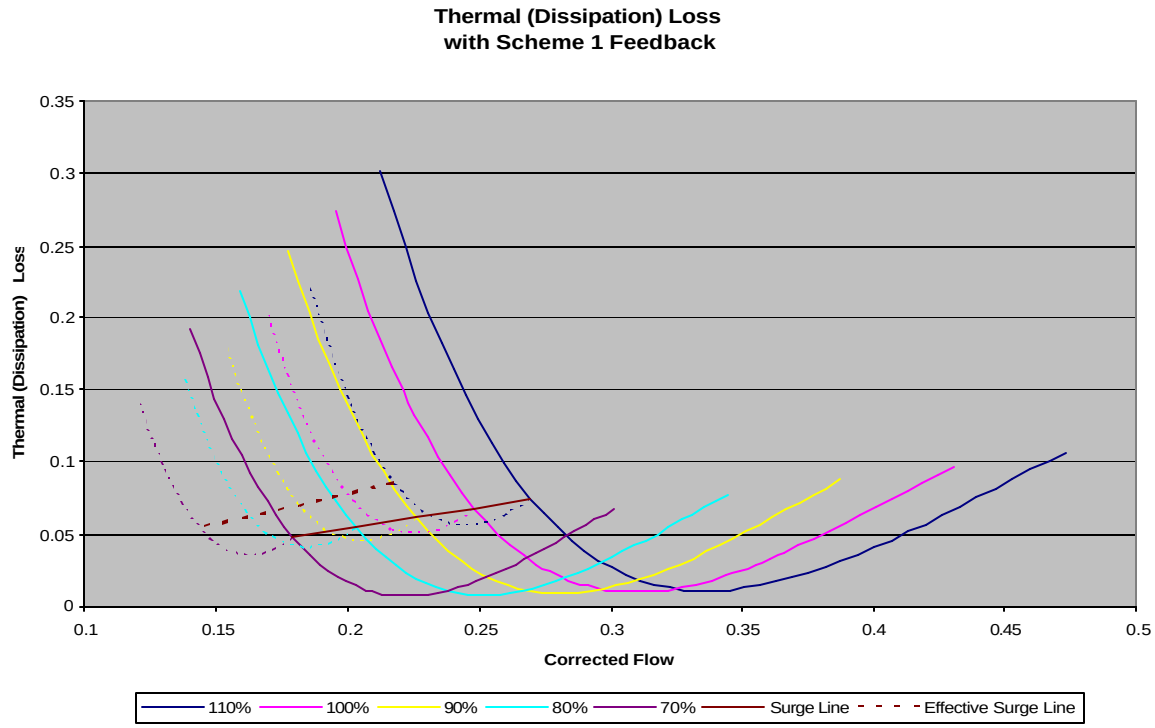

Fig. 4.5.1 b Thermal Loss versus Corrected Flow of a MIT single-stage compressor with aeromechanical feedback at various speeds.

4.5.2 Propulsive Loss *(refer to equation 2-9)*

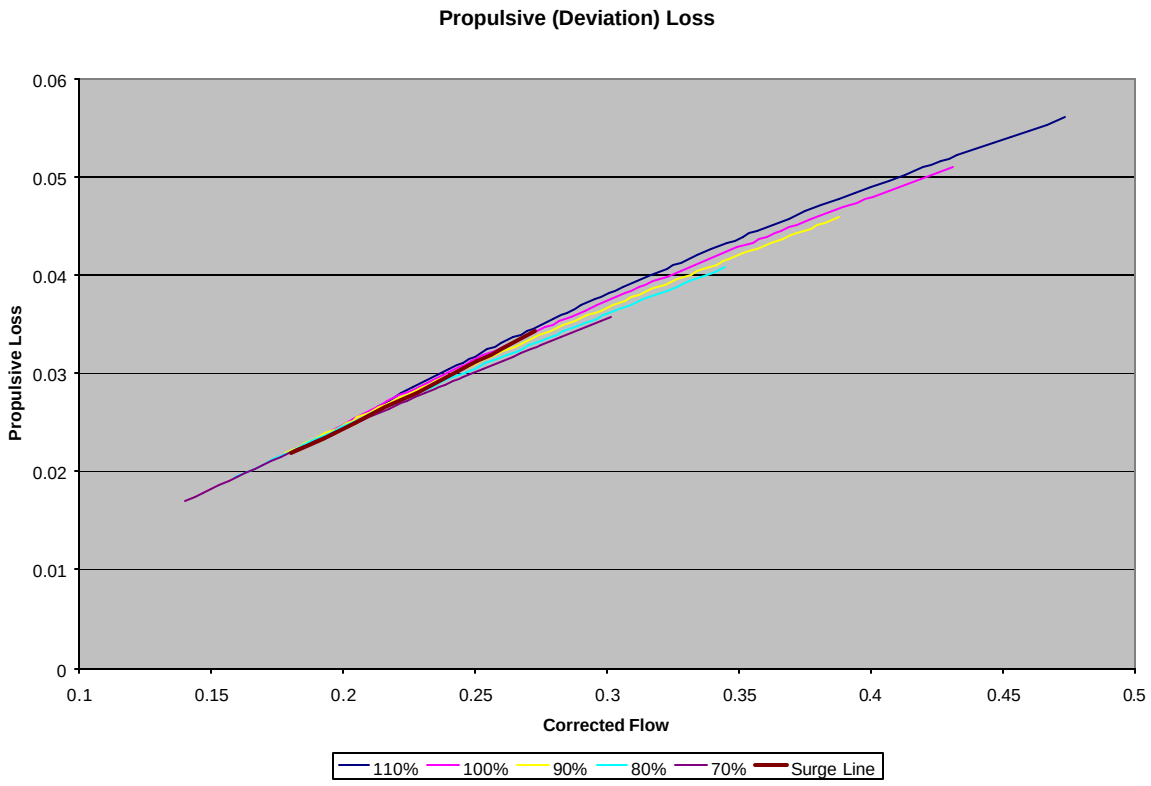

Fig. 4.5.2a Propulsive Loss versus Corrected Flow of a MIT single-stage compressor at various speeds.

Note: Propulsive loss is not affected by changes in the total-to-static characteristic according to its definition. Hence, aeromechanical feedback will not affect the propulsive loss of the machine. Refer to section on Losses and Efficiency.

4.5.3 Overall Loss *(refer to equation 2-15)*

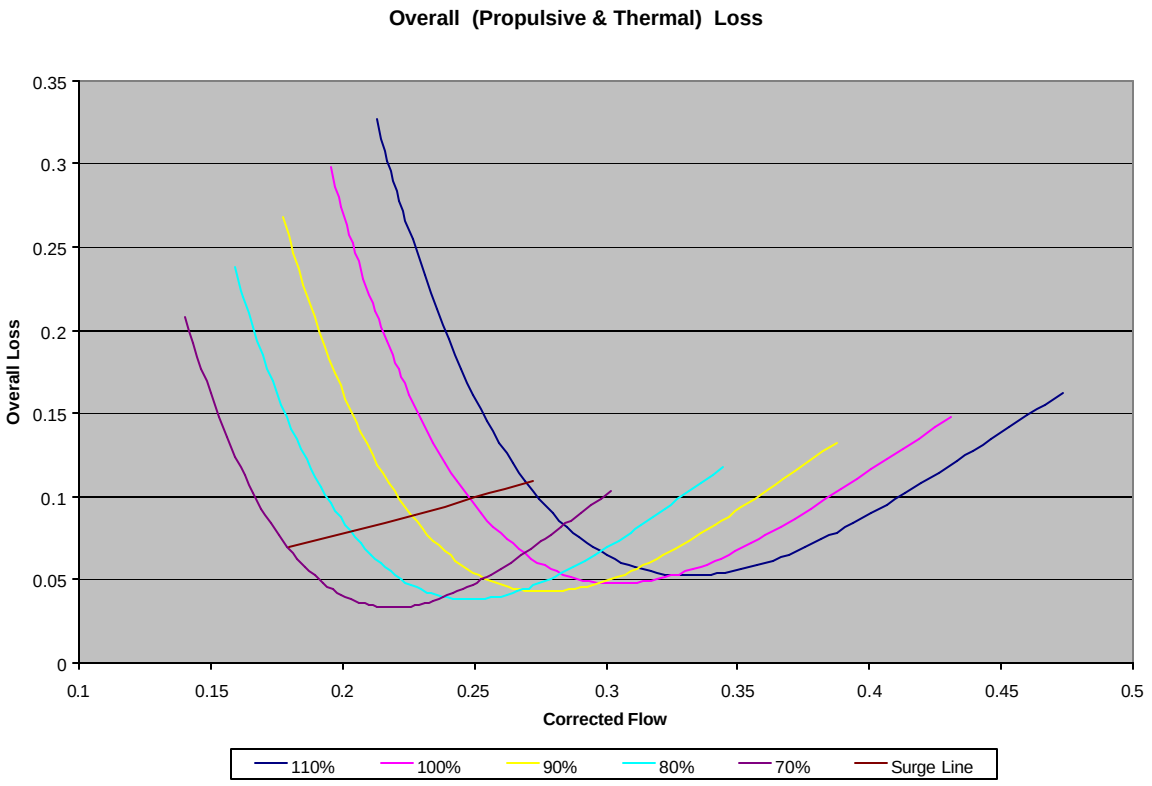

Fig. 4.5.3a Overall Loss versus Corrected Flow of a MIT single-stage compressor at various speeds.

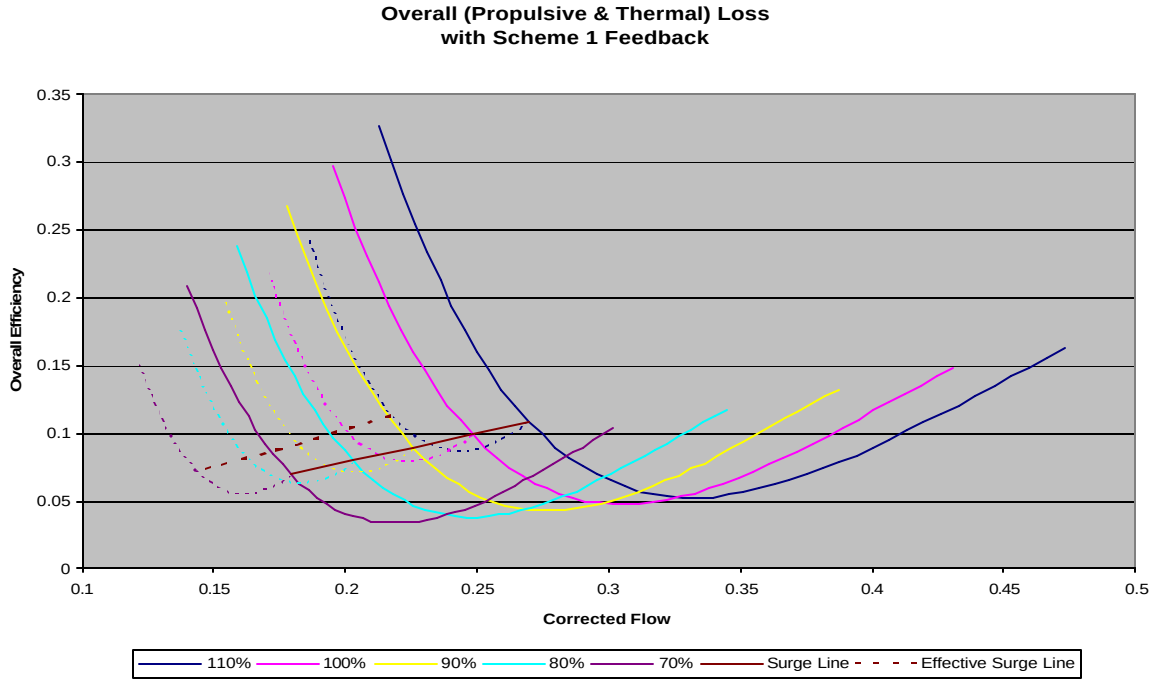

Fig. 4.5.3b Overall Loss versus Corrected Flow of a MIT single-stage compressor with aeromechanical feedback at various speeds.

4.5.4 Loss Ratio (Propulsive/Thermal)

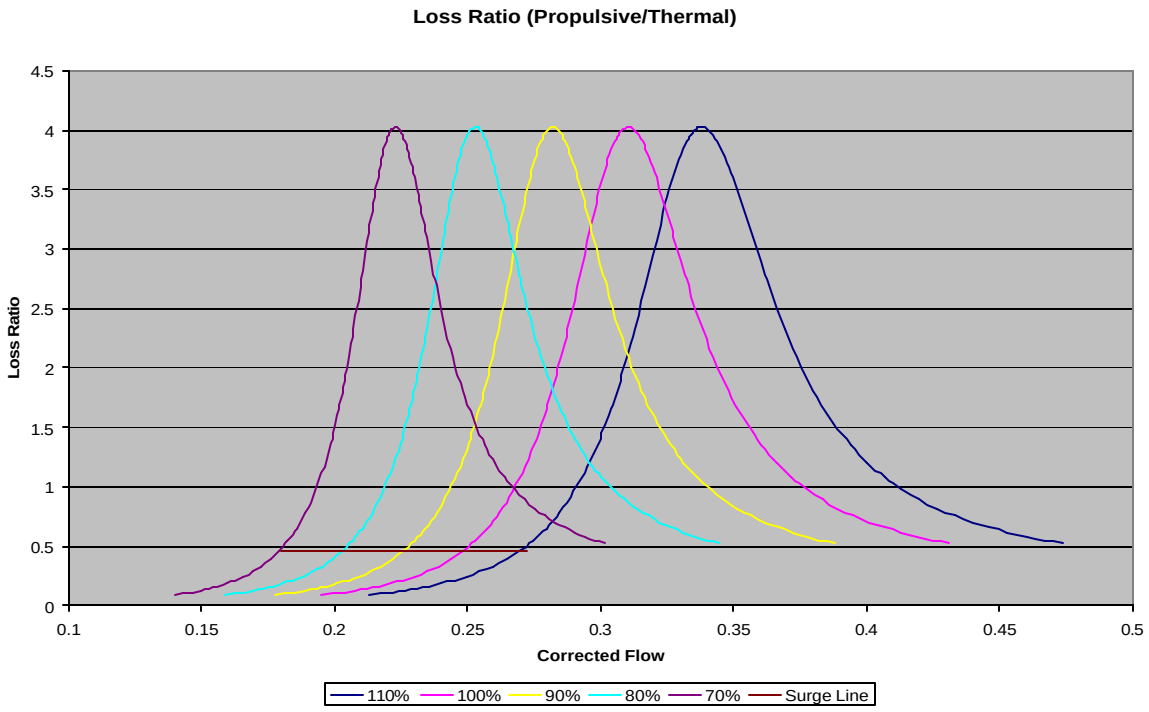

Fig. 4.5.4a Loss Ratio (Propulsive/Thermal) versus Corrected Flow of a MIT single-stage compressor at various speeds.

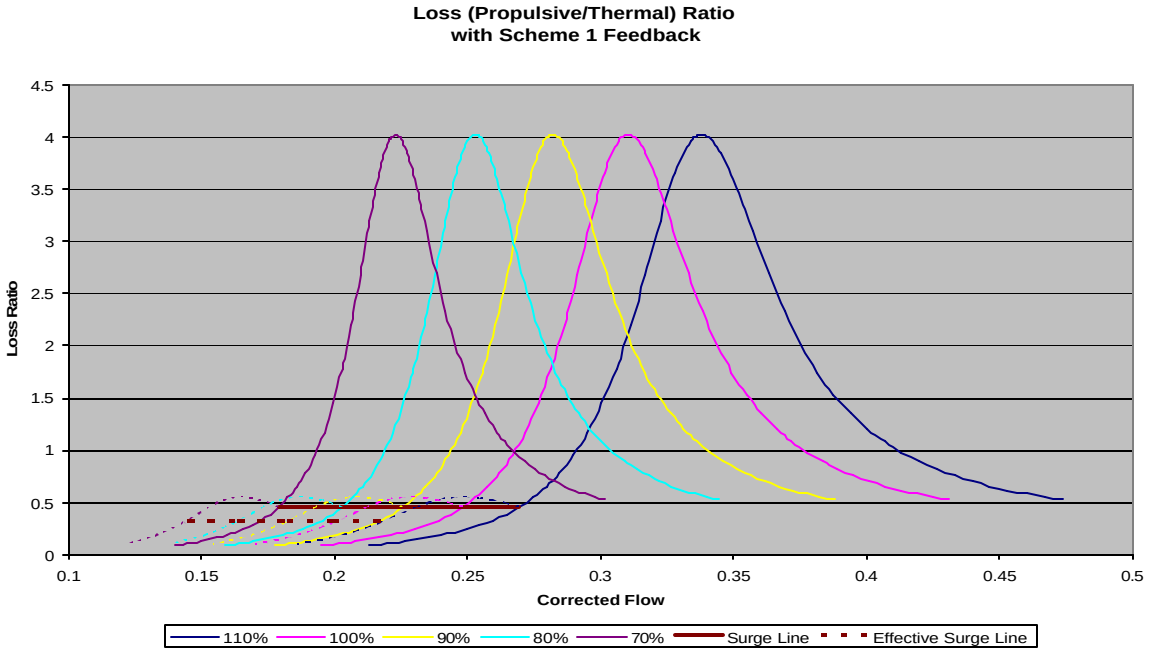

Fig. 4.5.4b Loss Ratio (Propulsive/Thermal) versus Corrected Flow of a MIT single-stage compressor at various speeds.

CHAPTER 5: Compressor Elasticity

5.1 Introduction

Compressor *elasticity* is a measure of the unsteadiness in the compression system. This chapter will explain how to develop an elasticity quantity. Further explanation is discussed in the *Appendix*. This chapter will also demonstrate the affect of aeromechanical feedback on two elasticity measures (corrected pressure-flow and corrected pressure-density). The effect of aeromechanical feedback on the other elasticity measures will be left for future study. However, the open-loop (without aeromechanical feedback) results are presented. In the subsequent sections, findings shown illustrate the unsteadiness of the compression system with respect to several different thermodynamic properties. Also introduced in this chapter is the concept of *relative non-dimensional flow*, which will be briefly explained. Finally, the chapter ends with presenting the results of the pumping and aeroelastic characteristic for a gas generator based on the MIT single-stage compressor with and without aeromechanical feedback. The aeroelastic characteristic was only measured for the corrected pressure-flow and corrected pressure-density elasticities, the measurement of the other aeroelastic characteristics are left for future study. The results of other elasticities, pumping, and aeroelastic characteristics for the MIT single-stage and MIT three-stage compressor for the remaining schemes can be found in the *Appendix*.

5.2 Corrected Pressure-Flow (Pf) Elasticity

In order to create an elasticity, or unsteadiness, measure you first need to develop a relationship between two quantities- in this case corrected pressure ratio and corrected flow. In *Section 4.2* this relationship was formed and plotted (see Fig. 4.2a). Once the relationship of the corrected pressure ratio and corrected flow has been obtained, the relative change in the corrected pressure ratio to the relative change in the flow (or the slope of the corrected pressure ratio vs. corrected flow curve) is measured. This quantity is then multiplied by the original corrected flow to corrected pressure ratio. The result is a corrected pressure-flow elasticity quantity. Mathematically, it is:

$$Pj_{elasticity} = \left(\frac{\Delta P}{\Delta j}\right)\left(\frac{j_o}{P_o}\right)$$

All other elasticities (other than the corrected pressure-density elasticity) were derived in a similar manner. See the *Appendix* for a more general formulation.

Figures 5.2a and 5.2b show the corrected pressure-flow elasticity of a MIT single-stage compressor at various speeds with and without feedback, respectively. Note the similarity of the relationship between the slope of the pressure rise characteristic versus corrected flow (Fig. 4.3b) and the corrected pressure-flow elasticity versus corrected flow (Fig. 5.2b), which both show *scheme #1* feedback enabling stability at lower flow; however, the slope of the latter is flatter than the slope of the former, which suggests that the corrected pressure-flow elasticity is less prone to fluctuate when the corrected flow changes.

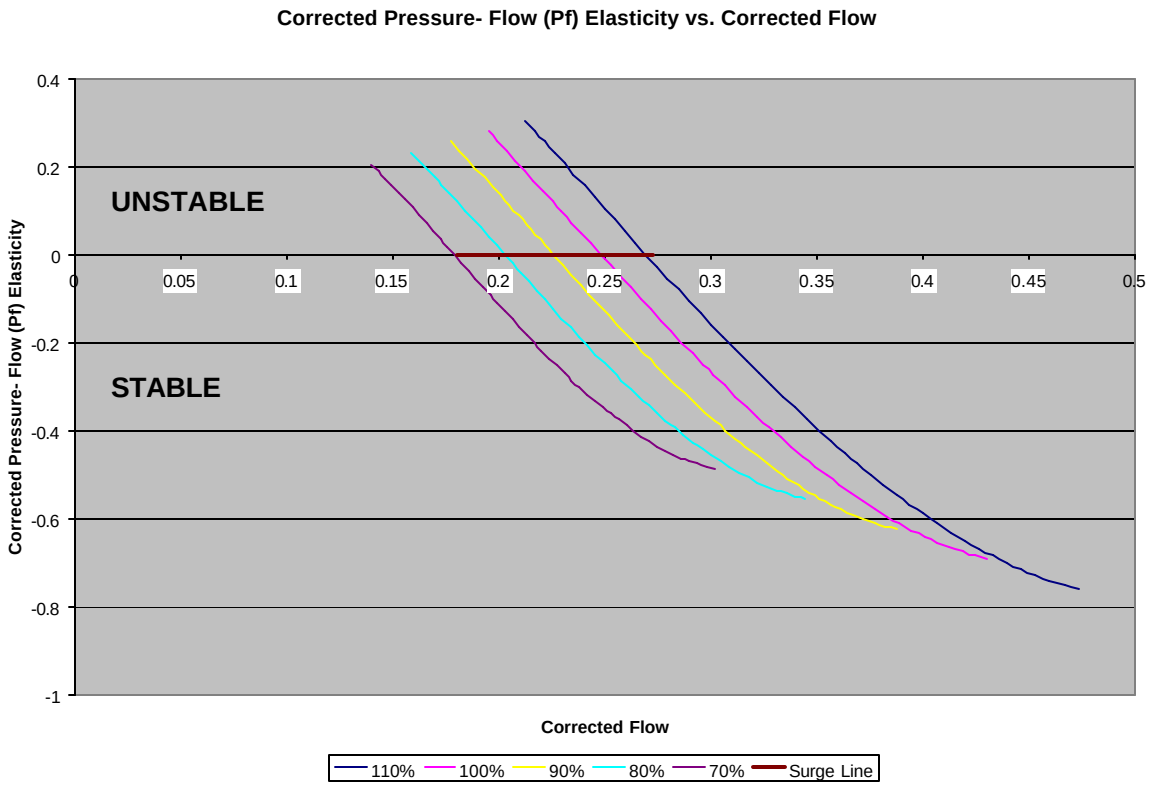

Fig. 5.2a Corrected Pressure-Flow Elasticity versus Corrected Flow of a MIT single-stage compressor at various speeds.

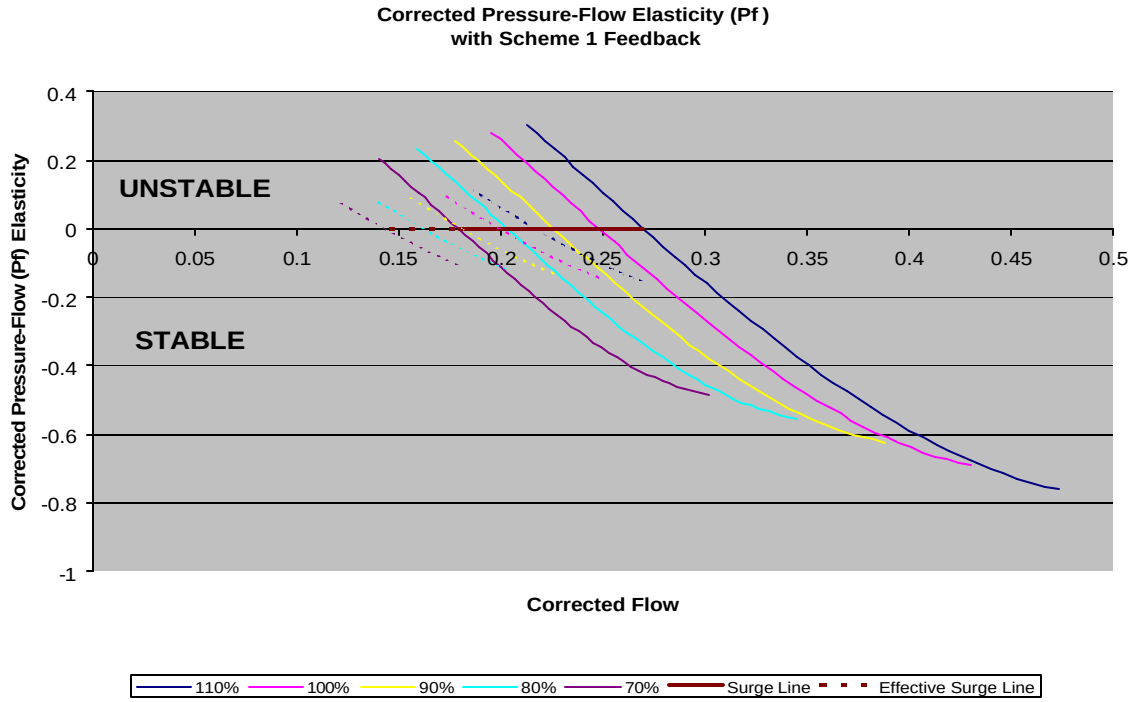

Fig. 5.2 b Corrected Pressure-Flow Elasticity versus Corrected Flow of a MIT single-stage compressor with aeromechanical feedback at various speeds.

5.3 Corrected Pressure-Density (P?) Elasticity

The corrected pressure-density elasticity is the polytropic exponent, n, and was derived from the propulsive efficiency, h_p, and specific heat ratio, k. It is described as follows (Gresh 2001):

$$Pr_{elasticity} = n = \frac{h_p\left(k/k-1\right)}{h_p\left(k/k-1\right)-1}$$

Note that it is assumed that aeromechanical feedback doesn't affect the corrected pressure-density elasticity because neither propulsive efficiency nor the specific heat ratio is affected by changes in the total-to-static pressure characteristic.

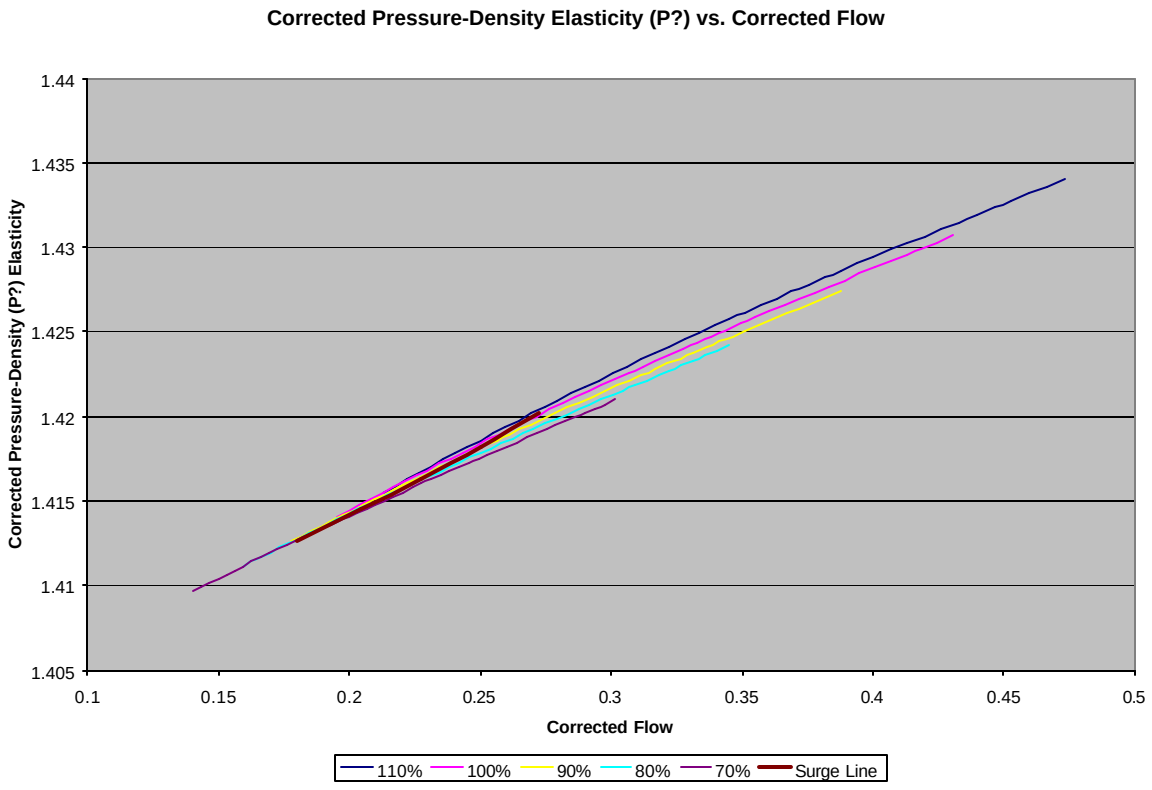

Fig. 5.3a Corrected Pressure-Density Elasticity versus Corrected Flow of a MIT single-stage compressor with aeromechanical feedback at various speeds. ***Note: Corrected Pressure-Density Elasticity is not affected by changes in the total-to-static characteristic but rather changes in the polytropic exponent.***

5.4 Corrected Pressure-Specific Volume Elasticity (Pv) *(see Appendix for basic elasticity derivation)*

Since this is the first section where it is derived, it is fitting to discuss the relative non-dimensional corrected flow. The relative non-dimensional corrected flow is simply a quantity that measures the relative change in the corrected flow with respect to the original flow. It is defined as follows:

$$j' = \frac{\Delta j}{j_o}$$

Altering the x-axis from corrected flow to relative non-dimensional corrected flow has significant consequences; particularly, the surge line becomes almost vertical, which means that the relative non-dimensional corrected flow at surge is constant (see Fig. 5.4c).

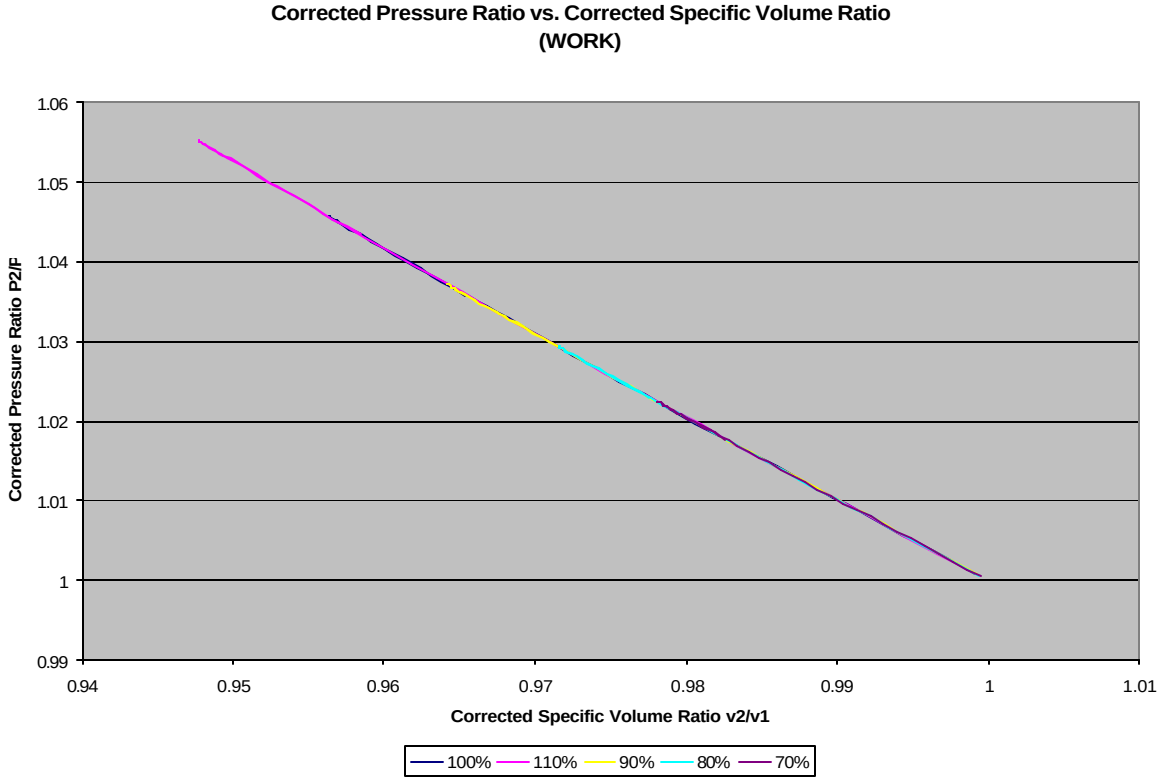

Fig. 5.4a Corrected Pressure Ratio versus Corrected Specific Volume Ratio of a MIT single-stage compressor at various speeds.

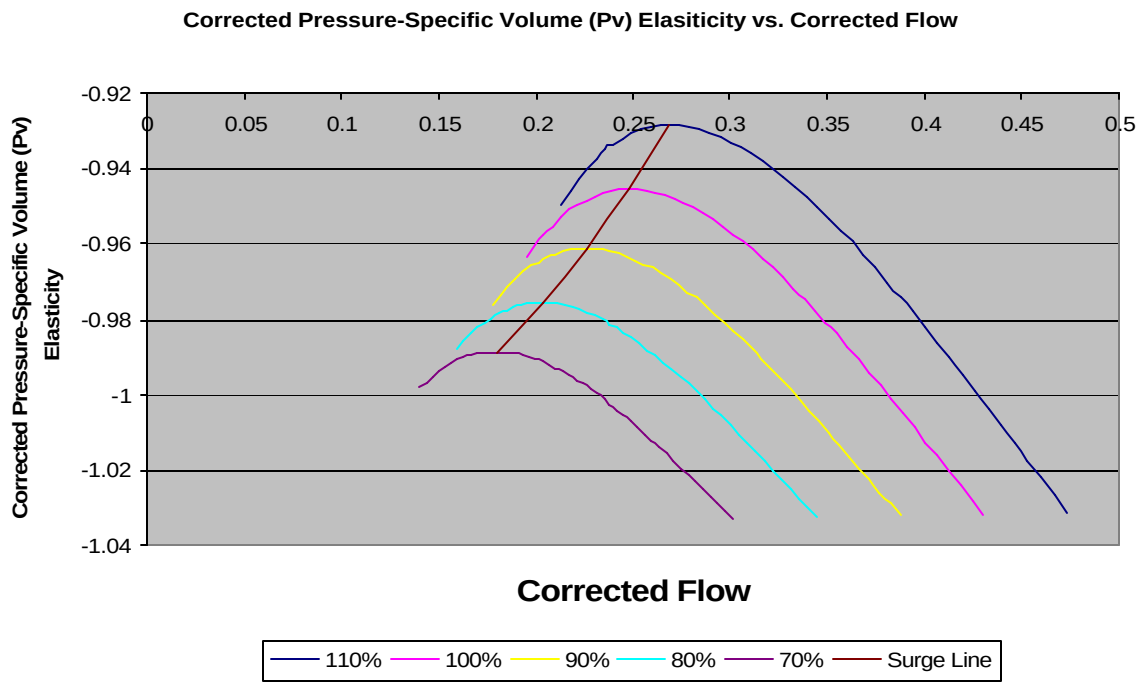

Fig. 5.4b Corrected Pressure-Specific Volume Elasticity versus Corrected Flow of a MIT single-stage compressor at various speeds.

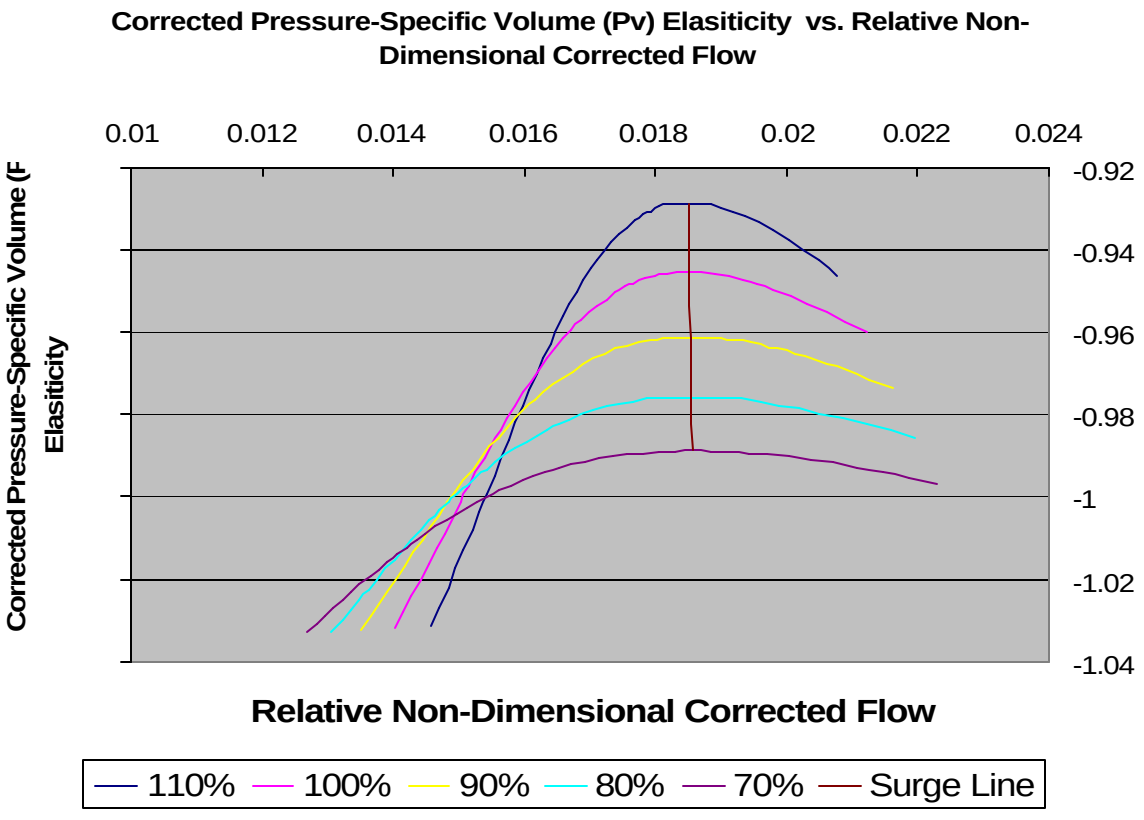

Fig. 5.4c Corrected Pressure-Specific Volume Elasticity versus Relative Non-Dimensional Corrected Flow of a MIT single-stage compressor at various speeds.

5.5 Corrected Pressure-Temperature (PT) Elasticity *(see Appendix for basic elasticity derivation)*

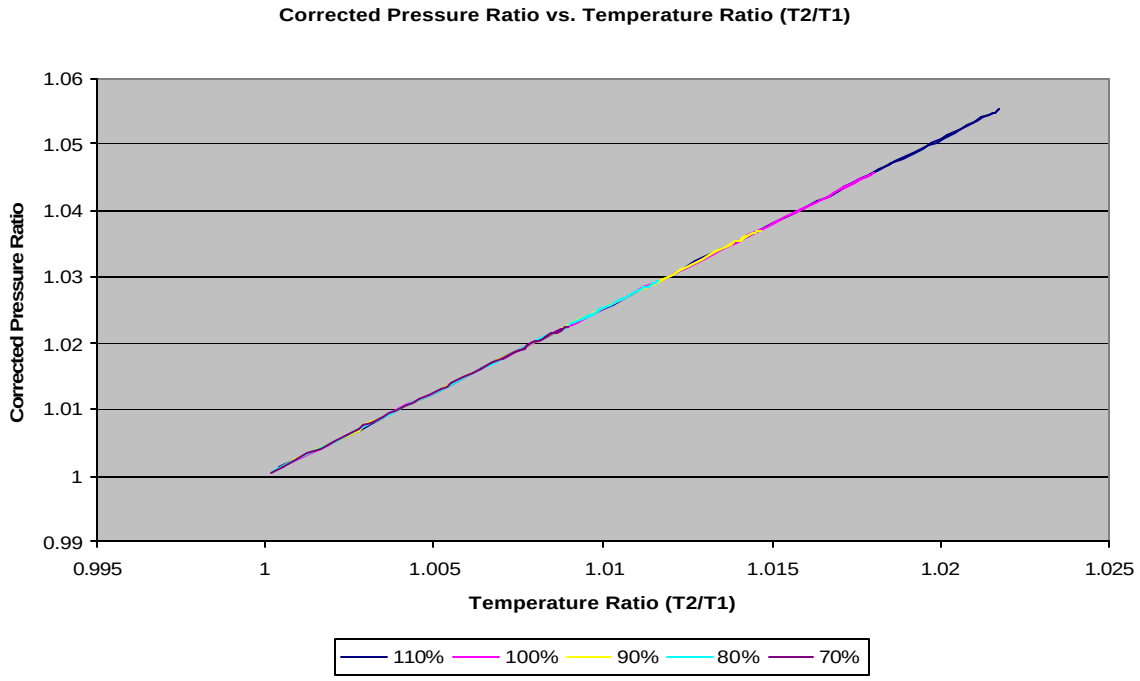

Fig. 5.5a Corrected Pressure Ratio versus Corrected Temperature Ratio (T_2/T_1) of a MIT single-stage compressor at various speeds.

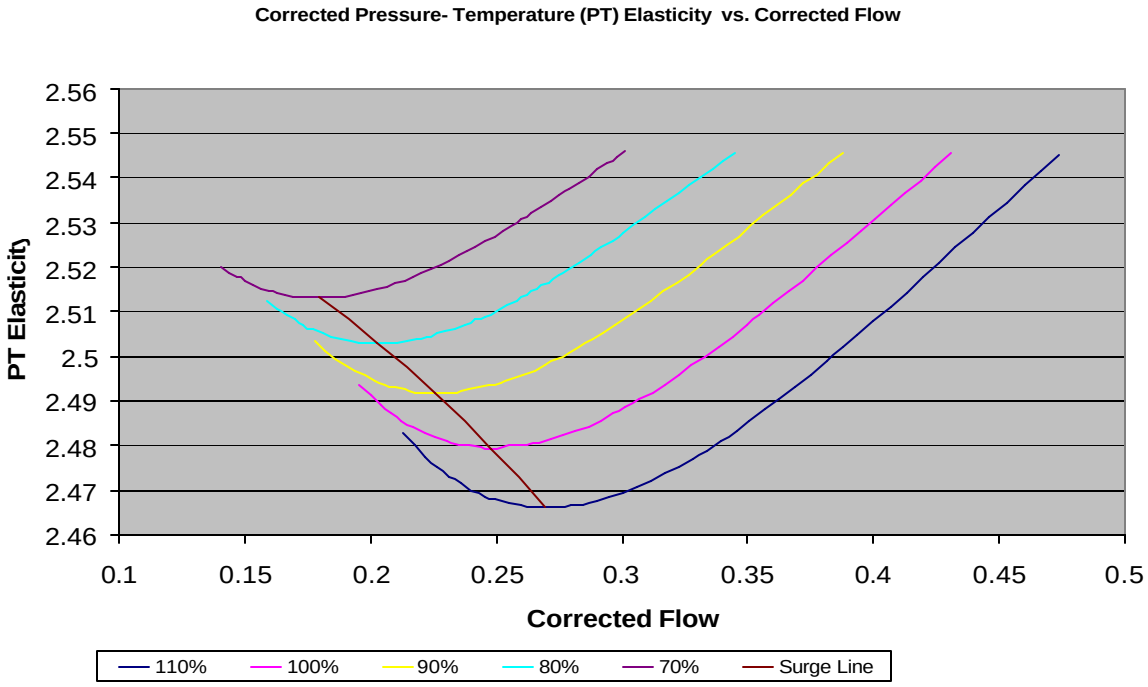

Fig. 5.5b Corrected Pressure-Temperature Elasticity versus Corrected Flow of a MIT single-stage compressor at various speeds.

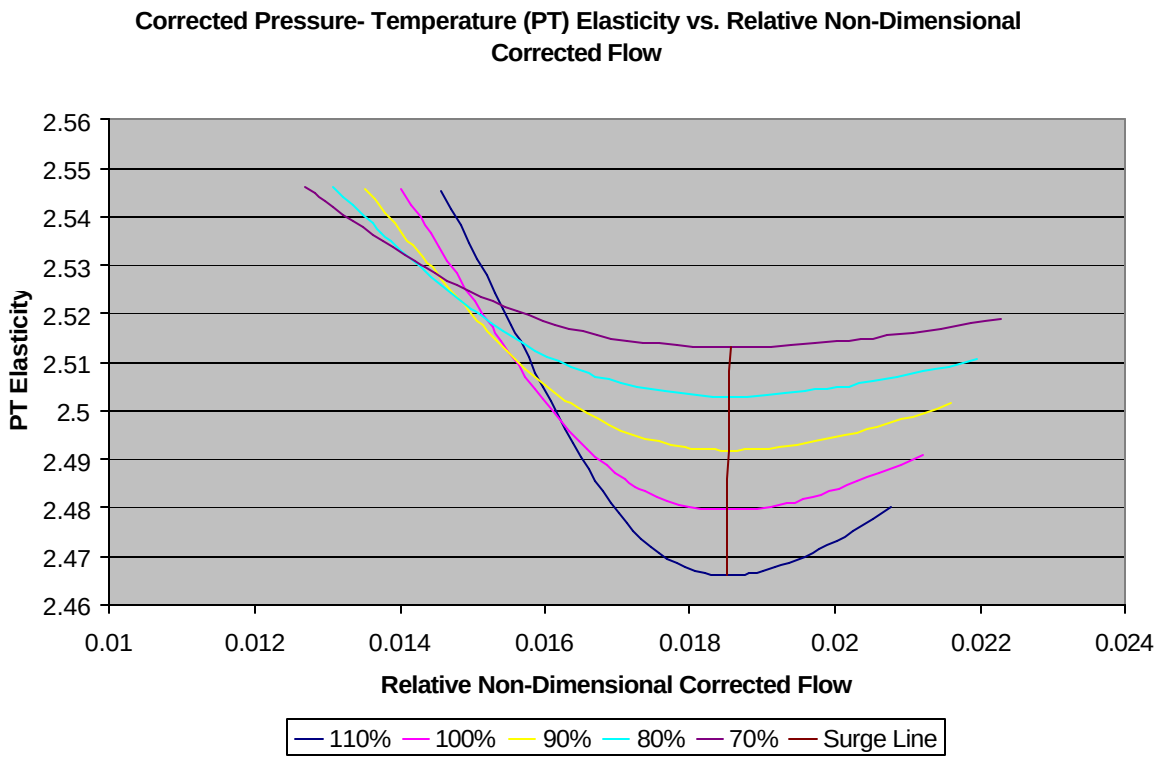

Fig. 5.5c Corrected Pressure-Temperature Elasticity versus Relative Non-Dimensional Corrected Flow of a MIT single-stage compressor at various speeds.

5.6 Corrected Temperature-Loss (Ts) Elasticity *(see Appendix for basic elasticity derivation)*

The elasticities that contain losses (thermal & propulsive) also have rather interesting effects- most likely because of the strange relationships that it has with the other thermodynamic properties in this study. In this section, the corrected temperature ratio (T_2/T_1) and losses are compared (see Fig. 5.6a). Note the considerable amount of thermal loss in comparison to propulsive loss during operation. As a result, it is apparent that when considering the overall efficiency of the compressor, it is more appropriate to consider the thermal efficiency versus the propulsive efficiency of the machine. The peculiar shape of the temperature ratio versus thermal loss curve leads to asymptotic elasticity curves around the x-axis (Fig. 5.6b). In addition, because the surge line is also along the x-axis ranging from about 0.18 to 0.27 in Fig. 5.6b, it becomes a point at about 0.0186 when this axis is altered in Fig. 5.6c. This phenomenon occurs in a similar manner in all the elasticities that involve loss. (see *Sections 5.7 and 5.9)*

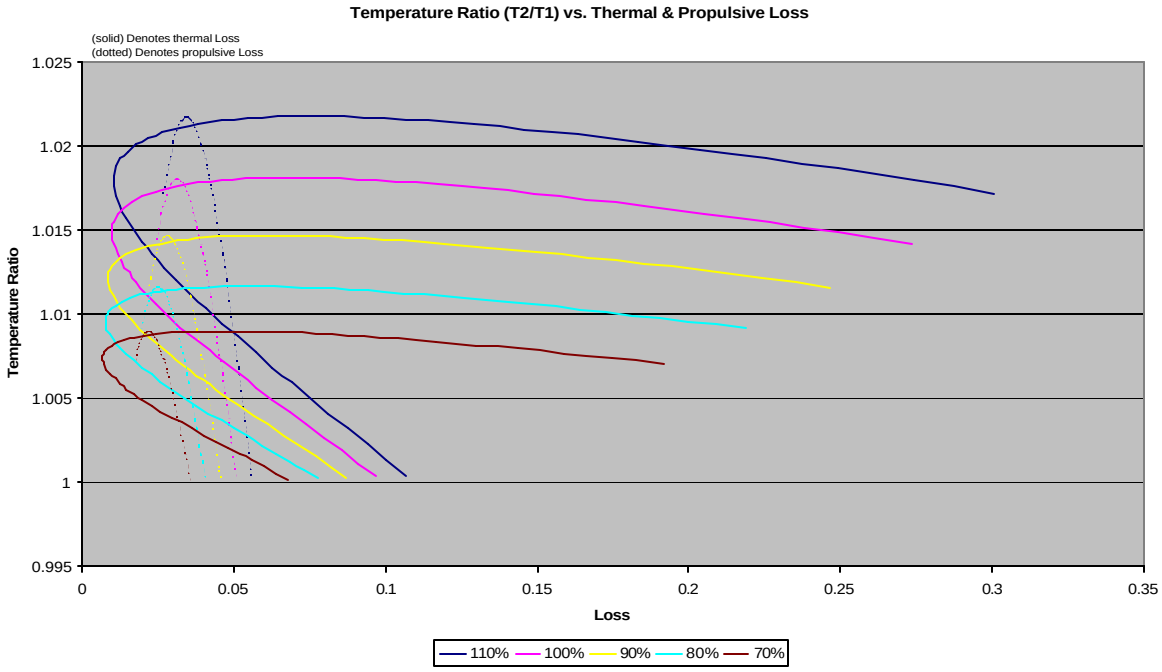

Fig. 5.6a Corrected Temperature Ratio (T_2/T_1) versus Thermal & Propulsive Loss of a MIT single-stage compressor at various speeds.

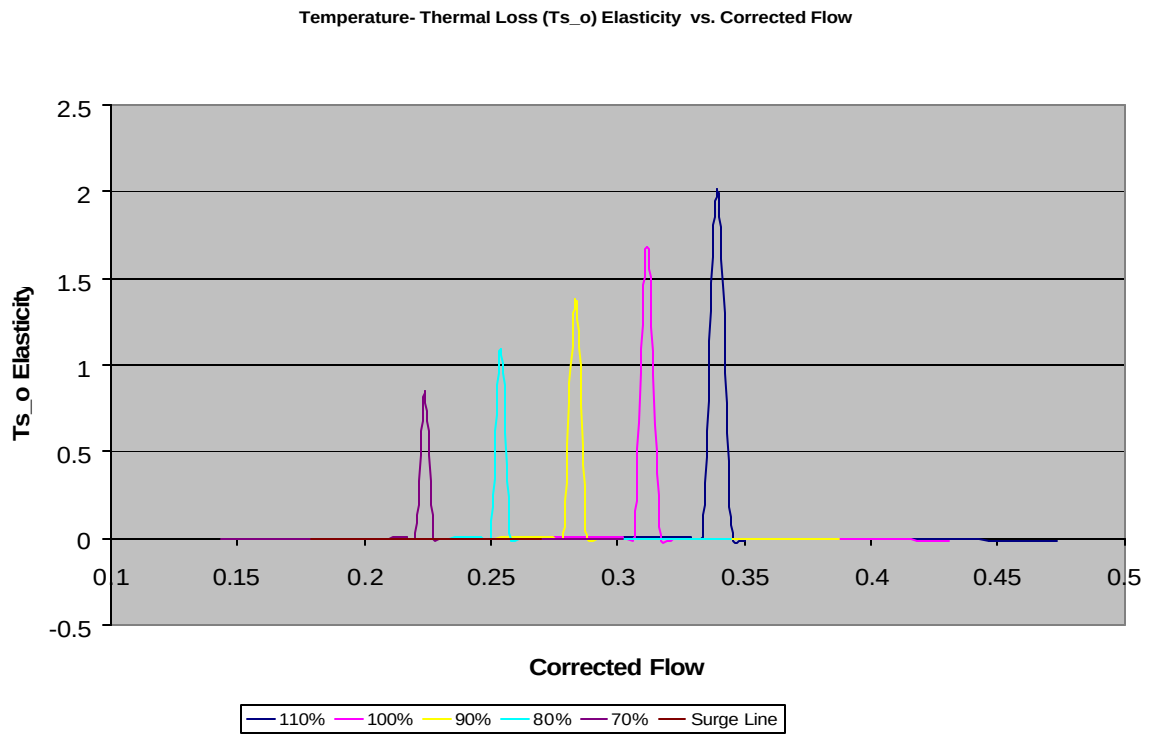

Fig. 5.6b Corrected Temperature-Thermal Loss Elasticity versus Corrected Flow of a MIT single-stage compressor at various speeds.

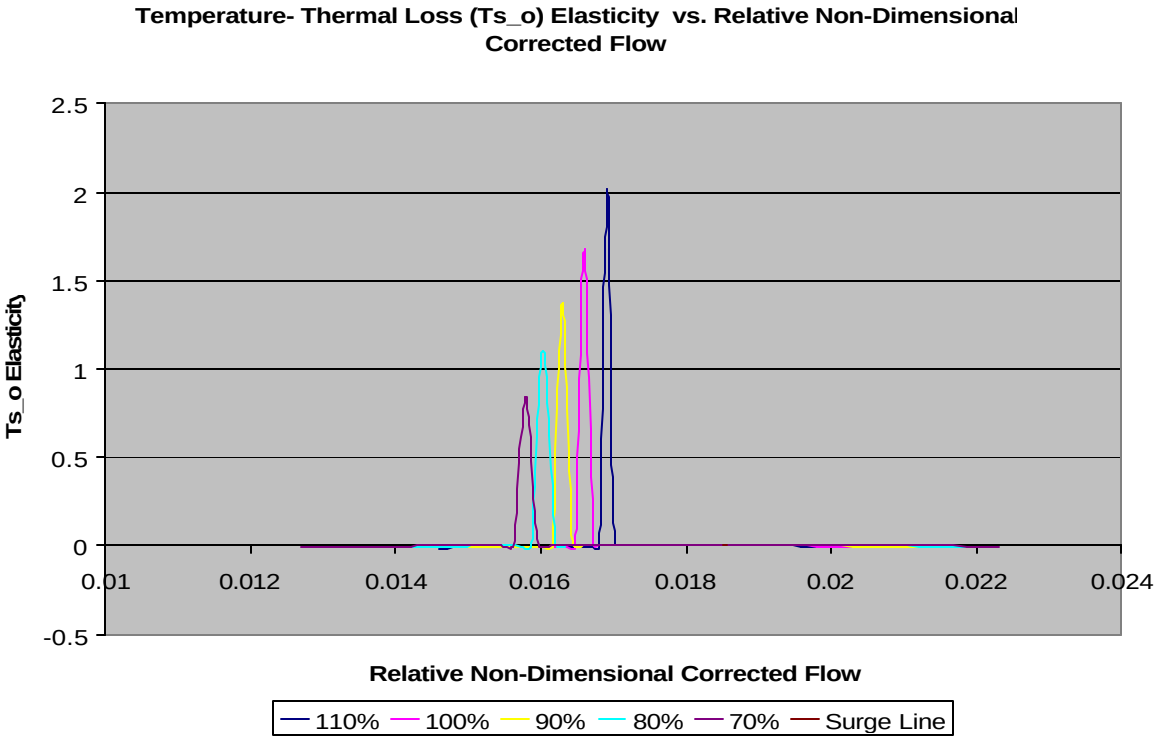

Fig. 5.6c Corrected Temperature-Thermal Loss Elasticity versus Relative Non-dimensional Corrected Flow of a MIT single-stage compressor at various speeds.

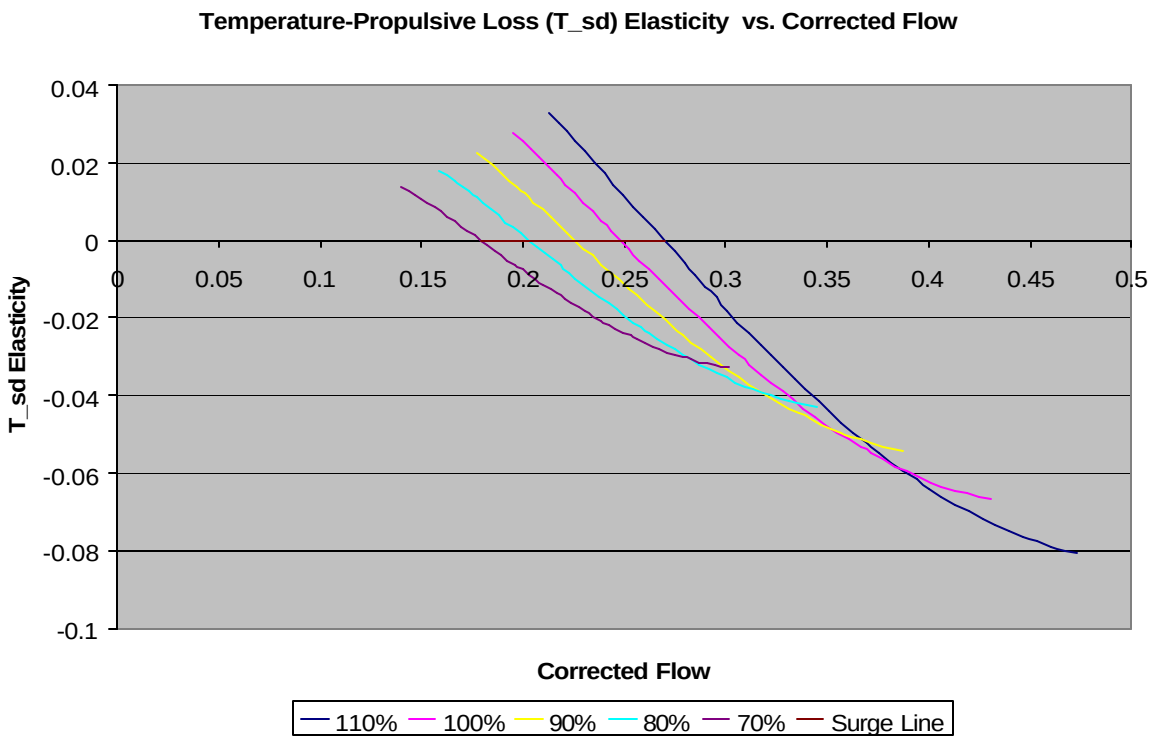

Fig. 5.6d Corrected Temperature-Propulsive Loss Elasticity versus Corrected Flow of a MIT single-stage compressor at various speeds.

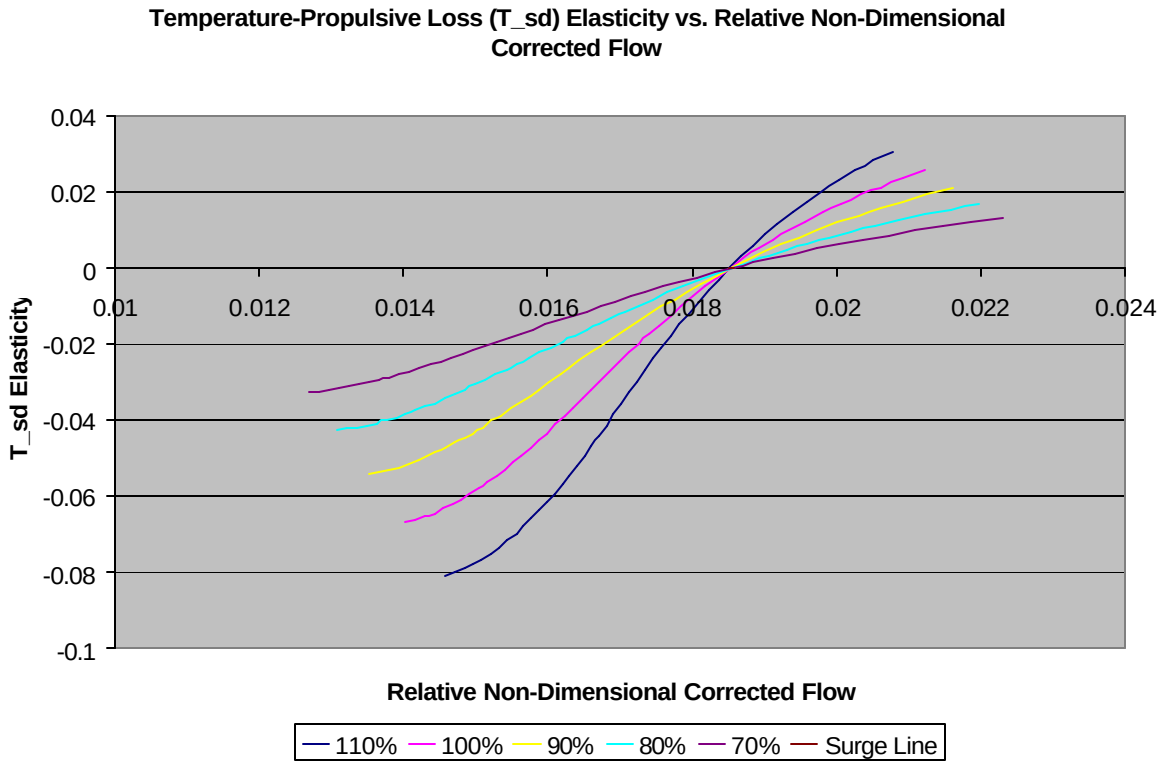

Fig. 5.6e Corrected Temperature-Propulsive Loss Elasticity versus Relative Non-Dimensional Corrected Flow of a MIT single-stage compressor at various speeds.

5.7 Corrected Pressure-Loss (Ps) Elasticity Elasticity *(see Appendix for basic elasticity derivation)*

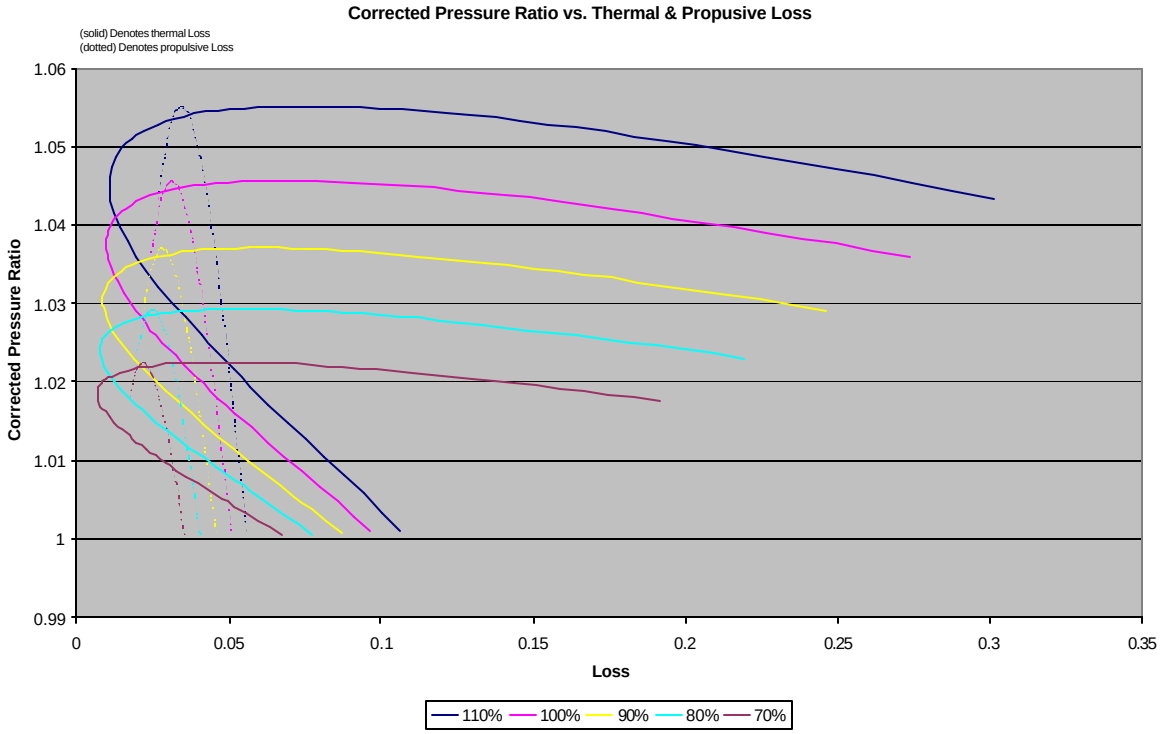

Fig. 5.7a Corrected Pressure Ratio versus Thermal & Propulsive Loss of a MIT single-stage compressor at various speeds.

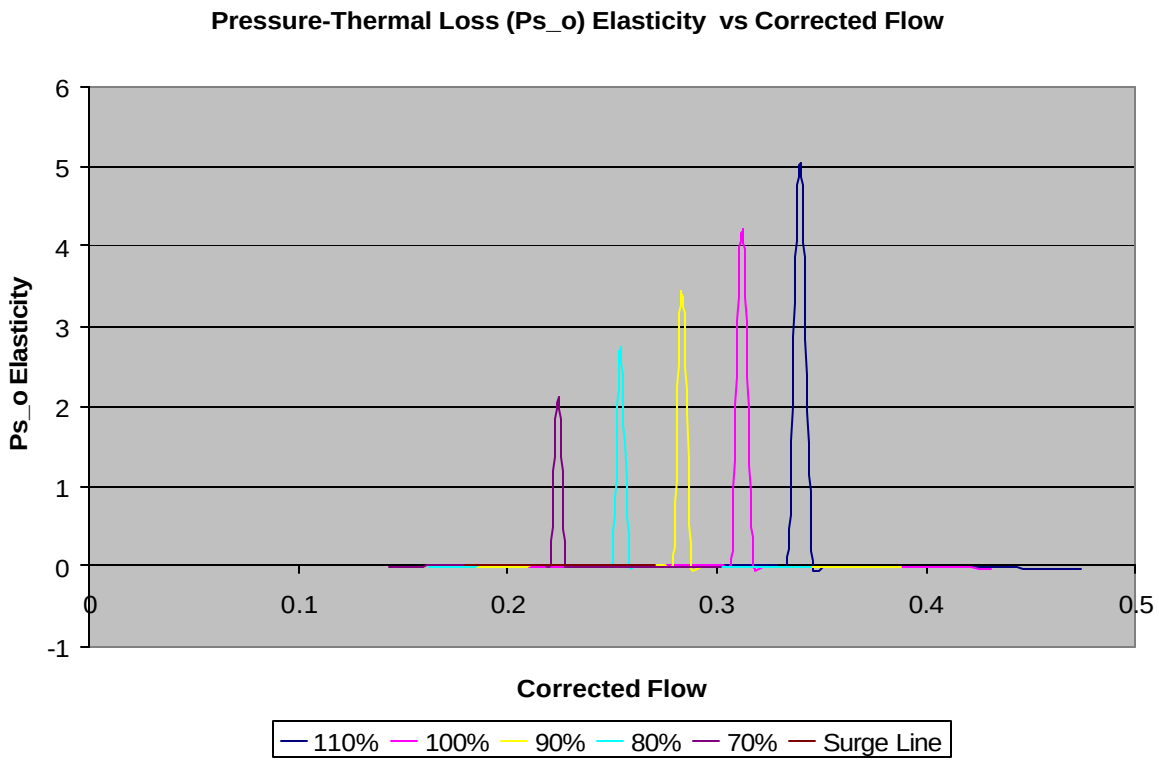

Fig. 5.7b Corrected Pressure-Thermal Loss Elasticity versus Corrected Flow of a MIT single-stage compressor at various speeds.

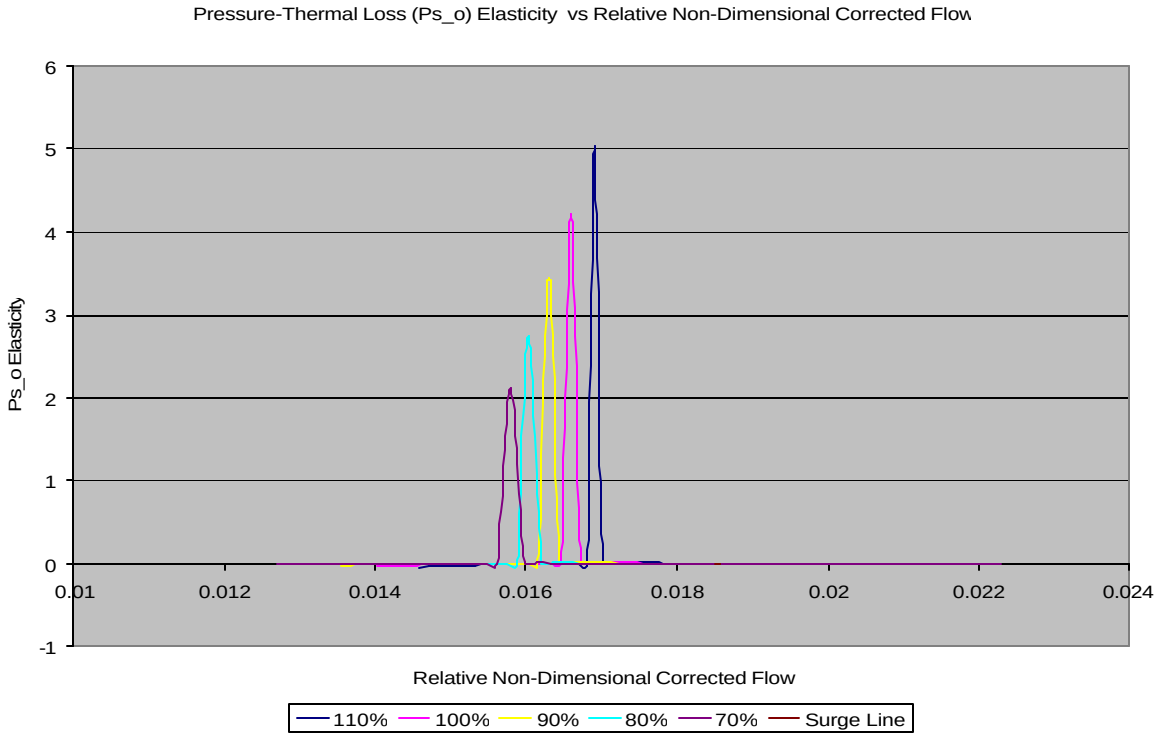

Fig. 5.7c Corrected Pressure-Thermal Loss Elasticity versus Relative Non-dimensional Corrected Flow of a MIT single-stage compressor at various speeds.

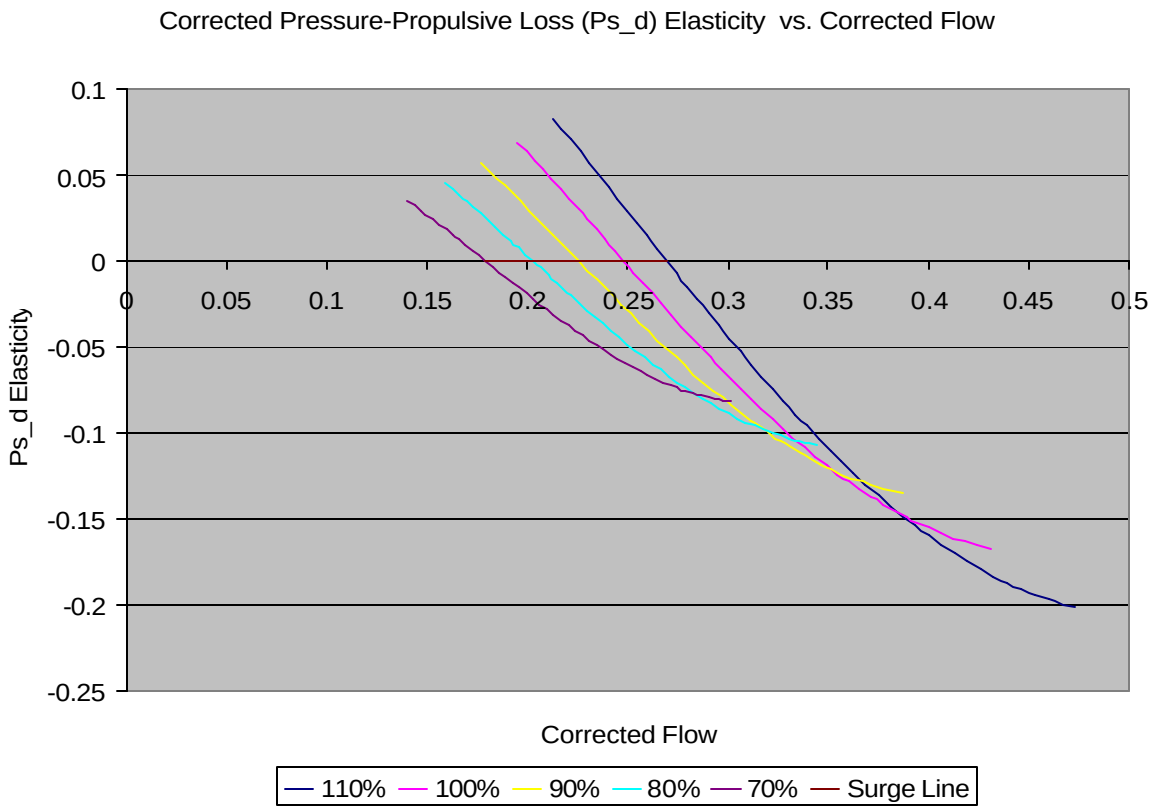

Fig. 5.7d Corrected Pressure-Propulsive Loss Elasticity versus Corrected Flow of a MIT single-stage compressor at various speeds.

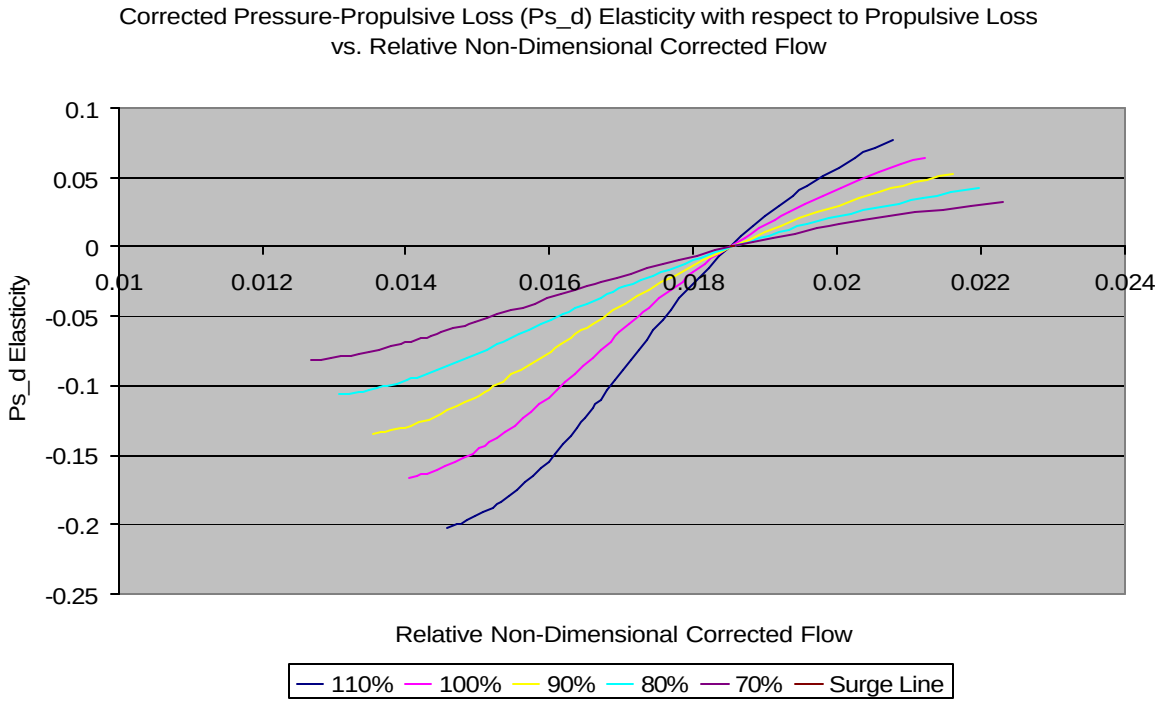

Fig. 5.7e Corrected Pressure-Propulsive Loss Elasticity versus Relative Non-Dimensional Corrected Flow of a MIT single-stage compressor at various speeds.

5.8 Corrected Specific Volume-Temperature (vT) Elasticity Elasticity *(see Appendix for basic elasticity derivation)*

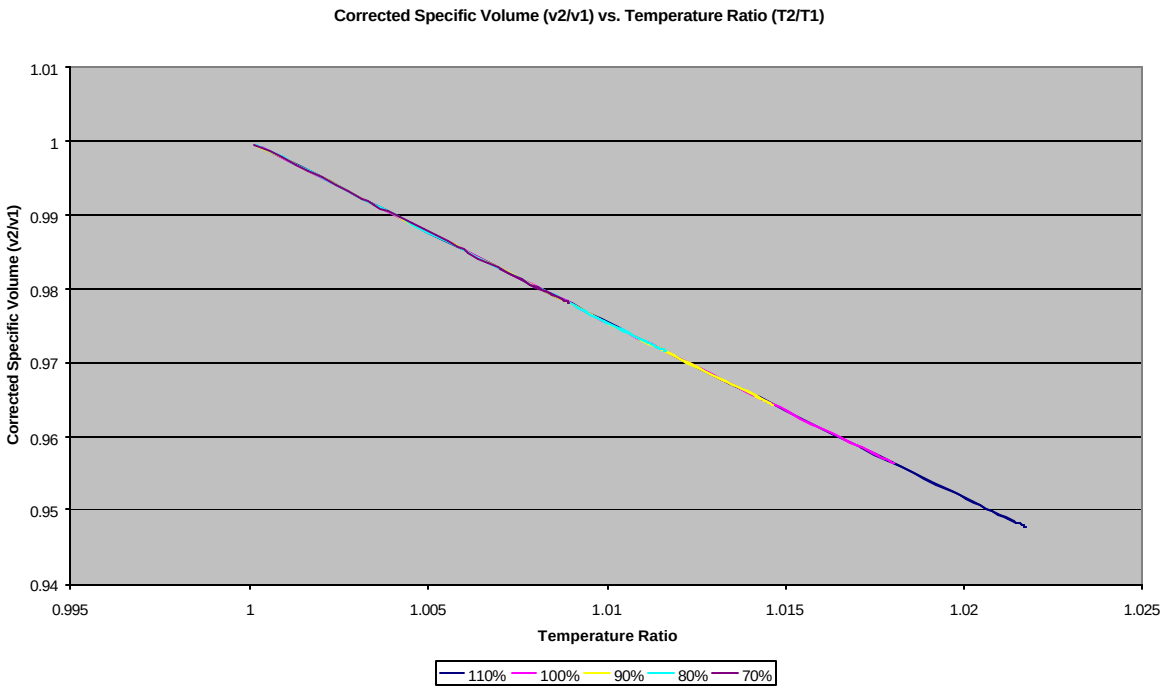

Fig. 5.8a Corrected Specifc Volume (v_2/v_1) versus Temperature Ratio (T_2/T_1) of a MIT single-stage compressor at various speeds.

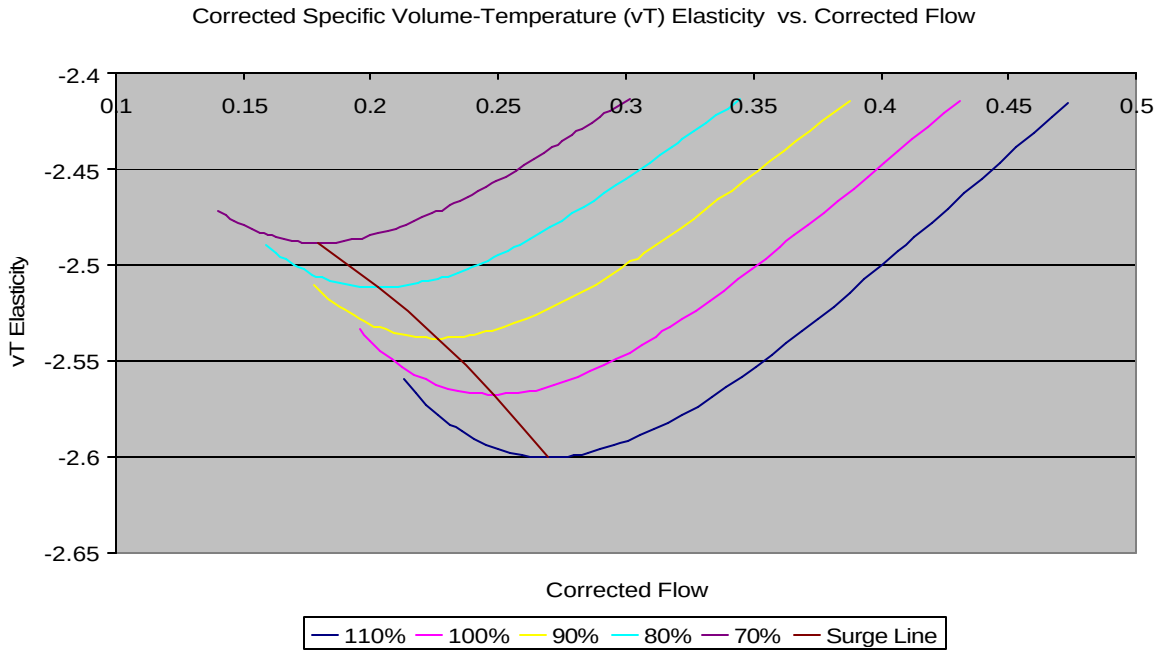

Fig. 5.8b Corrected Specifc Volume-Temperature Elasticity versus Corrected Flow of a MIT single-stage compressor at various speeds.

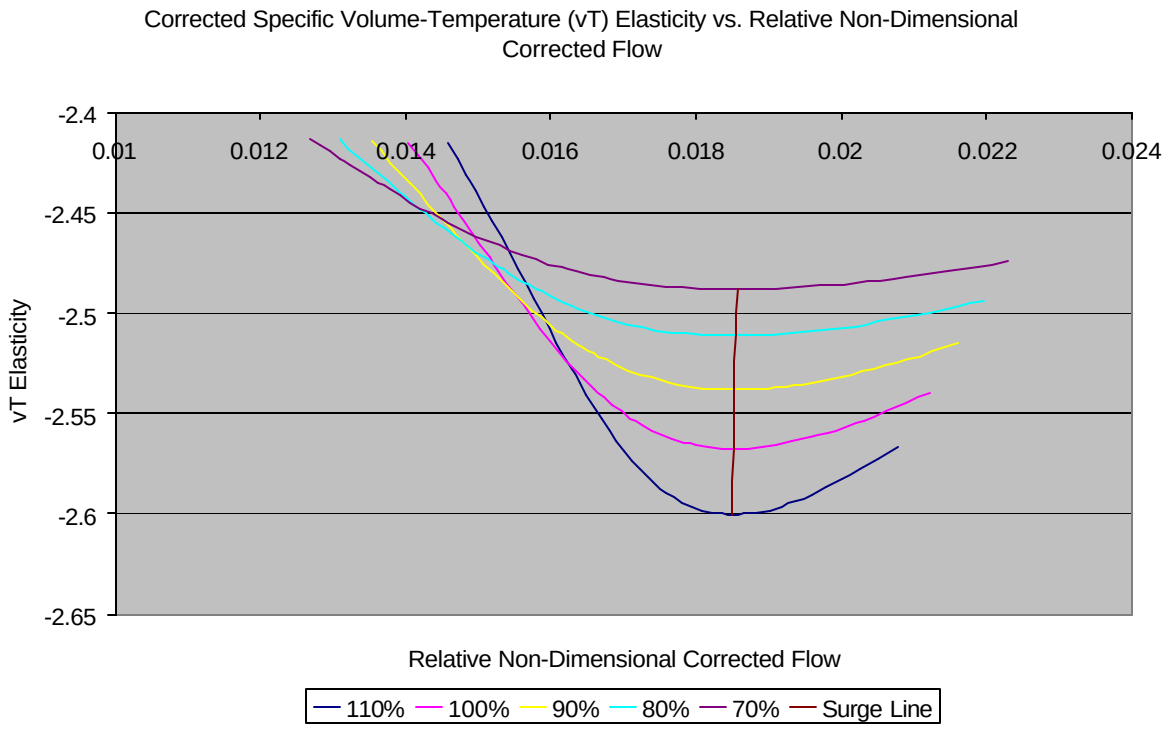

Fig. 5.8c Corrected Specifc Volume-Temperature Elasticity versus Non-dimensional Corrected Flow of a MIT single-stage compressor at various speeds.

5.9 Corrected Specific Volume-Loss (vs) Elasticity Elasticity *(see Appendix for basic elasticity derivation)*

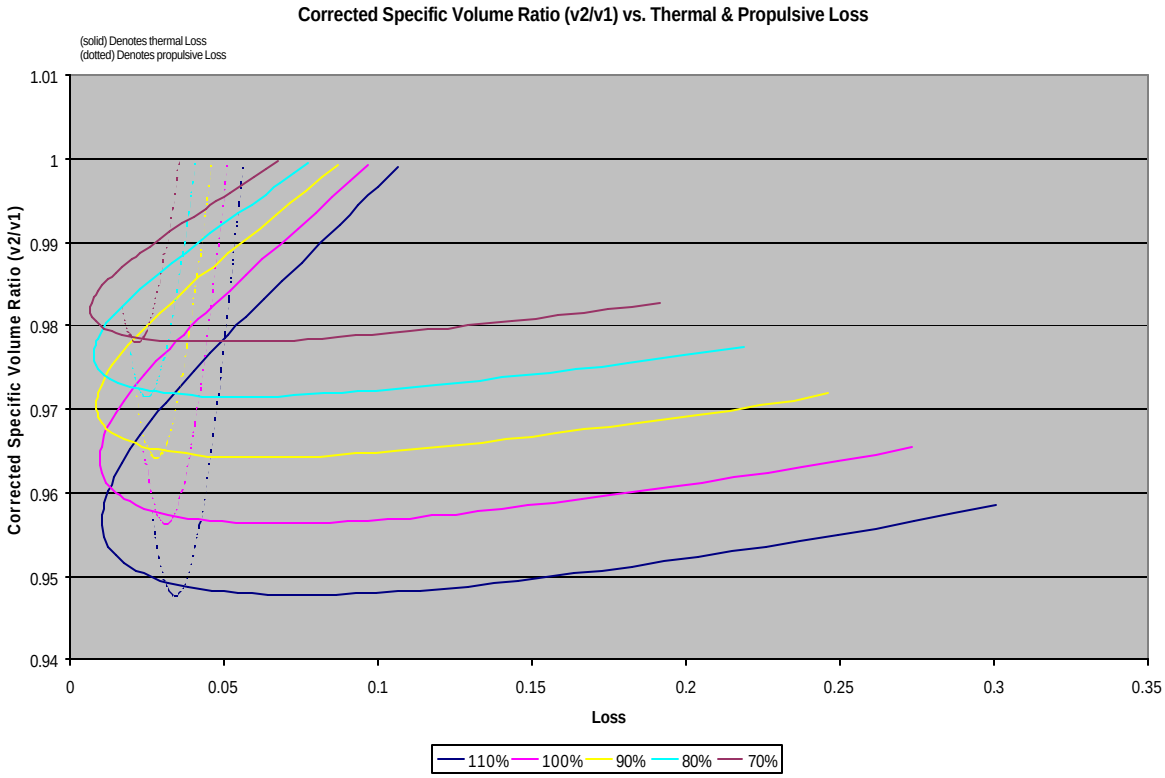

Fig. 5.9a Corrected Specific Volume Ratio (v2/v1) versus Thermal & Propulsive Loss of a MIT single-stage compressor at various speeds.

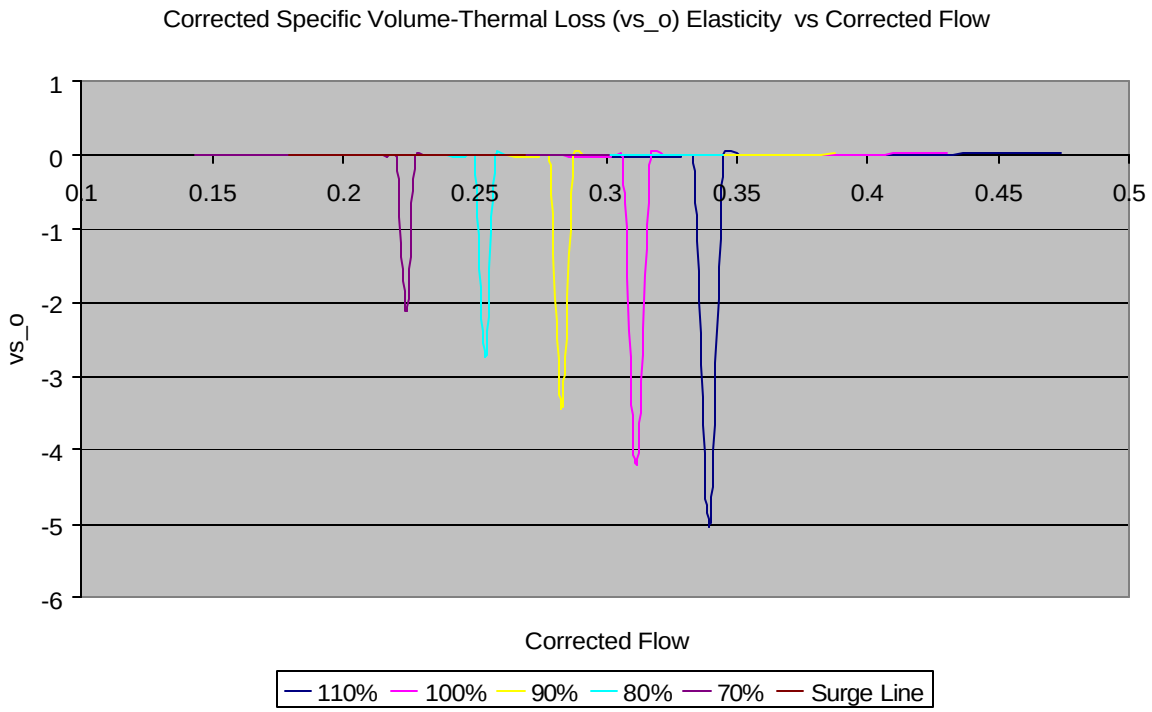

Fig. 5.9b Corrected Specific Volume–Thermal Loss Elasticity versus Corrected Flow of a MIT single-stage compressor at various speeds.

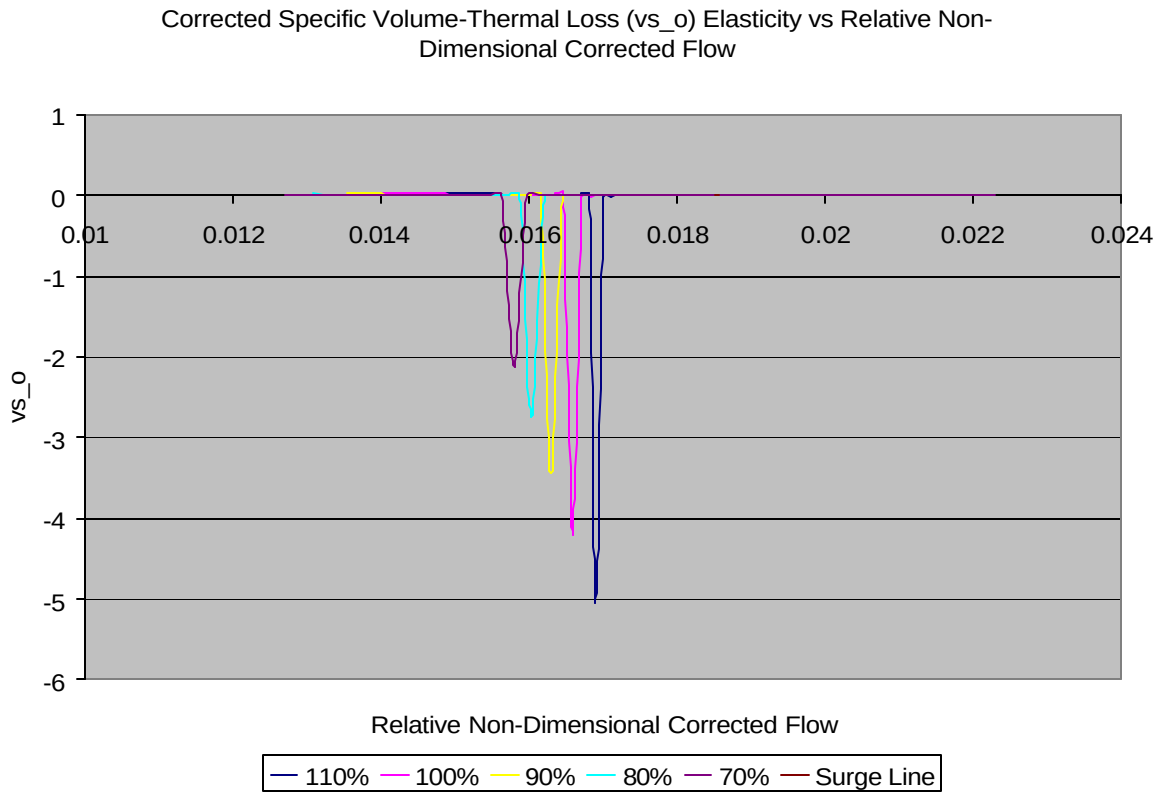

Fig. 5.9c Corrected Specific Volume–Thermal Loss Elasticity versus Relative Non-dimensional Corrected Flow of a MIT single-stage compressor at various speeds.

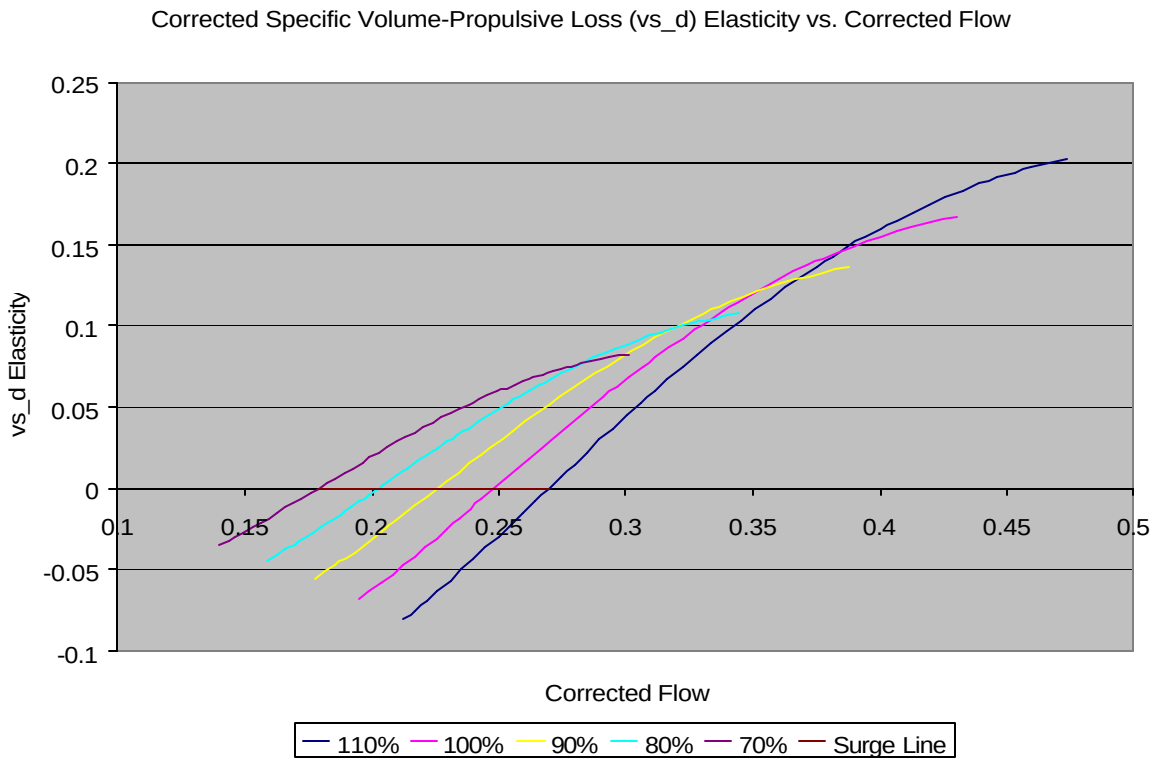

Fig. 5.9d Corrected Specific Volume–Propulsive Loss Elasticity versus Corrected Flow of a MIT single-stage compressor at various speeds.

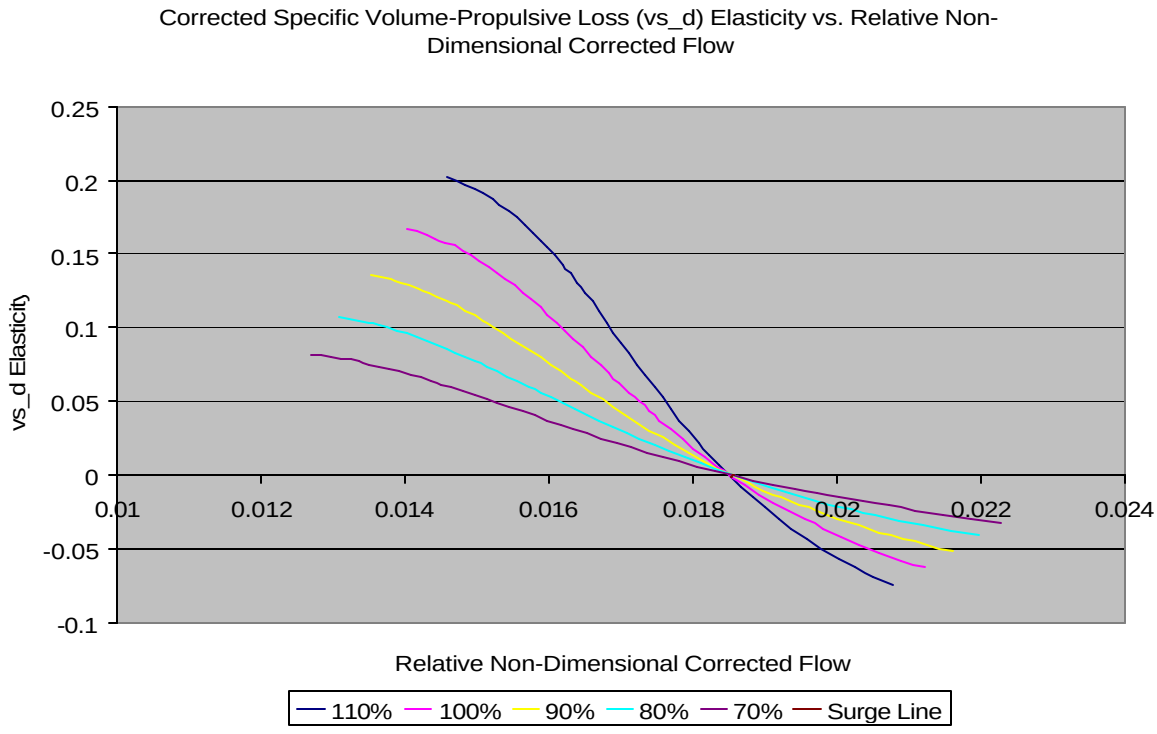

Fig. 5.9e Corrected Specific Volume–Propulsive Loss Elasticity versus Relative Non-dimensional Corrected Flow of a MIT single-stage compressor at various speeds.

5.10 Pumping and Aeroelastic Characteristics. Using the compressor map in *Section 5.1* the pumping characteristic of a gas generator can be determined. In a similar manner the aeroelastic characteristic with respect to density and flow can also be determined. The purpose of these characteristics is to reveal the changes that occur to certain quantities when the engine changes speed. The changes in corrected pressure ratio, corrected temperature ratio, and corrected flow were measured at stall. The changes in these quantities at maximum efficiency before and after stall were also compared.

5.10.1 Pumping Characteristic.

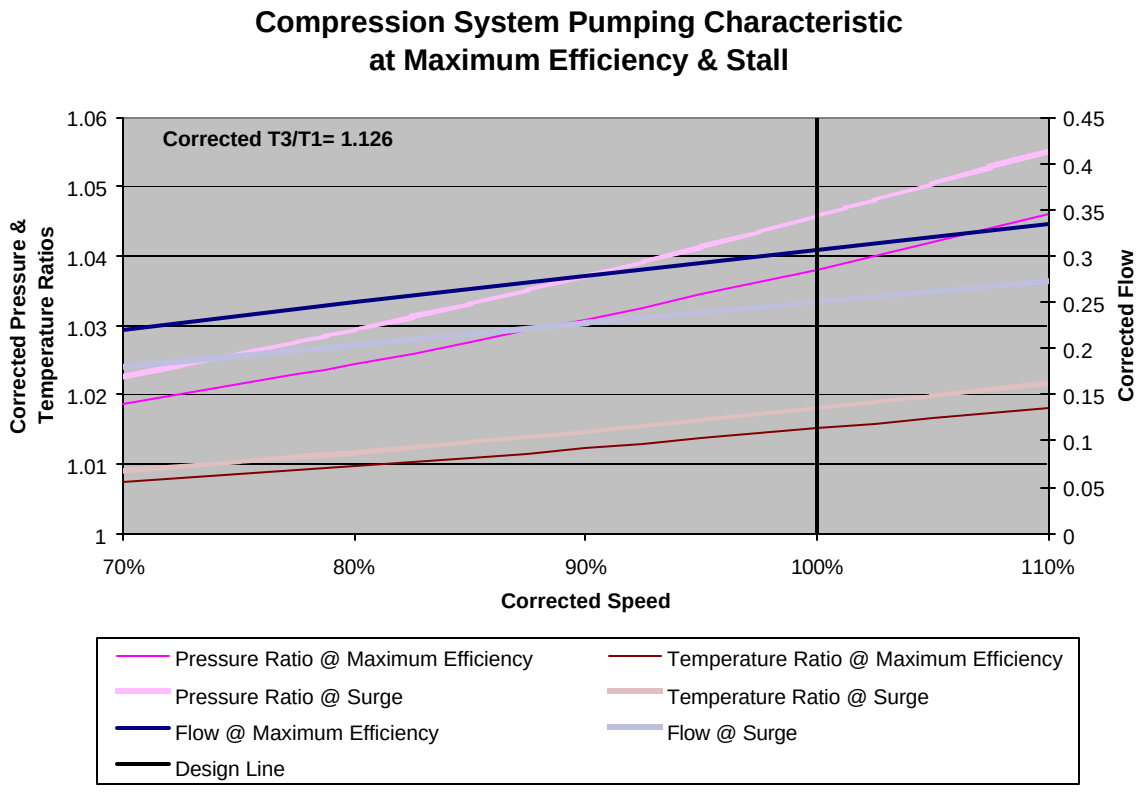

Fig. 5.10.1a Pumping Characteristic for a gas generator based on a MIT single-stage compressor.

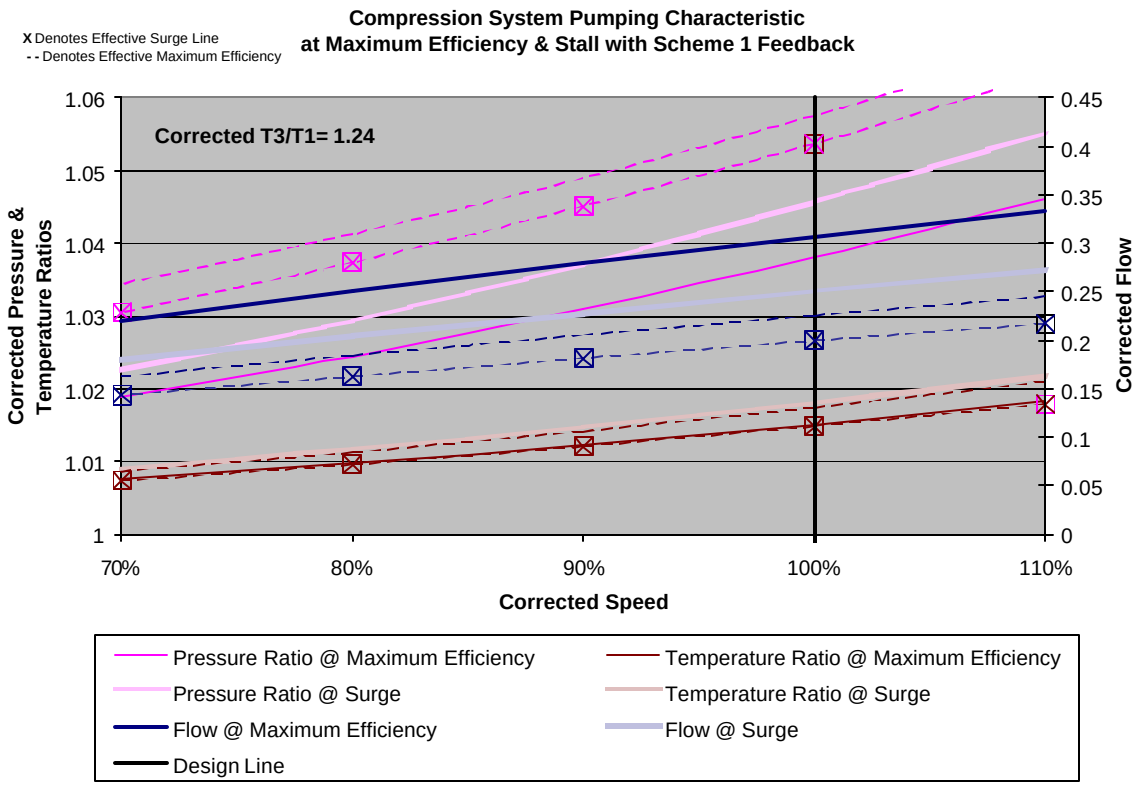

Fig. 5.10.1b Pumping Characteristic for a gas generator based on a MIT single-stage compressor with aeromechanical feedback .

5.10.2 Aeroelastic Characteristic.

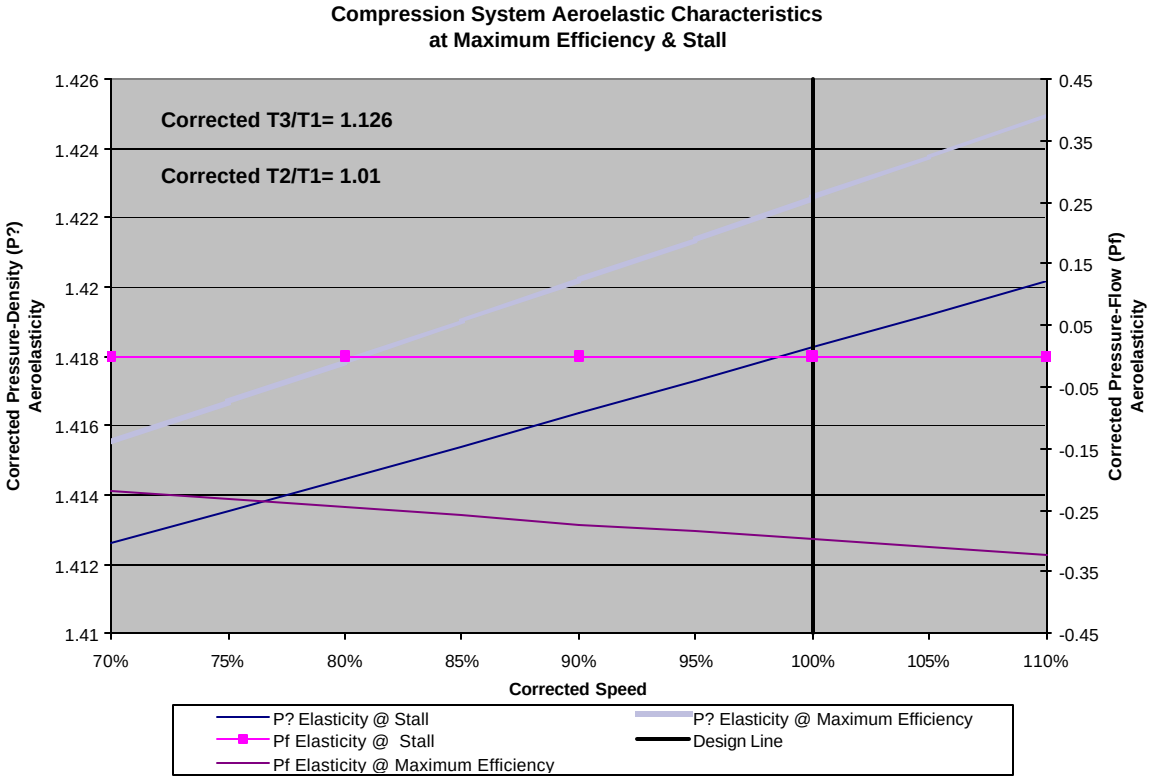

Fig. 5.10.2a Aeroelastic Characteristic for a gas generator based on a MIT single-stage compressor.

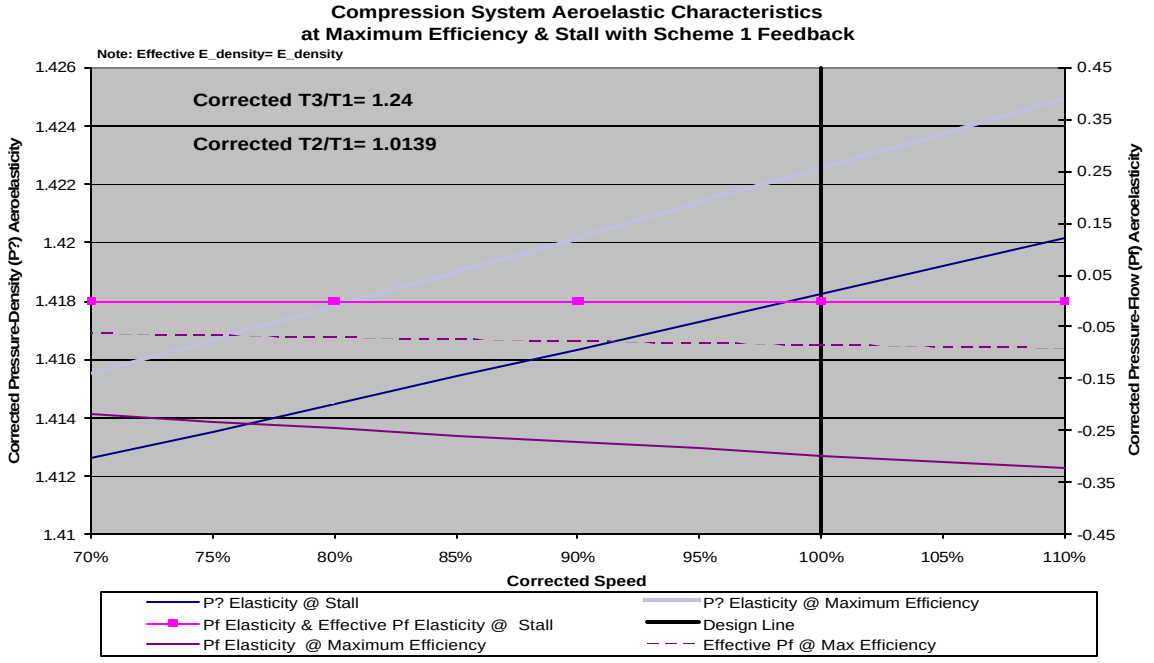

Fig. 5.10.2b Aeroelastic Characteristic for a gas generator based on a MIT single-stage compressor with aeromechanical feedback.

CHAPTER 6: Summary and Future Work

6.1 Summary

General methods were developed in this work to evaluate passive high-speed stabilization of two laboratory gas generator devices - the MIT single-stage and MIT three-stage compressors. A high-speed compressible rotating stall inception model was developed and compressible flow was analyzed along with the effects of changes in its thermodynamic properties. Ten passive stabilization schemes that could potentially be used by industry were discussed and examined in a high-speed compressible flow environment. The concept of elasticity was introduced and implemented to examine the effects of flow non-uniformity, entropic loss, and unsteadiness on thermodynamic state changes within the compression system. Finally, pumping and aeroelastic characteristics of these laboratory compressors both with and without feedback were analyzed.

6.1 Future Work

In the present research, we were able to answer two questions that lingered for high-speed aeroengine devices: (1) Are there high speed fluid-structural interactions associated flow non-uniformity, entropic loss, and unsteadiness, which can be avoided using tailored structural design to dynamically compensate compression systems through aeromechanical feedback passive control? (2) How do aeromechanical feedback dynamics combine with the pre-stall compressible fluid dynamics to postpone or induce the inception of high-speed rotating stall of aeroengine compressors? However, two additional questions still remain: (1) *What are other stabilization schemes associated with geometry, steady flow, fluidic compressibility, and operating performance of high-speed (compressible flow) compressors and engines in contrast to those fundamental to low-speed (incompressible flow) devices*? (2) *How do changes in the parameters that govern the pre-stall dynamics affect the stability of not only the compression system, but also the matching components (compressor, combustion, turbine) of the entire pumping system of the engine*?

It is proposed here that in addition to the ten aeromechanical schemes presented in the current research, other innovative aeromechanical schemes exist, through a careful sensitivity analysis on geometric, steady flow, fluidic compressibility, and operating performance parameters that can indeed inhibit the inception of rotating stall in high-speed engine devices. As a result, the stable operating range will be effectively extended, allowing higher performance operating conditions.

In order to achieve the goals presented in this proposal, a reduced-order model of fluid-structure interaction inside an axial compressor system used in modern aircraft engines has been devised. First, proof-of-concept schemes of innovative aeromechanical control technologies to describe how such feedback can be utilized to stabilize high-speed compressor stall of axial compressors, and how different tailored structural designs impact

high-speed compression system stability will be developed. Optimal structural parameters for these unique aeromechanical compensators will be determined to maximize the stable operating range of the high-speed compression system. The use of optimized aeromechanical feedback control to stabilize the system and extend the operating range will be discussed. The theoretical basis of additional control methods examined here will be evaluated under a compressible flow environment. To complete the evaluation of the aeromechanical control methodologies developed, a sensitivity analysis of the parameters that govern the pre-stall dynamics will be conducted. Thirteen input parameters are required in a high-speed compressor stall inception model, which include: geometry, steady flow values, fluidic compressibility, and overall performance slopes of the compressor device. Specifically these parameters are (Fréchette, 1997):

1. Geometry
    - axial chords (c_x/r_o)
    - stagger angles (g)
2. Steady flow values
    - inlet axial flow coeffient ($\bar{j}$)
    - inlet swirl angle ($\bar{a}_{in}$)
    - axial velocity ratios ($\frac{\bar{j}_2}{\bar{j}_1}$)
    - density ratios ($\frac{r_2}{r_1}$)
3. Overall compressor performance slopes
    - overall pressure rise sensitivity to inlet flow coefficient ($\frac{\partial \Psi_{ts}}{\partial j}$)
    - overall pressure rise sensitivity to inlet swirl angle ($\frac{\partial \Psi_{ts}}{\partial \tan a_{in}}$)
    - last blade row deviation sensitivity to inlet flow coefficient ($\frac{\partial \tan a_{ex}}{\partial j}$)

- last blade row deviation sensitivity to inlet swirl angle ($\frac{\partial \tan a_{ex}}{\partial \tan a_{in}}$)

4. Fluidic Compressibility Parameters
   - axial velocity-density ratio (AVDR)
   - axial momentum ratio (Y)
   - blade row continuity parameter (I_{br})

These parameters are all part of Fréchette's extended stability model which is:

$$s = \frac{TS_R - |n| Y \bar{j}^{-2} d_{I,ex}}{\left(\frac{AVDR + 1}{|n|} + m \right)}$$

where:

$$TS_R = \frac{\partial \Psi_{ts}}{\partial j} - \frac{\tan \bar{a}_{in}}{\partial \bar{j}} \frac{\partial \Psi_{ts}}{\partial \tan a_{in}}$$

$$d_{I,ex} = \frac{1}{|n| \bar{j}} \frac{\partial \tan a_{ex}}{\partial \tan a_{in}}$$

$$m = \left(\sum_{rotors+stators} \frac{c_x / r_o}{\cos^2 g} \right) I_{br} AVDR$$

$$AVDR = \frac{r_2 V_{x,2}}{r_1 V_{x,1}}$$

$$I_{br} = \frac{1 + \frac{V_{x,2}}{V_{x,1}}}{2}$$

$$Y = \frac{r_2}{r_1} \left(\frac{V_{x,2}}{V_{x,1}} \right)^2$$

Differentiating this extended stability equation with respect to each of these parameters results in the following:

1. Geometry

- axial chords (c_x/r_o)

$$\frac{\partial s}{\partial\left(c_x/r_o\right)} = -\frac{TS_R - |n|Y\bar{J}^2 d_{I,ex}}{\left(\frac{AVDR+1}{|n|}+m\right)^2}\left(\frac{AVDR}{\cos^2 g}\right)$$

- stagger angles (g)

$$\frac{\partial s}{\partial(g)} = \frac{TS_R - |n|Y\bar{J}^2 d_{I,ex}}{\left(\frac{AVDR+1}{|n|}+m\right)^2}\left(\frac{c_x/r_o}{\cos^2 g}\right) I_{br} AVDR$$

2. Steady flow values

- inlet axial flow coefficient ($\bar{J}$)

$$\frac{\partial s}{\partial(\bar{J})} = \frac{\left[\frac{\tan\bar{a}_{in}}{\bar{J}^2}\frac{\partial\Psi_{ts}}{\partial\tan a_{in}} - 2\bar{J}|n|Yd_{I,ex}\right]\left[\frac{AVDR+1}{|n|}+m\right]}{\left(\frac{AVDR+1}{|n|}+m\right)^2}$$

- inlet swirl angle ($\bar{a}_{in}$)

$$\frac{\partial s}{\partial(\tan a_{in})} = -\frac{\left[\frac{1}{\bar{J}}\frac{\partial\Psi_{ts}}{\partial\tan a_{in}}\right]}{\left(\frac{AVDR+1}{|n|}+m\right)}$$

- axial velocity ratios ($\frac{\bar{J}_2}{\bar{J}_1}$)

$$\frac{\partial s}{\partial\left(\bar{J}_2/\bar{J}_1\right)} = \frac{\left[-2\bar{J}^2|n|\left(\frac{\bar{J}_2}{\bar{J}_1}\right)d_{I,ex}\right]\left[\frac{AVDR+1}{|n|}+m\right] - \left[TS_R - |n|Y\bar{J}^2 d_{I,ex}\right]\left[\frac{r_2}{r_1}\right]\left[\frac{1}{|n|} + \frac{c_x/r_o}{\cos^2 g}\left(1/2 + \left(\frac{\bar{J}_2}{\bar{J}_1}\right)\right)\right]}{\left(\frac{AVDR+1}{|n|}+m\right)^2}$$

- density ratios ($\frac{r_2}{r_1}$)

$$\frac{\partial s}{\partial\left(r_2/r_1\right)} = \frac{\left[-|n|\left(\frac{\bar{J}_2}{\bar{J}_1}\right)^2 d_{I,ex}\right]\left[\frac{AVDR+1}{|n|}+m\right]-\left[TS_R-|n|Y\bar{J}^{-2}d_{I,ex}\right]\left[\frac{j_2}{j_1}\right]\left[\frac{1}{|n|}+\frac{c_x/r_o}{\cos^2 g}I_{br}\right]}{\left(\frac{AVDR+1}{|n|}+m\right)^2}$$

3. Overall performance slopes

   - overall pressure rise sensitivity to inlet flow coefficient ($\frac{\partial\Psi_{ts}}{\partial j}$)

$$\frac{\partial s}{\partial\left(\frac{\partial\Psi_{ts}}{\partial j}\right)} = \frac{1}{\left(\frac{AVDR+1}{|n|}+m\right)^2}$$

   - overall pressure rise sensitivity to inlet swirl angle ($\frac{\partial\Psi_{ts}}{\partial\tan a_{in}}$)

$$\frac{\partial s}{\partial\left(\frac{\partial\Psi_{ts}}{\partial\tan a_{in}}\right)} = -\frac{\frac{\tan a_{in}}{\bar{J}}}{\left(\frac{AVDR+1}{|n|}+m\right)}$$

   - last blade row deviation sensitivity to inlet flow coefficient ($\frac{\partial\tan a_{ex}}{\partial j}$)

$$\frac{\partial s}{\partial\left(\frac{\partial\tan a_{ex}}{\partial j}\right)} = 0$$

   - last blade row deviation sensitivity to inlet swirl angle ($\frac{\partial\tan a_{ex}}{\partial\tan a_{in}}$)

$$\frac{\partial s}{\partial\left(\frac{\partial\tan a_{ex}}{\partial\tan a_{in}}\right)} = -\frac{Y\bar{J}}{\left(\frac{AVDR+1}{|n|}+m\right)}$$

4. Fluidic Compressibility Parameters

   - axial velocity-density ratio (AVDR)

$$\frac{\partial s}{\partial(AVDR)} = \frac{-\left[TS_R - |n|\bar{Y}\bar{J}^{-2}d_{I,ex}\right]\left[\frac{1}{|n|} + \frac{c_x/r_o}{\cos^2 g} I_{br}\right]}{\left(\frac{AVDR+1}{|n|} + m\right)^2}$$

- axial momentum ratio (Y)

$$\frac{\partial s}{\partial(Y)} = -\frac{\left[|n|\bar{J}^{-2}d_{I,ex}\right]}{\left(\frac{AVDR+1}{|n|} + m\right)}$$

- blade row continuity parameter (I_{br})

$$\frac{\partial s}{\partial(I_{br})} = \frac{-\left[TS_R - |n|\bar{Y}\bar{J}^{-2}d_{I,ex}\right]\left[\frac{c_x/r_o}{\cos^2 g} AVDR\right]}{\left(\frac{AVDR+1}{|n|} + m\right)^2}$$

which is the basis for the sensitivity analysis posed.

References

Emmons, H.W., Pearson, C.E., and Grant, H.P., 1955, "Compressor Surge and Stall Propagation," *Trans. ASME*, 77, pp. 455-469.

Frechette, L.G., 1997, "Implications of Stability Modeling for High-Speed Axial Compressor Design," Master Thesis, Department of Aeronautics and Astronautics, M.I.T., Cambridge, MA.

Frechette, L.G., McGee, O.G., and Graf, M.B., 2004, "Tailored Structural Design and Aeromechanical Control of Axial Compressor Stall – Part II: Evaluation of Approaches," *ASME J. Turbomachinery*, 126, pp. 63-72.

Greitzer, E.M., 1976, "Surge and Rotating Stall in Axial Flow Compressors, Part I & II," *ASME J. Eng. Power*, 99, pp. 190-217.

Greitzer, E.M., 1980, "Review: Axial Compressor Stall Phenomenon," *ASME J. Fluids Eng.*, 102, pp. 134-151.

Greitzer, E.M., 1981, "The Stability of Pumping Systems, The 1980 Freeman Scholar Lecture," *ASME J. Fluids Eng*., 103, pp. 193-242.

Gresh, M. Theodore, 2001, "Compressor Performance: Aerodynamics for the User," Butterworth & Heinemann, Boston.

Gysling, D.L., and Greitzer, E.M., 1995, "Dynamic Control of Rotating Stall in Axial Flow Compressors Using Aeromechanical Feedback," *ASME J. Turbomachinery*, 117, pp. 307-319.

Haynes, J.M., Hendricks, G.J., and Epstein, A.H., 1994, "Active Stabilization of Rotating Stall in a Three-Stage Axial Compressor, "*ASME J. Turbomachinery*, 116, pp. 226-239.

McGee, O.G., Graf, M.B., and Frechette, L.G., 2004, "Tailored Structural Design and Aeromechanical Control of Axial Compressor Stall – Part I: Development of Models and Metrics, *ASME J. Turbomachinery*, 126, pp. 63-72.

McGee, O.G. and Coleman, K.L., 2006a, "Aeromechanical Control of High-Speed Axial Compressor Stall and Engine Performance– Part I: Development of Models, to be submitted, *ASME J. Turbomachinery*.

Coleman, K.L. and McGee, O.G., 2006b, "Aeromechanical Control of High-Speed Axial Compressor Stall and Engine Performance– Part II: Evaluation of Approaches, to be submitted, *ASME J. Turbomachinery*.

APPENDIX

A.1 Introduction

This appendix contains the formulation of the elasticity concept and the results of the nonlinear measured high-speed compression system dynamics for the MIT single-stage and MIT three-stage compressor for schemes #1-#8 and schemes #1-#10 (including the open-loop problem), respectively.

A.2 Basic Elasticity Formulation

Step 1: Begin with a relationship between two quantities, X and Y.

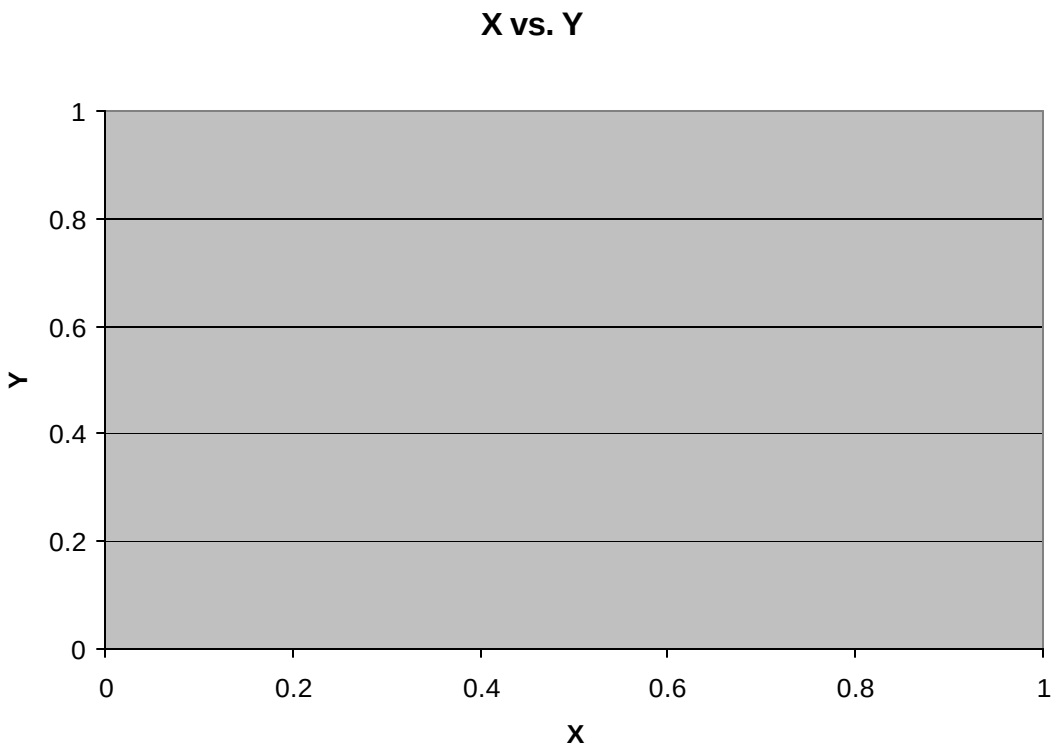

Fig. A.2 Plot of the relationship between X and Y.

Step 2: Find the slope, m, of the XY relationship.

$$m = \frac{\Delta Y}{\Delta X}$$

Step 3: Multiply the slope at point (X,Y) by the X to Y ratio at that point to obtain a cross-elasticity measure .

$$YX_{\,elasticity} = m\left(\frac{X}{Y}\right)$$

A.3 Additional Nonlinear Measured High Speed Compression System Dynamics

MIT 1 Scheme 2

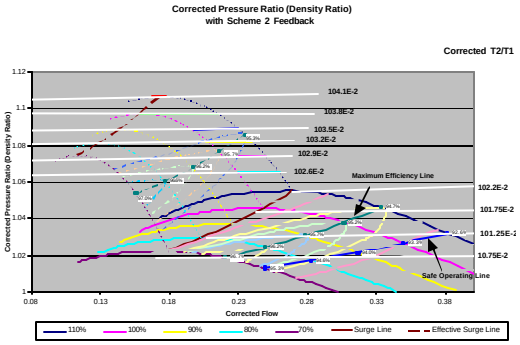

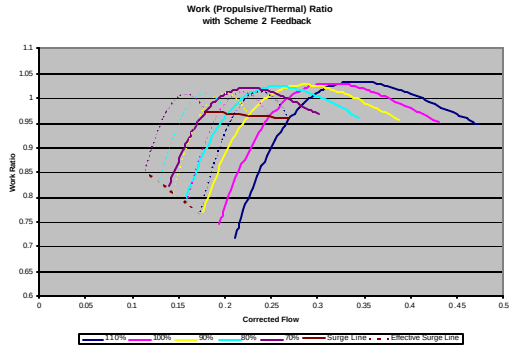

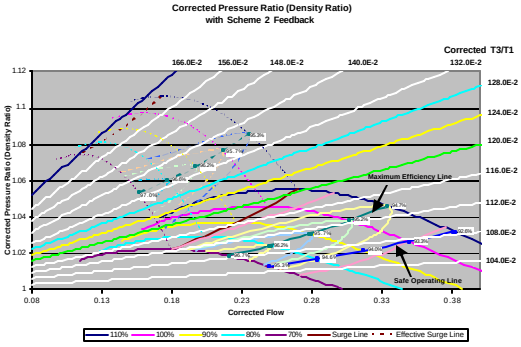

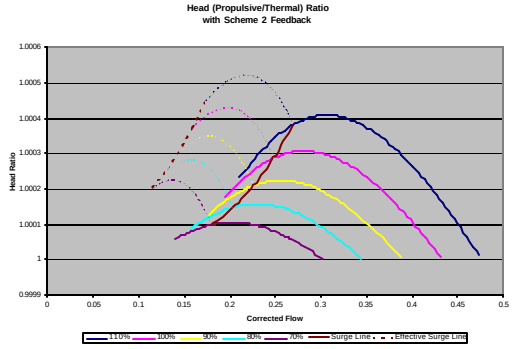

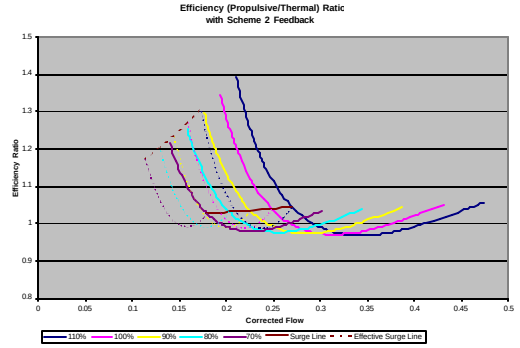

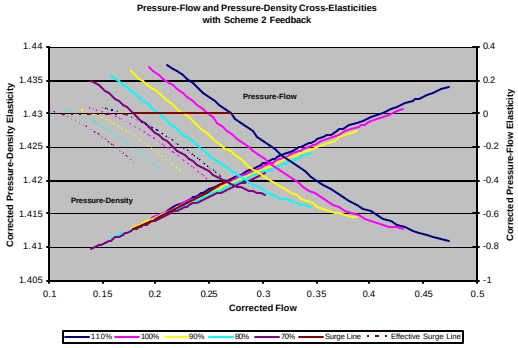

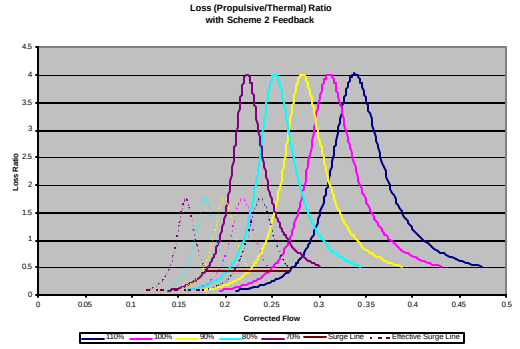

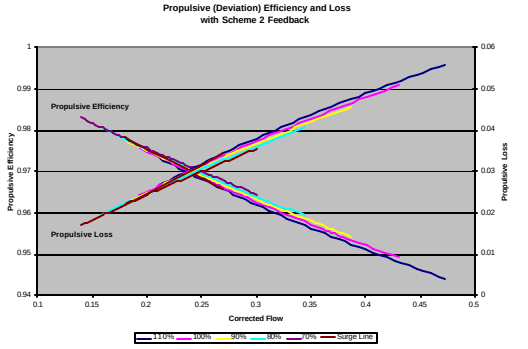

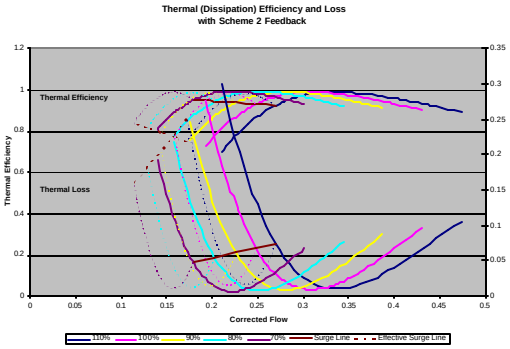
Thermal (Dissipation) Efficiency and Loss
with Scheme 2 Feedback
Thermal Efficiency
Thermal Loss
Thermal Efficiency
Corrected Flow
110%
100%
90%
80%
70%
Surge Line
Effective Surge Line

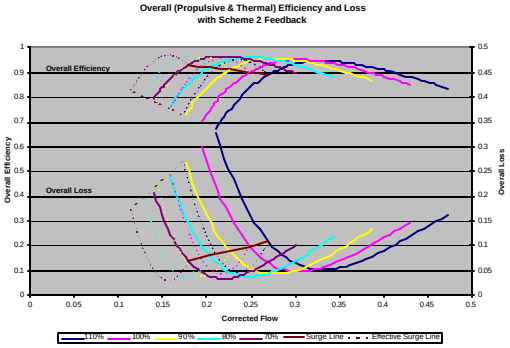
Overall (Propulsive & Thermal) Efficiency and Loss
with Scheme 2 Feedback
Overall Efficiency
Overall Loss
Overall Efficiency
Overall Loss
Corrected Flow
110%
100%
90%
80%
70%
Surge Line
Effective Surge Line

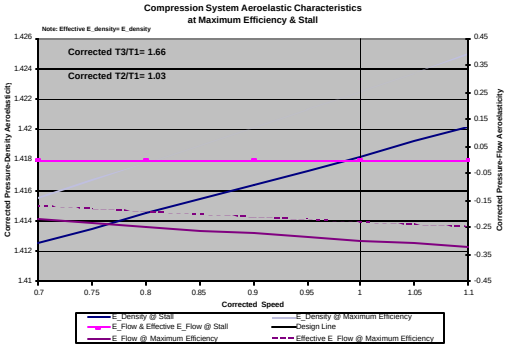
Compression System Aeroelastic Characteristics
at Maximum Efficiency & Stall
Note: Effective E_density= E_density
Corrected T3/T1= 1.66
Corrected T2/T1= 1.03
Corrected Pressure-Density Aeroelasticity
Corrected Pressure-Flow Aeroelasticity
Corrected Speed
E_Density @ Stall
E_Density @ Maximum Efficiency
E_Flow & Effective E_Flow @ Stall
Design Line
E_Flow @ Maximum Efficiency
Effective E_Flow @ Maximum Efficiency

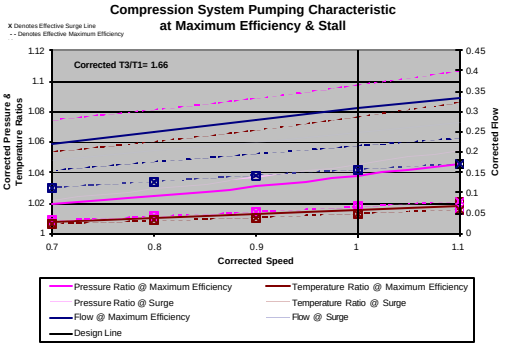
Compression System Pumping Characteristic
at Maximum Efficiency & Stall
X Denotes Effective Surge Line
- - Denotes Effective Maximum Efficiency
Corrected T3/T1= 1.66
Corrected Pressure & Temperature Ratios
Corrected Flow
Corrected Speed
Pressure Ratio @ Maximum Efficiency
Temperature Ratio @ Maximum Efficiency
Pressure Ratio @ Surge
Temperature Ratio @ Surge
Flow @ Maximum Efficiency
Flow @ Surge
Design Line

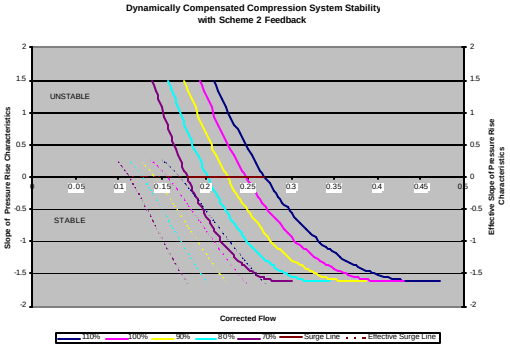
Dynamically Compensated Compression System Stability
with Scheme 2 Feedback
UNSTABLE
STABLE
Slope of Pressure Rise Characteristics
Effective Slope of Pressure Rise Characteristics
Corrected Flow
110%
100%
90%
80%
70%
Surge Line
Effective Surge Line

MIT 1 Scheme 3

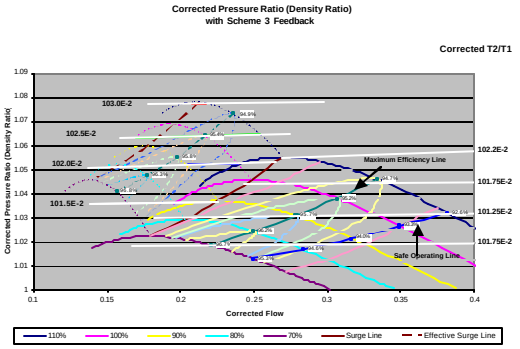

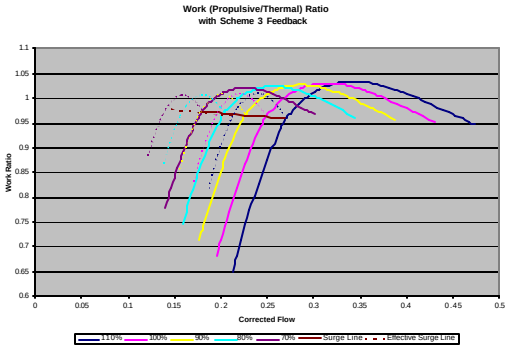

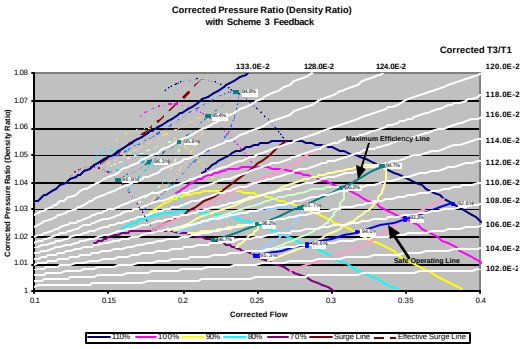

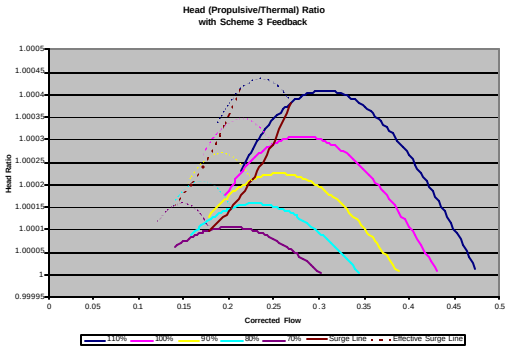

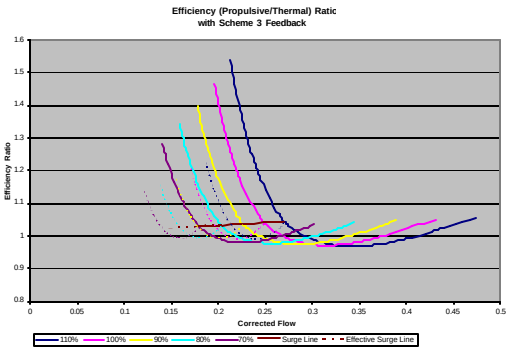

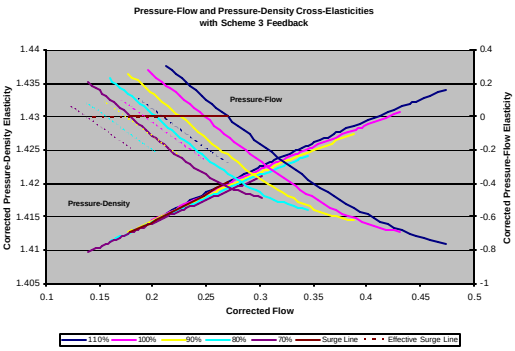

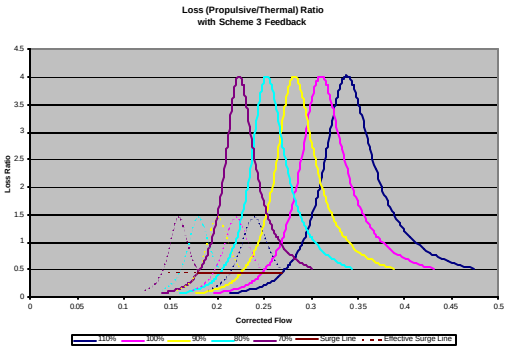

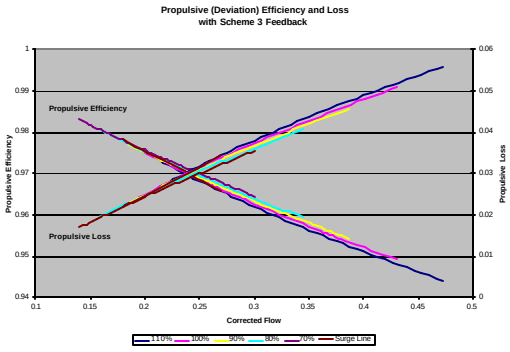

Thermal (Dissipation) Efficiency and Loss with Scheme 3 Feedback

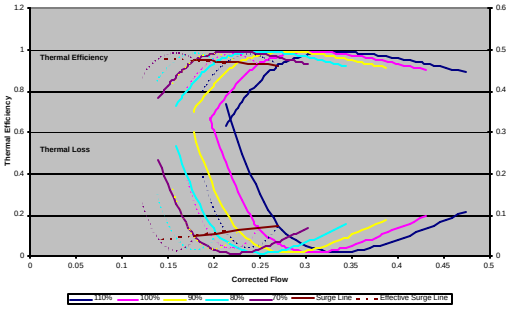

Overall (Propulsive & Thermal) Efficiency and Loss with Scheme 3 Feedback

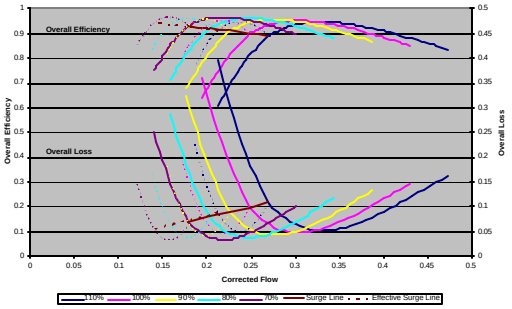

Compression System Aeroelastic Characteristics at Maximum Efficiency & Stall

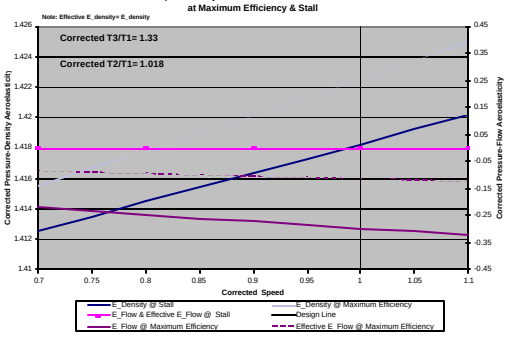

Compression System Pumping Characteristic at Maximum Efficiency & Stall

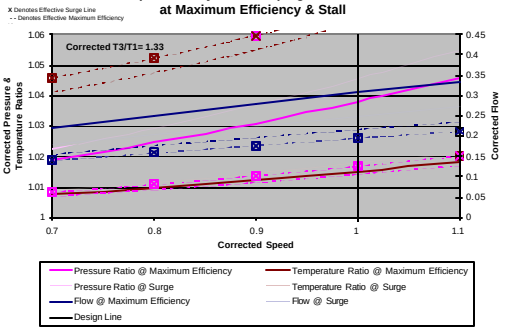

Dynamically Compensated Compression System Stability with Scheme 3 Feedback

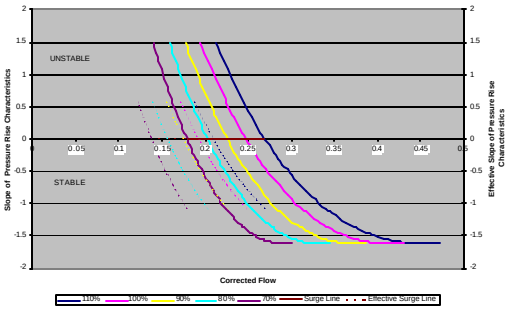

MIT 1 Scheme 4

Corrected Pressure Ratio (Density Ratio) with Scheme 4 Feedback

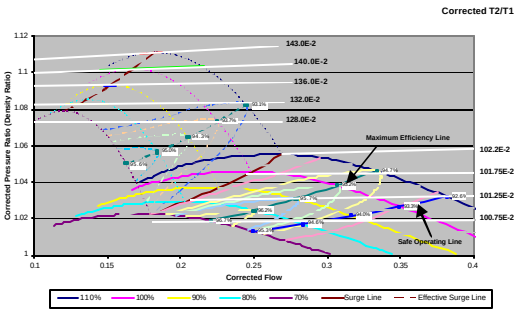

Work (Propulsive/Thermal) Ratio with Scheme 4 Feedback

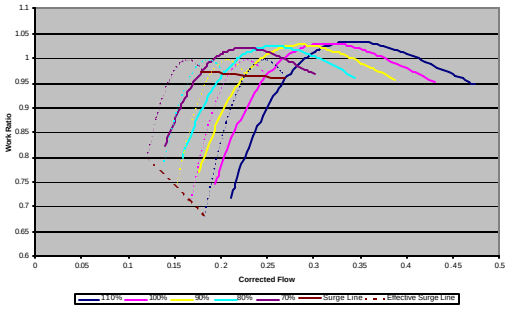

Corrected Pressure Ratio (Density Ratio) with Scheme 4 Feedback

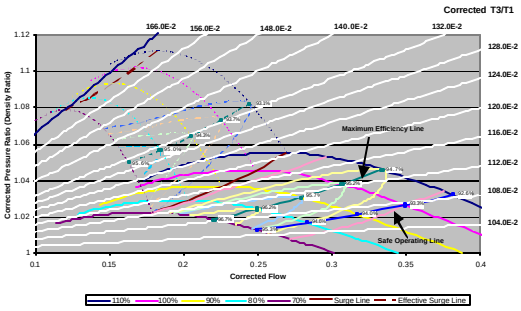

Head (Propulsive/Thermal) Ratio with Scheme 4 Feedback

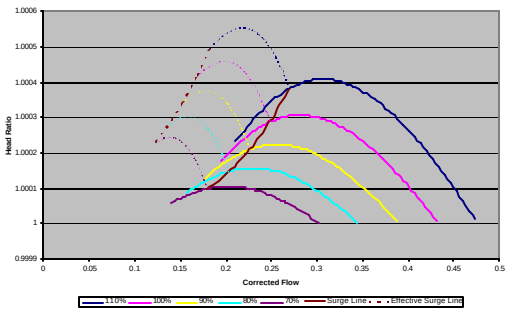

Efficiency (Propulsive/Thermal) Ratic with Scheme 4 Feedback

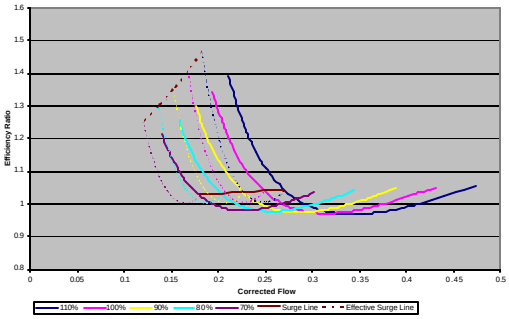

Pressure-Flow and Pressure-Density Cross-Elasticities with Scheme 4 Feedback

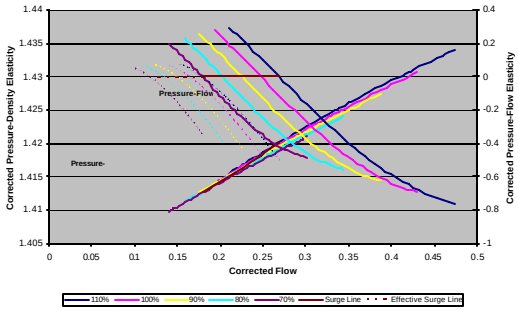

Loss (Propulsive/Thermal) Ratio with Scheme 4 Feedback

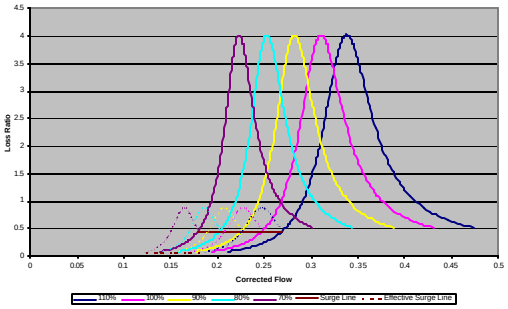

Propulsive (Deviation) Efficiency and Loss with Scheme 4 Feedback

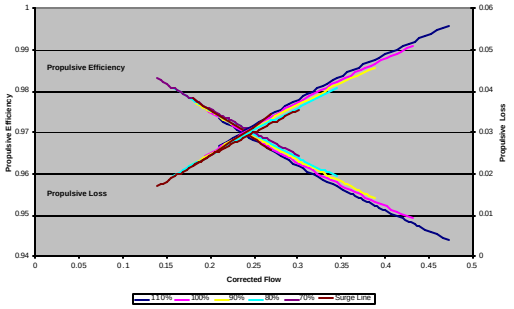

Thermal (Dissipation) Efficiency and Loss with Scheme 4 Feedback

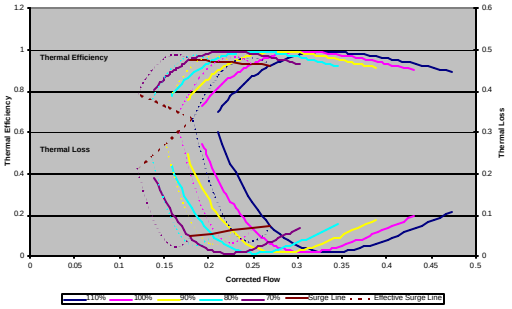

Overall (Propulsive & Thermal) Efficiency and Loss with Scheme 4 Feedback

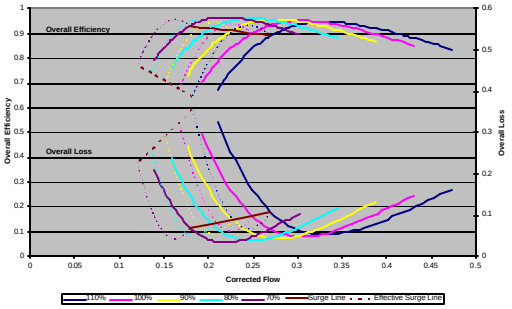

Compression System Aeroelastic Characteristics at Maximum Efficiency & Stall

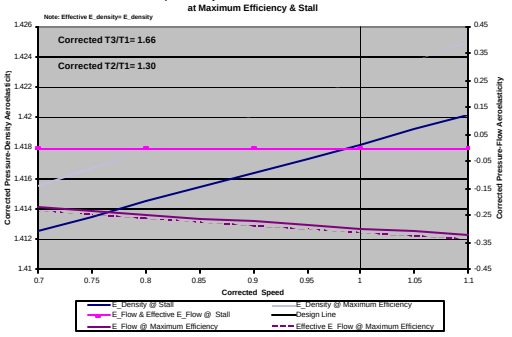

Compression System Pumping Characteristic at Maximum Efficiency & Stall

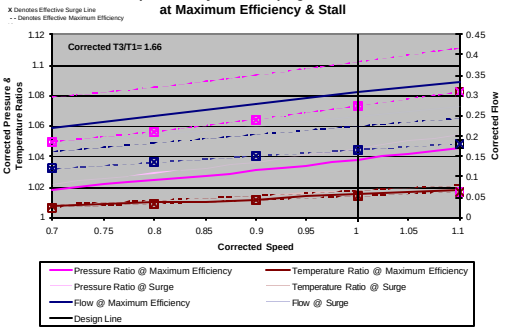

Dynamically Compensated Compression System Stability with Scheme 4 Feedback

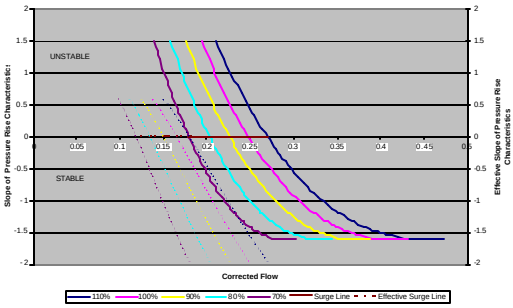

MIT 1 Scheme 5

Corrected Pressure Ratio (Density Ratio)
with Scheme 5 Feedback

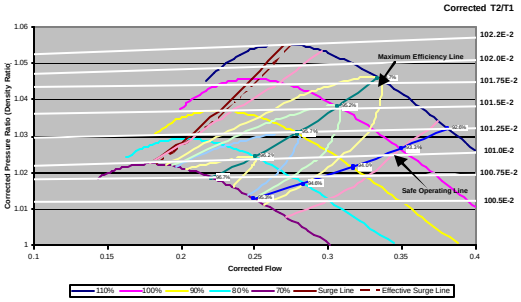

Work (Propulsive/Thermal) Ratio
with Scheme 5 Feedback

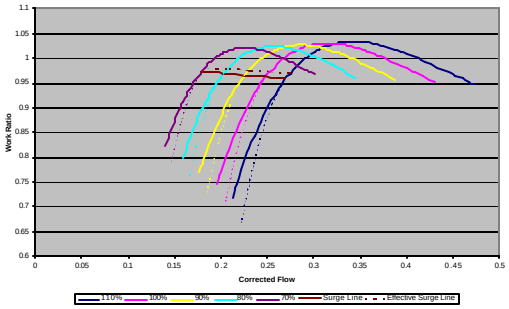

Corrected Pressure Ratio (Density Ratio)
with Scheme 5 Feedback

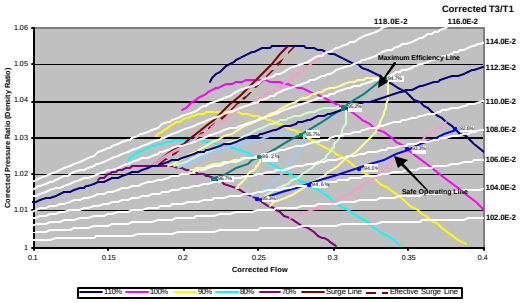

Head (Propulsive/Thermal) Ratio
with Scheme 5 Feedback

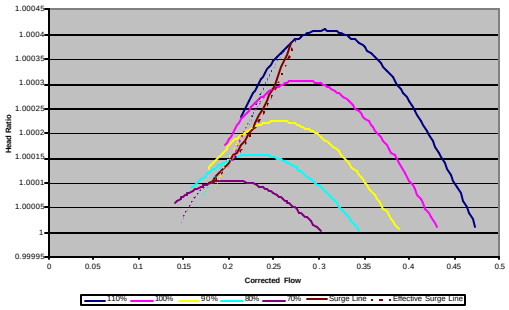

Efficiency (Propulsive/Thermal) Ratic
with Scheme 5 Feedback

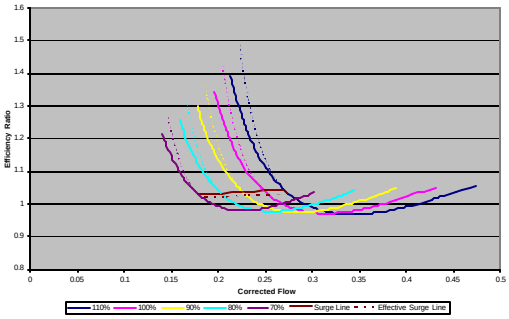

Pressure-Flow and Pressure-Density Cross-Elasticities
with Scheme 5 Feedback

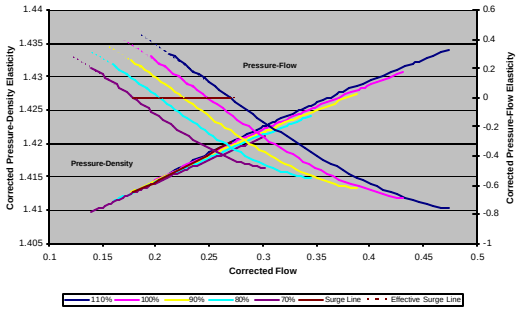

Loss (Propulsive/Thermal) Ratio
with Scheme 5 Feedback

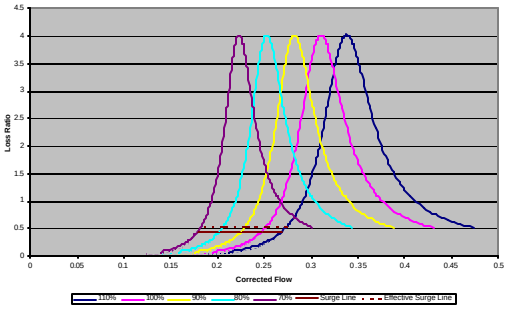

Propulsive (Deviation) Efficiency and Loss
with Scheme 5 Feedback

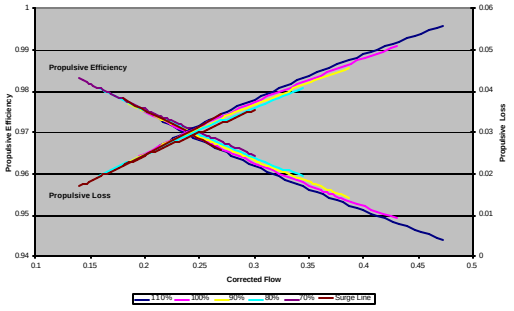

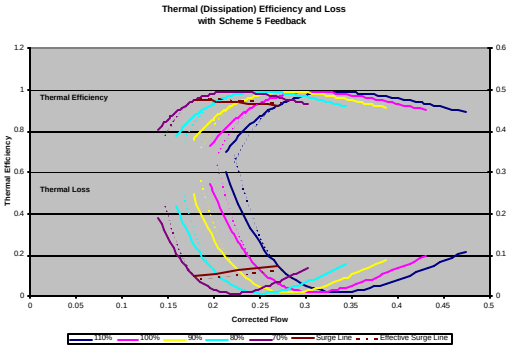
Thermal (Dissipation) Efficiency and Loss
with Scheme 5 Feedback
Thermal Efficiency
Thermal Loss
Thermal Efficiency
Corrected Flow
110%
100%
90%
80%
70%
Surge Line
Effective Surge Line

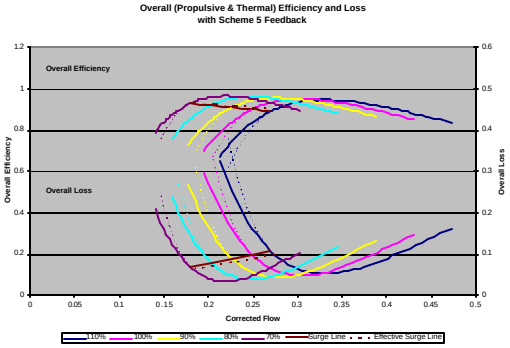
Overall (Propulsive & Thermal) Efficiency and Loss
with Scheme 5 Feedback
Overall Efficiency
Overall Loss
Overall Efficiency
Overall Loss
Corrected Flow
110%
100%
90%
80%
70%
Surge Line
Effective Surge Line

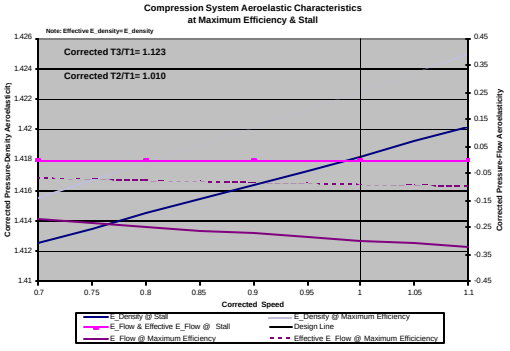
Compression System Aeroelastic Characteristics
at Maximum Efficiency & Stall
Note: Effective E_density=E_density
Corrected T3/T1= 1.123
Corrected T2/T1= 1.010
Corrected Pressure-Density Aeroelasticity
Corrected Pressure-Flow Aeroelasticity
Corrected Speed
E_Density @ Stall
E_Density @ Maximum Efficiency
E_Flow & Effective E_Flow @ Stall
Design Line
E_Flow @ Maximum Efficiency
Effective E_Flow @ Maximum Efficiency

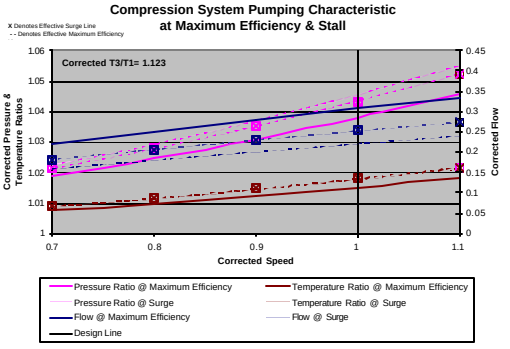
Compression System Pumping Characteristic
at Maximum Efficiency & Stall
X Denotes Effective Surge Line
- - Denotes Effective Maximum Efficiency
Corrected T3/T1= 1.123
Corrected Pressure & Temperature Ratios
Corrected Flow
Corrected Speed
Pressure Ratio @ Maximum Efficiency
Temperature Ratio @ Maximum Efficiency
Pressure Ratio @ Surge
Temperature Ratio @ Surge
Flow @ Maximum Efficiency
Flow @ Surge
Design Line

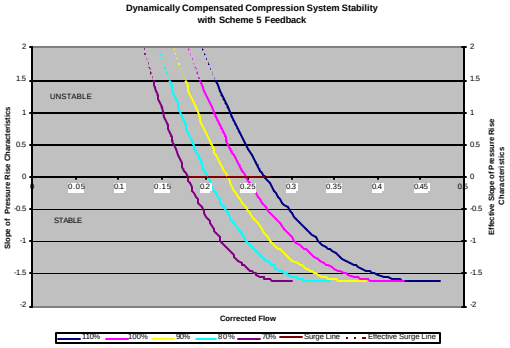
Dynamically Compensated Compression System Stability
with Scheme 5 Feedback
UNSTABLE
STABLE
Slope of Pressure Rise Characteristics
Effective Slope of Pressure Rise Characteristics
Corrected Flow
110%
100%
90%
80%
70%
Surge Line
Effective Surge Line

MIT 1 Scheme 6

Corrected Pressure Ratio (Density Ratio)
with Scheme 6 Feedback

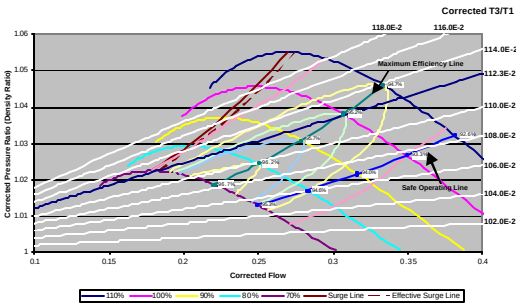

Head (Propulsive/Thermal) Ratio
with Scheme 6 Feedback

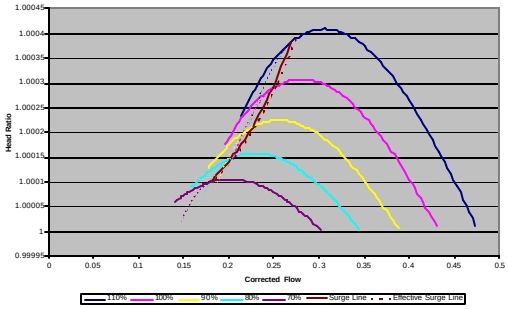

Efficiency (Propulsive/Thermal) Ratic
with Scheme 6 Feedback

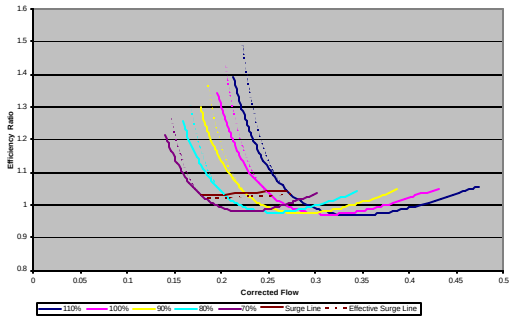

Pressure-Flow and Pressure-Density Cross-Elasticities
with Scheme 6 Feedback

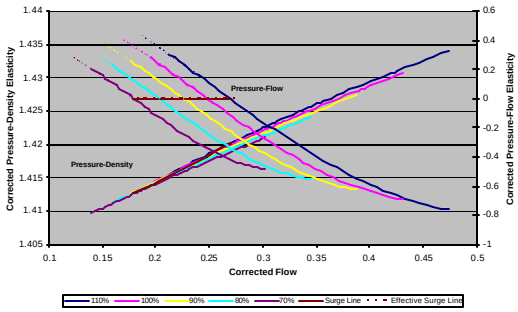

Loss (Propulsive/Thermal) Ratio
with Scheme 6 Feedback

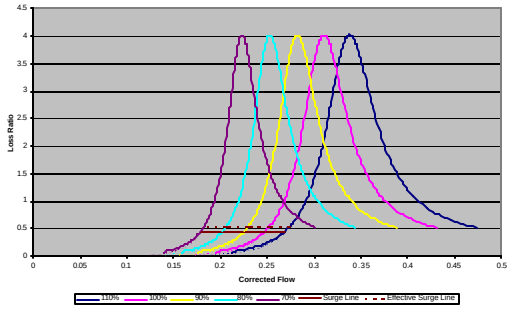

Propulsive (Deviation) Efficiency and Loss
with Scheme 6 Feedback

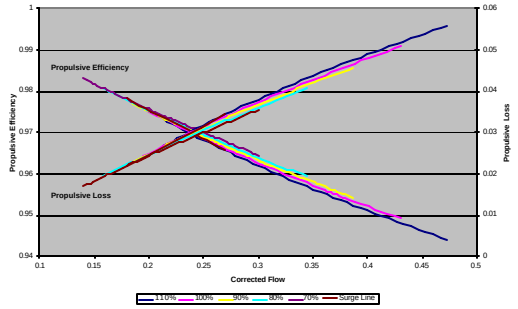

Work (Propulsive/Thermal) Ratio
with Scheme 6 Feedback

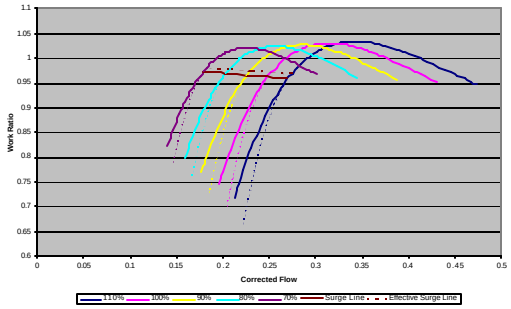

Thermal (Dissipation) Efficiency and Loss
with Scheme 6 Feedback

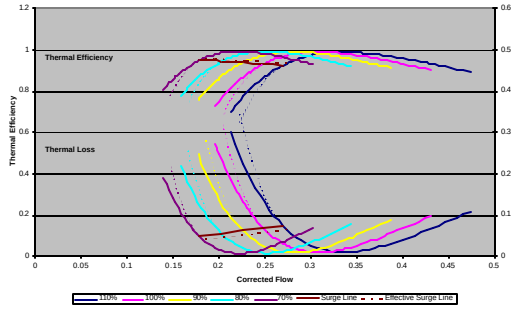

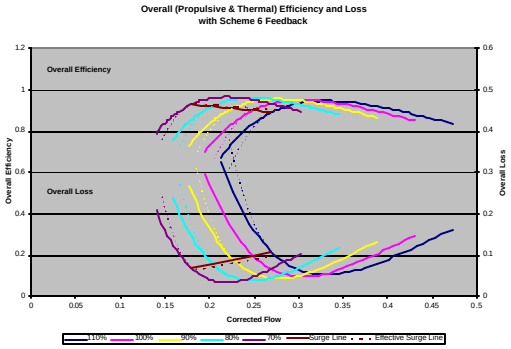
Overall (Propulsive & Thermal) Efficiency and Loss
with Scheme 6 Feedback
Overall Efficiency
Overall Loss
Overall Efficiency
Overall Loss
Corrected Flow
110%
100%
90%
80%
70%
Surge Line
Effective Surge Line

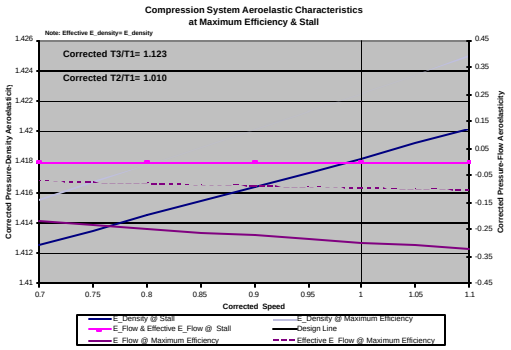
Compression System Aeroelastic Characteristics
at Maximum Efficiency & Stall
Note: Effective E_density= E_density
Corrected T3/T1= 1.123
Corrected T2/T1= 1.010
Corrected Pressure-Density Aeroelasticity
Corrected Pressure-Flow Aeroelasticity
Corrected Speed
E_Density @ Stall
E_Density @ Maximum Efficiency
E_Flow & Effective E_Flow @ Stall
Design Line
E_Flow @ Maximum Efficiency
Effective E_Flow @ Maximum Efficiency

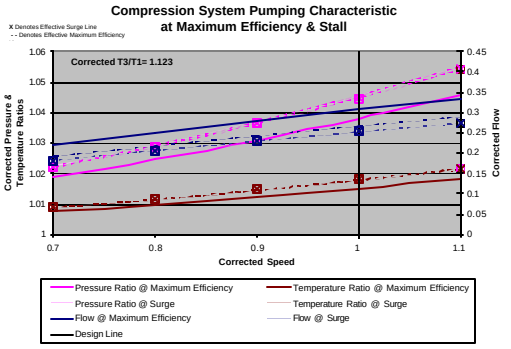
Compression System Pumping Characteristic
at Maximum Efficiency & Stall
X Denotes Effective Surge Line
- - Denotes Effective Maximum Efficiency
Corrected T3/T1= 1.123
Corrected Pressure &
Temperature Ratios
Corrected Flow
Corrected Speed
Pressure Ratio @ Maximum Efficiency
Temperature Ratio @ Maximum Efficiency
Pressure Ratio @ Surge
Temperature Ratio @ Surge
Flow @ Maximum Efficiency
Flow @ Surge
Design Line

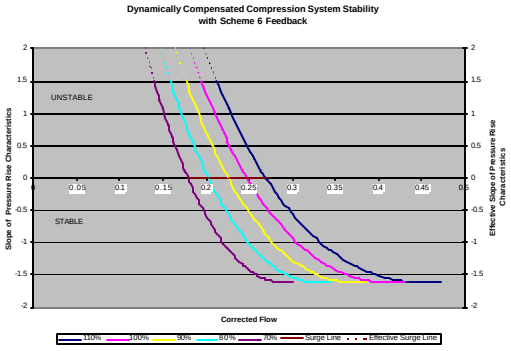
Dynamically Compensated Compression System Stability
with Scheme 6 Feedback
UNSTABLE
STABLE
Slope of Pressure Rise Characteristics
Effective Slope of Pressure Rise Characteristics
Corrected Flow
110%
100%
90%
80%
70%
Surge Line
Effective Surge Line

MIT 1 Scheme 7

Corrected Pressure Ratio (Density Ratio) with Scheme 7 Feedback

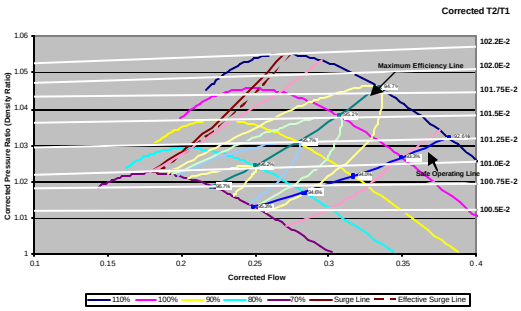

Work (Propulsive/Thermal) Ratio with Scheme 7 Feedback

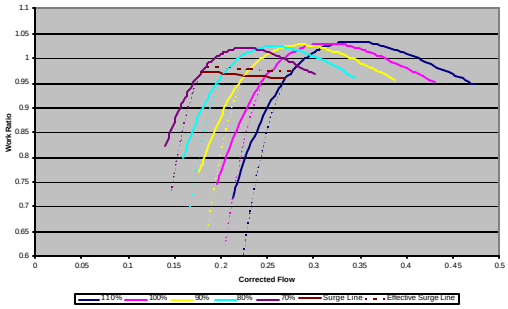

Corrected Pressure Ratio (Density Ratio) with Scheme 7 Feedback

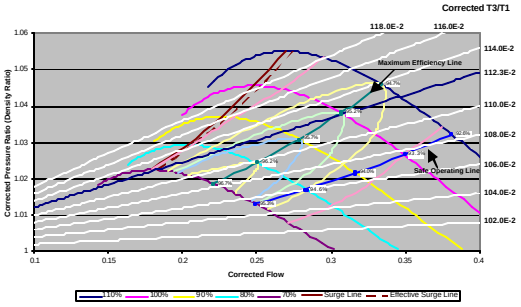

Head (Propulsive/Thermal) Ratio with Scheme 7 Feedback

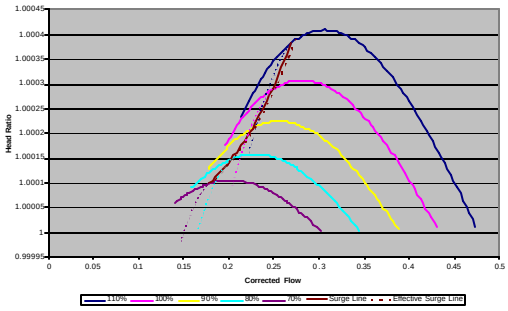

Efficiency (Propulsive/Thermal) Ratic with Scheme 7 Feedback

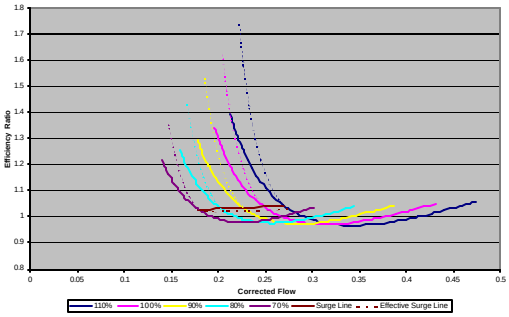

Pressure-Flow and Pressure-Density Cross-Elasticities with Scheme 7 Feedback

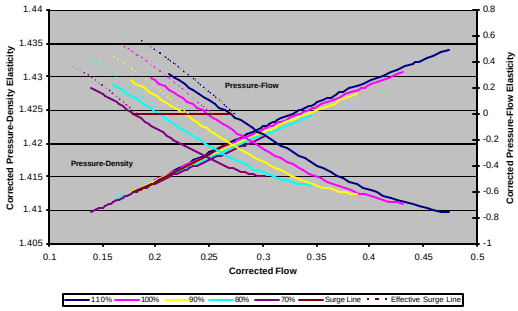

Loss (Propulsive/Thermal) Ratio with Scheme 7 Feedback

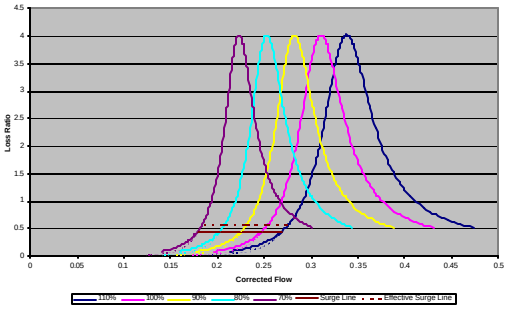

Propulsive (Deviation) Efficiency and Loss with Scheme 7 Feedback

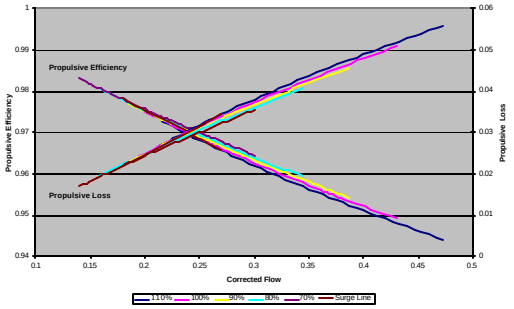

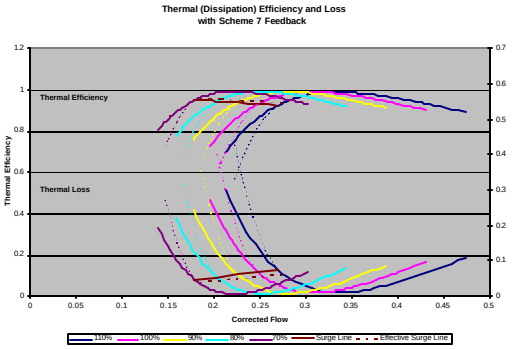
Thermal (Dissipation) Efficiency and Loss
with Scheme 7 Feedback
Thermal Efficiency
Thermal Loss
Thermal Efficiency
Corrected Flow
110%
100%
90%
80%
70%
Surge Line
Effective Surge Line

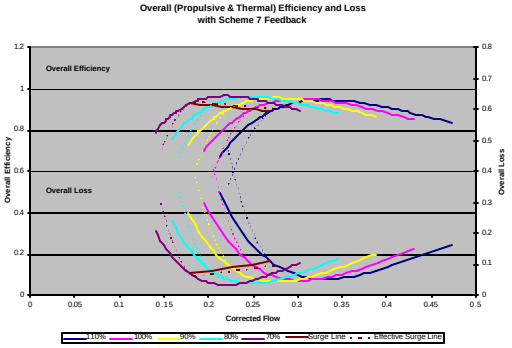
Overall (Propulsive & Thermal) Efficiency and Loss
with Scheme 7 Feedback
Overall Efficiency
Overall Loss
Overall Efficiency
Overall Loss
Corrected Flow
110%
100%
90%
80%
70%
Surge Line
Effective Surge Line

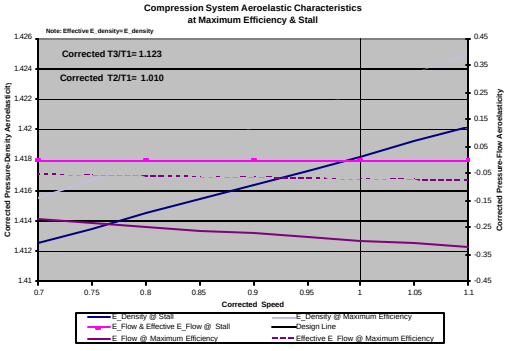
Compression System Aeroelastic Characteristics
at Maximum Efficiency & Stall
Note: Effective E_density=E_density
Corrected T3/T1= 1.123
Corrected T2/T1= 1.010
Corrected Pressure-Density Aeroelasticity
Corrected Pressure-Flow Aeroelasticity
Corrected Speed
E_Density @ Stall
E_Density @ Maximum Efficiency
E_Flow & Effective E_Flow @ Stall
Design Line
E_Flow @ Maximum Efficiency
Effective E_Flow @ Maximum Efficiency

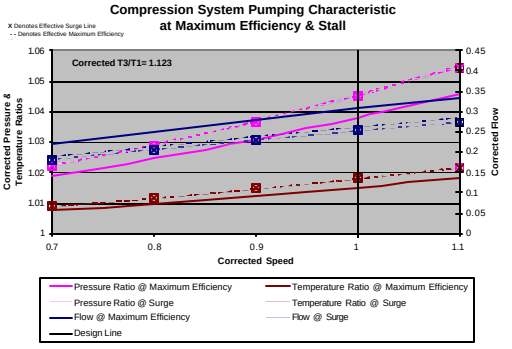
Compression System Pumping Characteristic
at Maximum Efficiency & Stall
X Denotes Effective Surge Line
- - Denotes Effective Maximum Efficiency
Corrected T3/T1= 1.123
Corrected Pressure & Temperature Ratios
Corrected Flow
Corrected Speed
Pressure Ratio @ Maximum Efficiency
Temperature Ratio @ Maximum Efficiency
Pressure Ratio @ Surge
Temperature Ratio @ Surge
Flow @ Maximum Efficiency
Flow @ Surge
Design Line

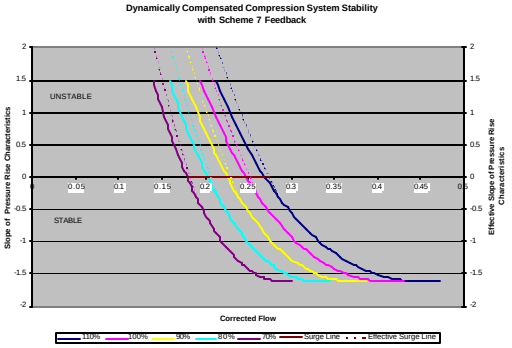
Dynamically Compensated Compression System Stability
with Scheme 7 Feedback
UNSTABLE
STABLE
Slope of Pressure Rise Characteristics
Effective Slope of Pressure Rise Characteristics
Corrected Flow
110%
100%
90%
80%
70%
Surge Line
Effective Surge Line

MIT 1 Scheme 8

Corrected Pressure Ratio (Density Ratio)
with Scheme 8 Feedback

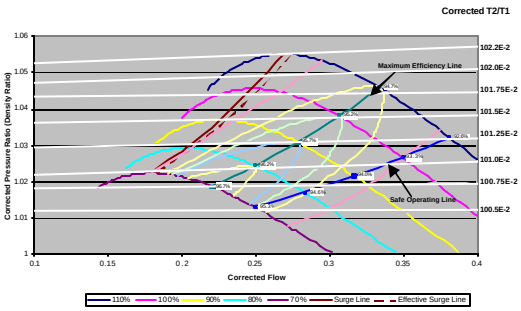

Work (Propulsive/Thermal) Ratio
with Scheme 8 Feedback

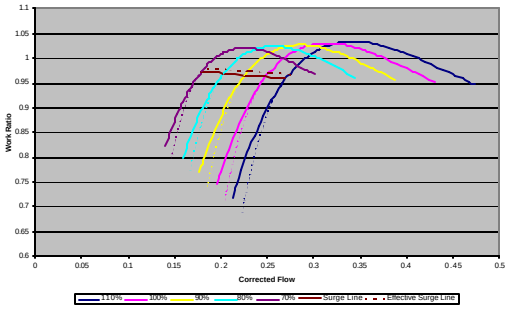

Corrected Pressure Ratio (Density Ratio)
with Scheme 8 Feedback

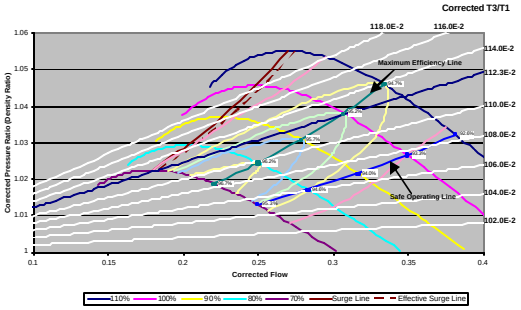

Head (Propulsive/Thermal) Ratio
with Scheme 8 Feedback

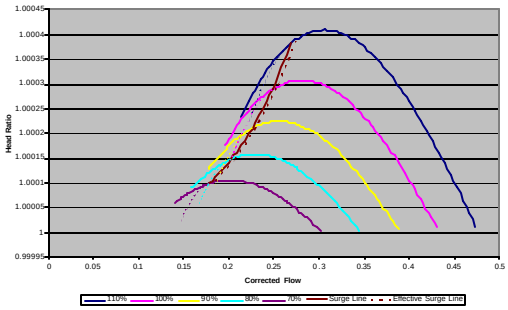

Efficiency (Propulsive/Thermal) Ratic
with Scheme 8 Feedback

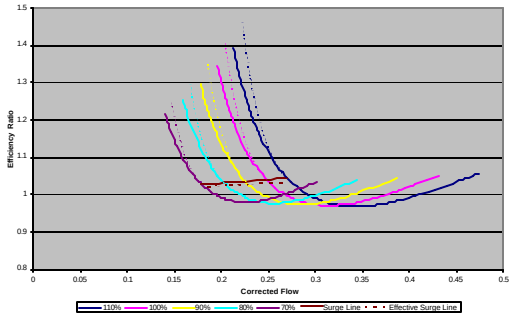

Pressure-Flow and Pressure-Density Cross-Elasticities
with Scheme 8 Feedback

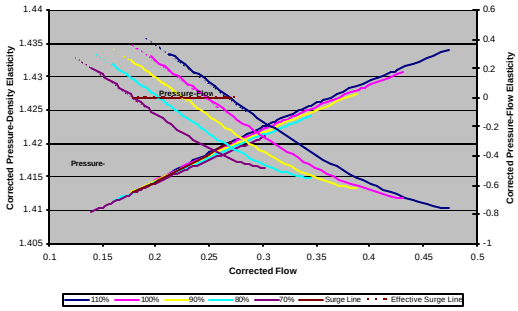

Loss (Propulsive/Thermal) Ratio
with Scheme 8 Feedback

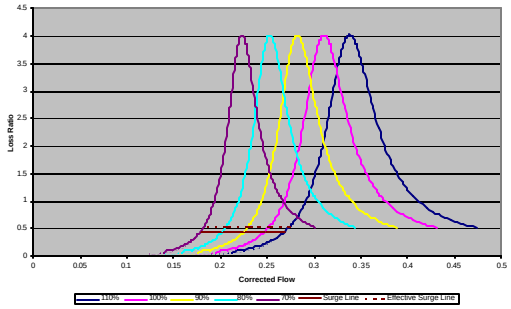

Propulsive (Deviation) Efficiency and Loss
with Scheme 8 Feedback

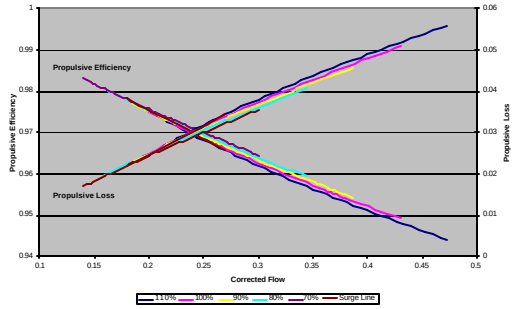

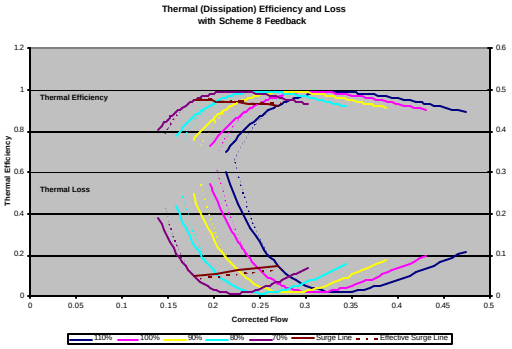
Thermal (Dissipation) Efficiency and Loss
with Scheme 8 Feedback
Thermal Efficiency
Thermal Loss
Thermal Efficiency
Corrected Flow
110%
100%
90%
80%
70%
Surge Line
Effective Surge Line

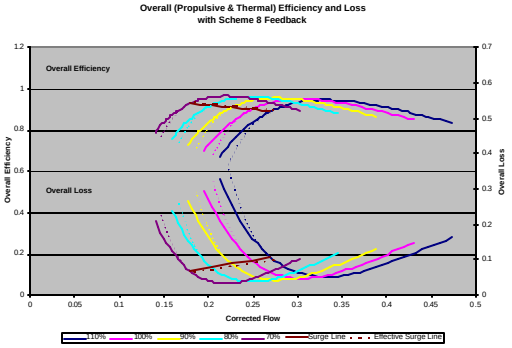
Overall (Propulsive & Thermal) Efficiency and Loss
with Scheme 8 Feedback
Overall Efficiency
Overall Loss
Overall Efficiency
Overall Loss
Corrected Flow
110%
100%
90%
80%
70%
Surge Line
Effective Surge Line

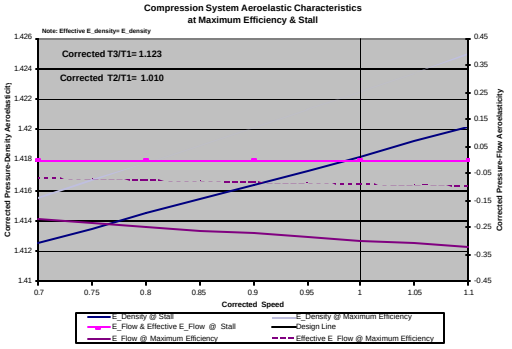
Compression System Aeroelastic Characteristics
at Maximum Efficiency & Stall
Note: Effective E_density= E_density
Corrected T3/T1= 1.123
Corrected T2/T1= 1.010
Corrected Pressure-Density Aeroelasticity
Corrected Pressure-Flow Aeroelasticity
Corrected Speed
E_Density @ Stall
E_Density @ Maximum Efficiency
E_Flow & Effective E_Flow @ Stall
Design Line
E_Flow @ Maximum Efficiency
Effective E_Flow @ Maximum Efficiency

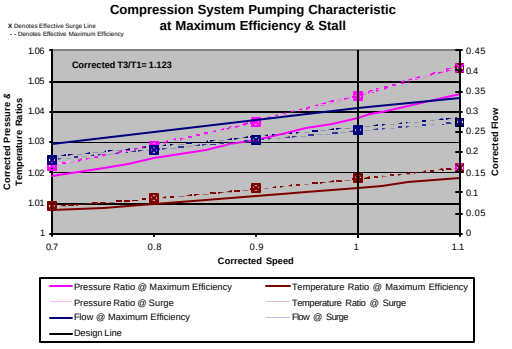
Compression System Pumping Characteristic
at Maximum Efficiency & Stall
X Denotes Effective Surge Line
- - Denotes Effective Maximum Efficiency
Corrected T3/T1= 1.123
Corrected Pressure & Temperature Ratios
Corrected Flow
Corrected Speed
Pressure Ratio @ Maximum Efficiency
Temperature Ratio @ Maximum Efficiency
Pressure Ratio @ Surge
Temperature Ratio @ Surge
Flow @ Maximum Efficiency
Flow @ Surge
Design Line

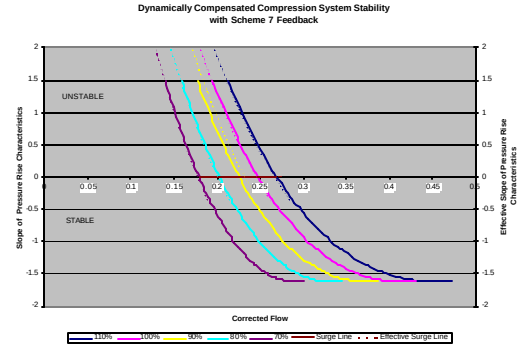
Dynamically Compensated Compression System Stability
with Scheme 7 Feedback
UNSTABLE
STABLE
Slope of Pressure Rise Characteristics
Effective Slope of Pressure Rise Characteristics
Corrected Flow
110%
100%
90%
80%
70%
Surge Line
Effective Surge Line

MIT 3 Open Loop

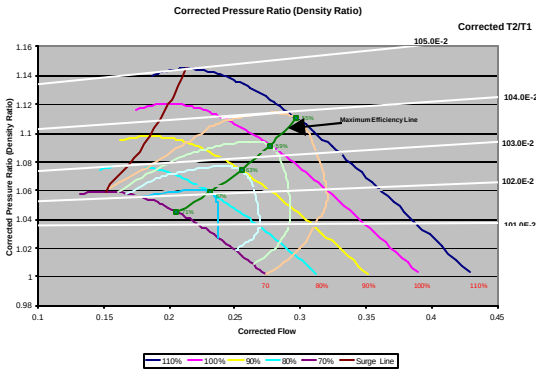

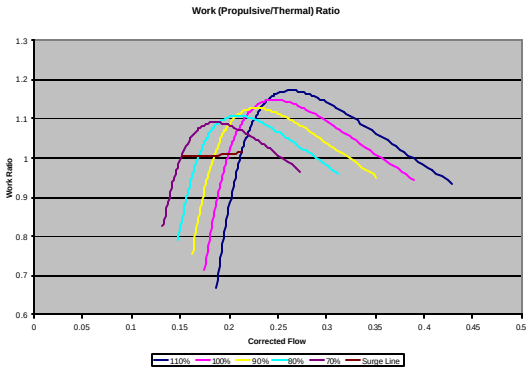

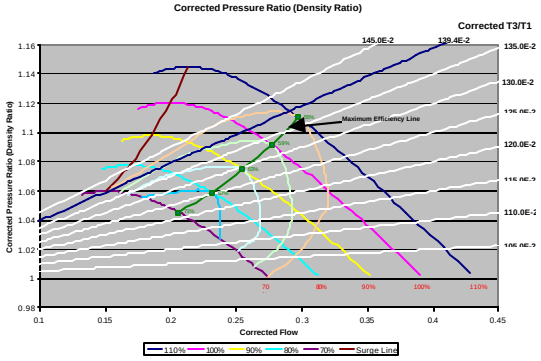

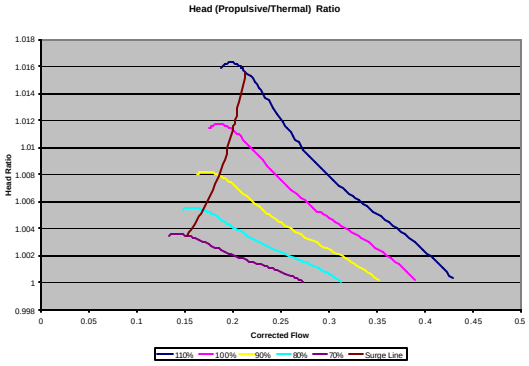

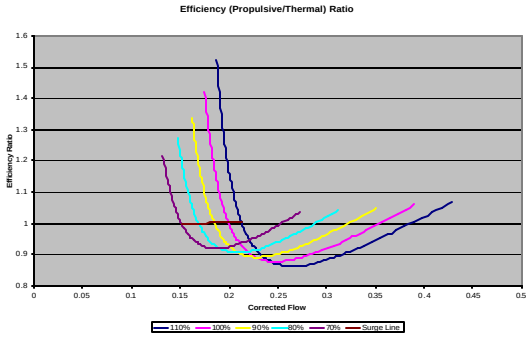

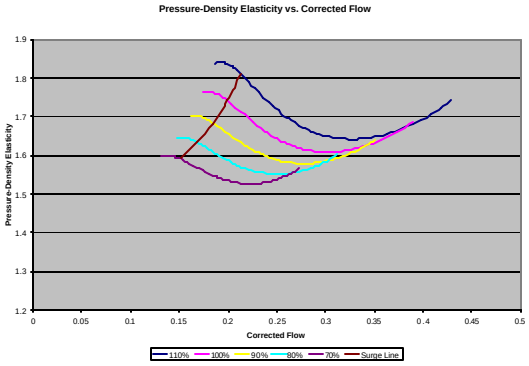

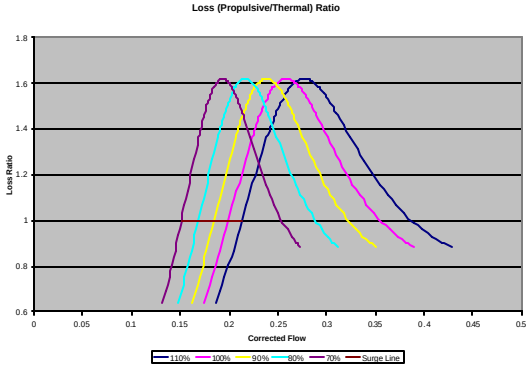

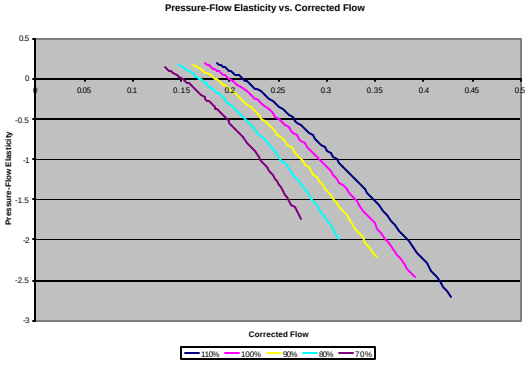

Propulsive Efficiency

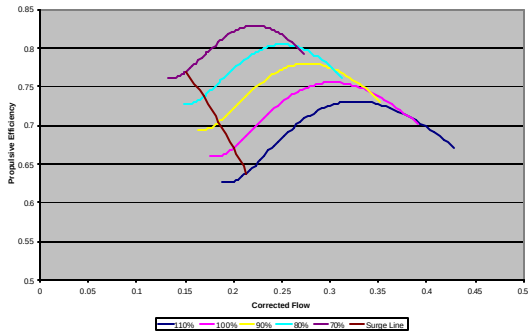

Overall (Propulsive & Thermal) Efficiency

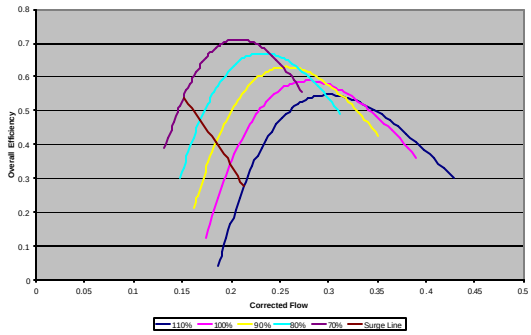

Propulsive (Deviation) Loss

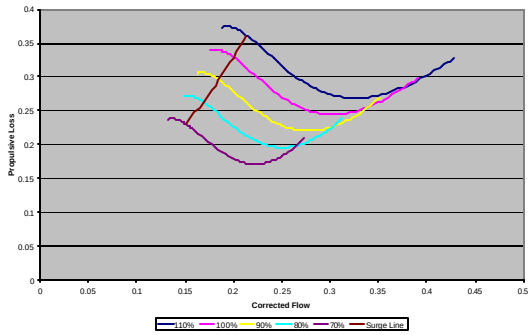

Overall (Viscous+Dissipation) Loss

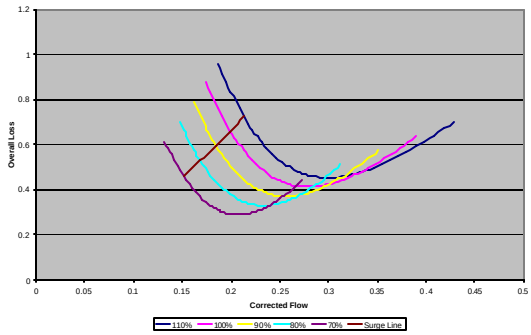

Thermal Efficiency

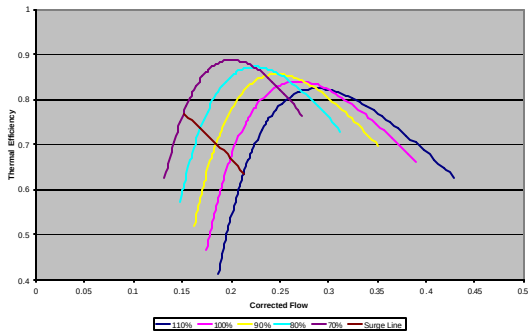

Compression System Aeroelastic Characteristics at Maximum Efficiency & Stall

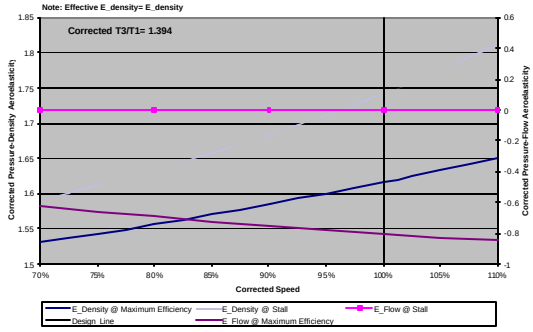

Thermal (Viscous) Loss

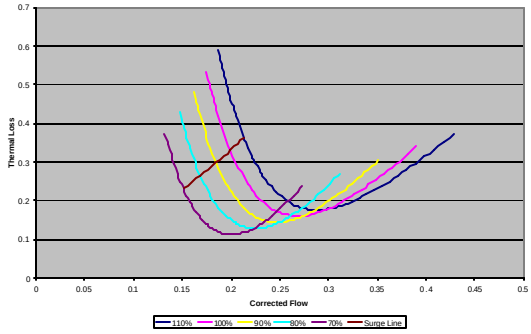

Compressor System Pumping Characteristic at Maximum Efficiency & Stall

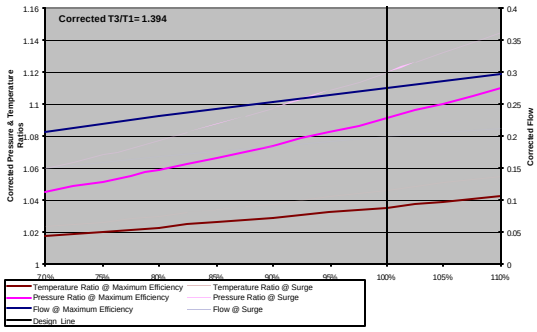

Temperature Ratio vs. Entropy

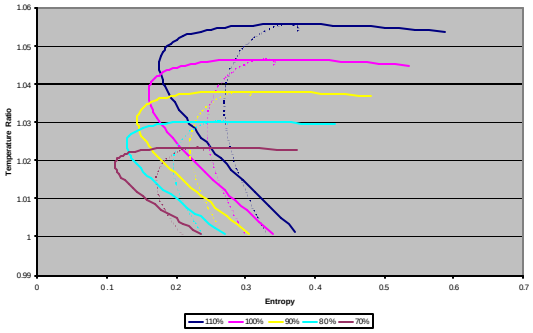

Temperature-Viscous Loss (Ts_o) Elasticity with respect to Viscous Loss vs. Relative Non-Dimensional Corrected Flow

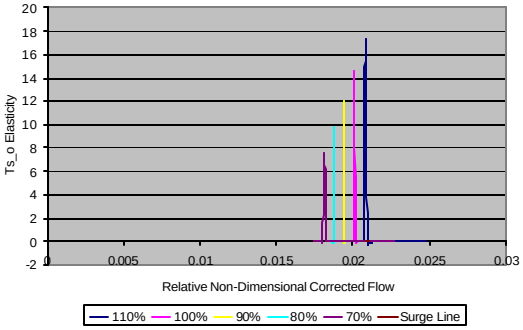

Temperature- Propulsive Loss (Ts_d) Elasticity with respect to Propulsive Loss vs. Corrected Flow

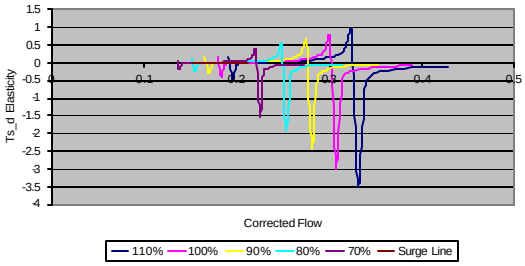

Corrected Specific Volume Ratio (v2/v1) vs. Entropy

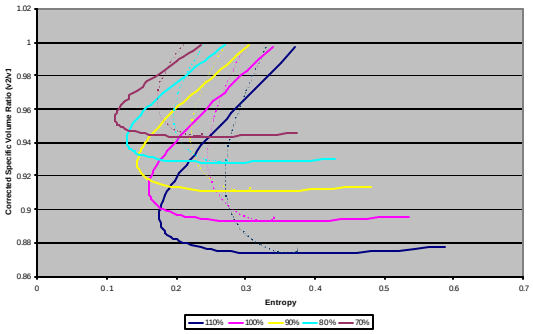

Temperature- Propulsive Loss (Ts_d) Elasticity with respect to Propulsive Loss vs. Relative Non-Dimensional Corrected Flow

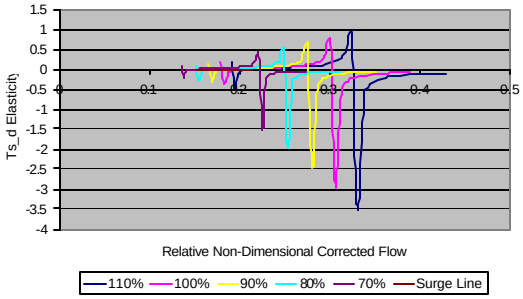

Corrected Specific Volume-Propulsive Loss (vs_d) Elasticity with respect to Propulsive Loss vs. Corrected Flow

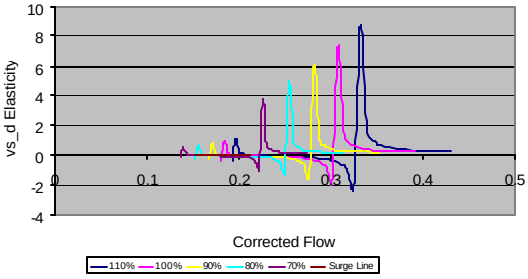

Temperature-Viscous Loss (Ts_o) Elasticity with respect to Viscous Loss vs. Corrected Flow

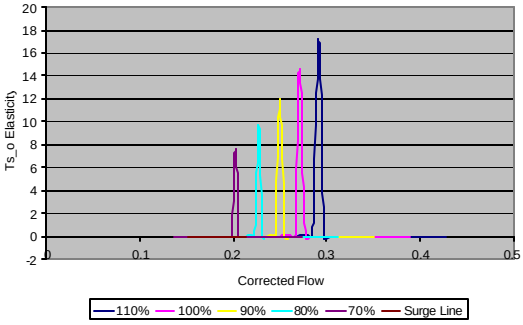

Corrected Specific Volume-Propulsive Loss (vs_d) Elasticity with respect to Propulsive Loss vs. Relative Non-Dimensional Corrected Flow

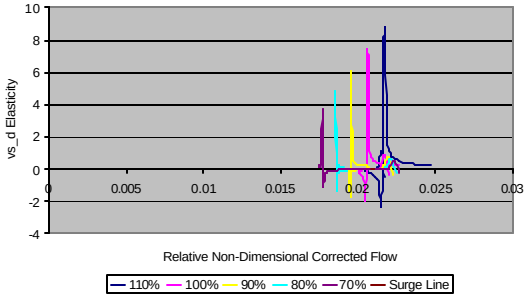

Corrected Specific Volume-Viscous Loss (vs_o) Elasticity with respect to Viscous Loss vs. Corrected Flow

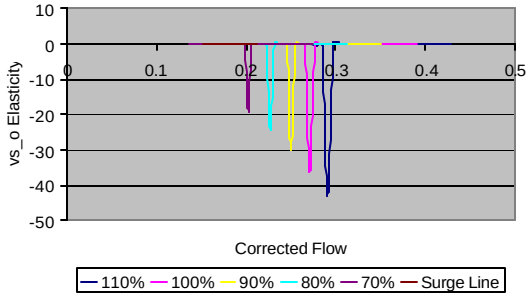

Corrected Specific Volume-Temperature (vT) Elasticity with respect to Temperature vs. Relative Non-Dimensional Corrected Flow

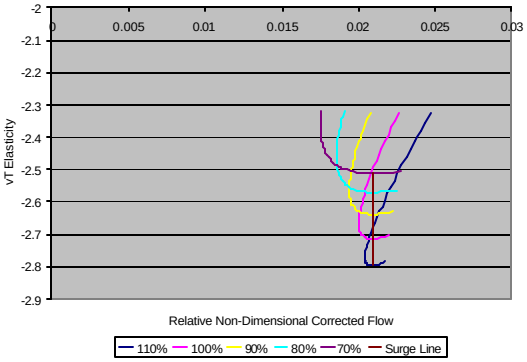

Corrected Specific Volume-Viscous Loss (vs_o) Elasticity with respect to Viscous Loss vs. Relative Non-Dimensional Corrected Flow

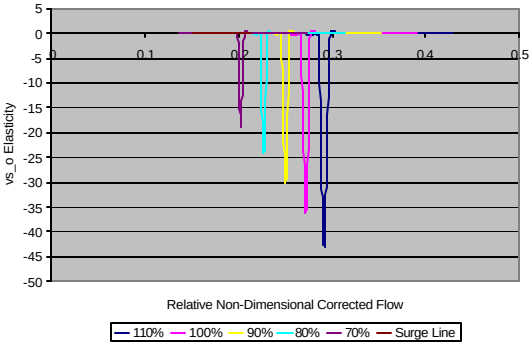

Corrected Pressure Ratio vs. Entropy

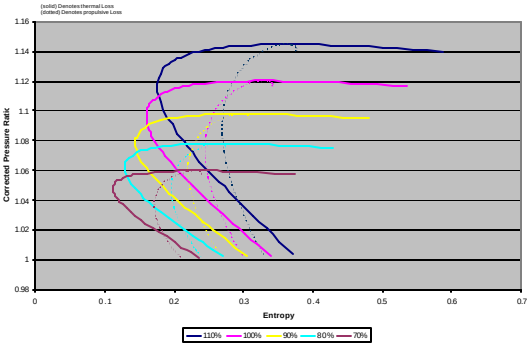

Corrected Specific Volume Ratio (v2/v1) vs. Temperature Ratio (T2/T1)

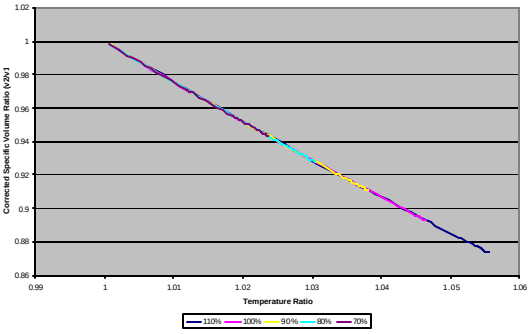

Pressure-Propusive Loss (Ps_d) Elasticity with respect to Propulsive Loss vs. Corrected Flow

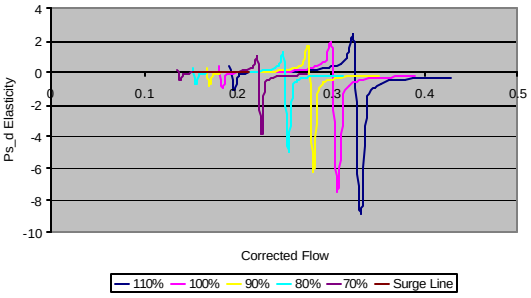

Corrected Specific Volume-Temperature (vT) Elasticity with respect to Temperature vs. Corrected Flow

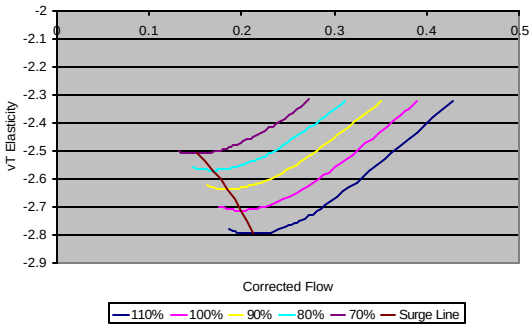

Pressure-Propusive Loss (Ps_d) Elasticity with respect to Propulsive Loss vs. Relative Non-Dimensional Corrected Flow

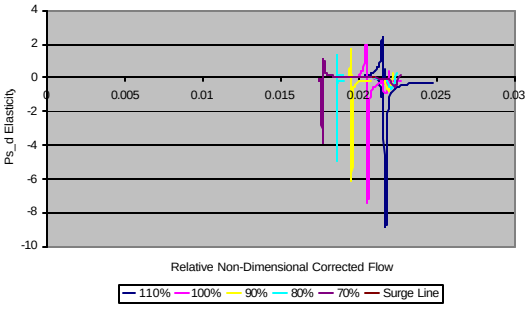

Pressure-Viscous Loss (Ps_o) Elasticity with respect to Viscous Loss vs. Corrected Flow

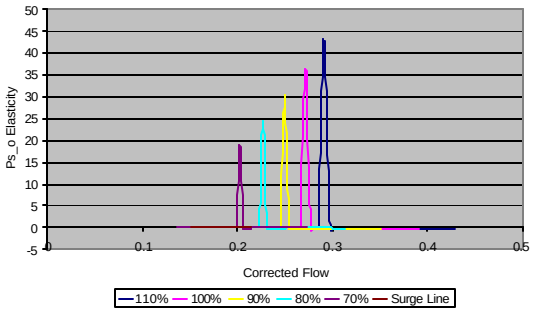

Corrected Pressure Ratio vs. Corrected Specific Volume Ratio (v2/v1)

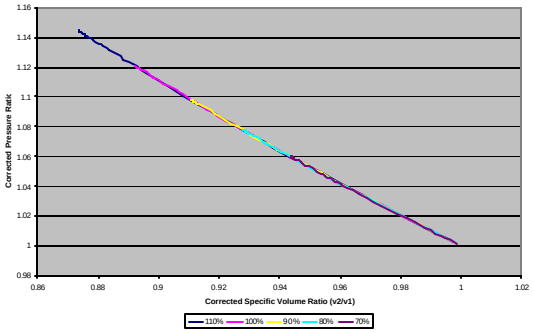

Pressure-Viscous Loss (Ps_o) Elasticity with respect to Viscous Loss vs. Relative Non-Dimensional Corrected Flow

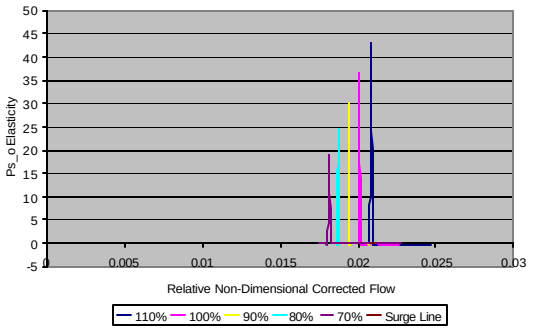

Corrected Pressure-Corrected Specific Volume (Pv) Elasticity with respect to Corrected Specific Volume vs. Corrected Flow

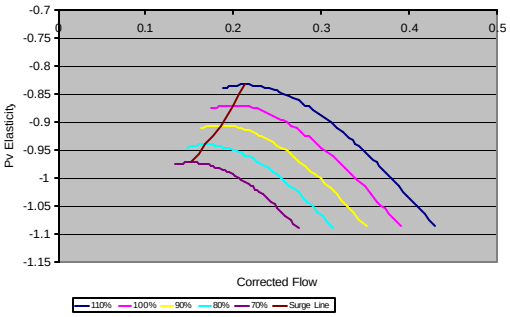

Corrected Pressure vs. Temperature Ratio

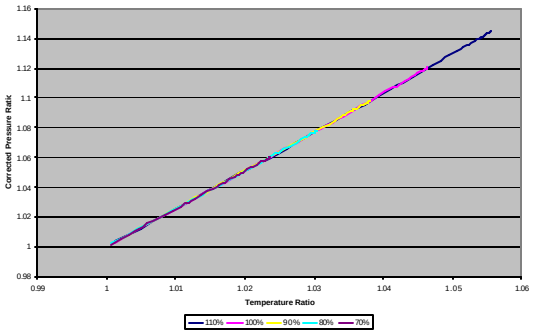

Corrected Pressure-Corrected Specific Volume (Pv) Elasticity with respect to Corrected Specific Volume vs. Relative Non-Dimensional Corrected Flow

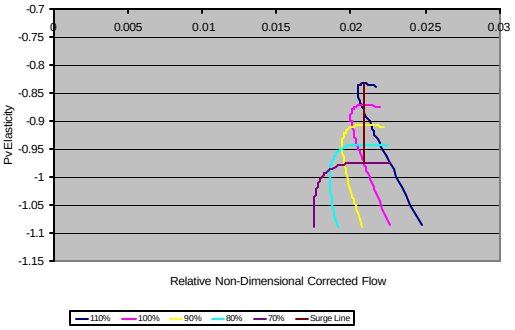

Corrected Pressure- Temperature (PT) Elasticity with respect to Temperature vs. Corrected Flow

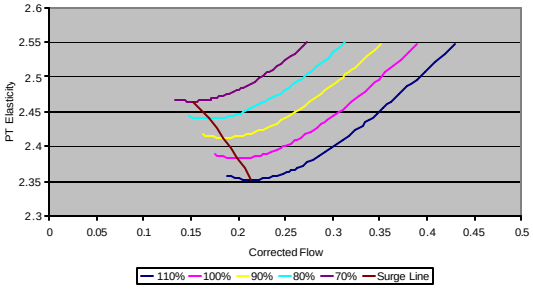

Corrected Pressure- Temperature (PT) Elasticity with respect to Temperature vs. Relative Non-Dimensional Corrected Flow

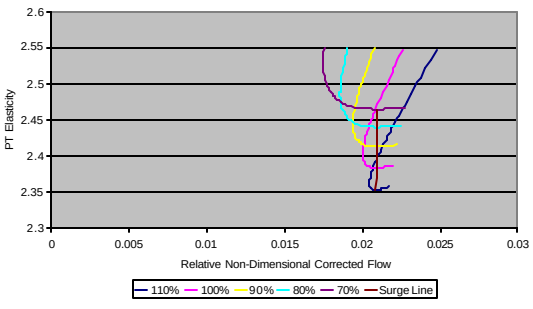

MIT 3 Scheme 1

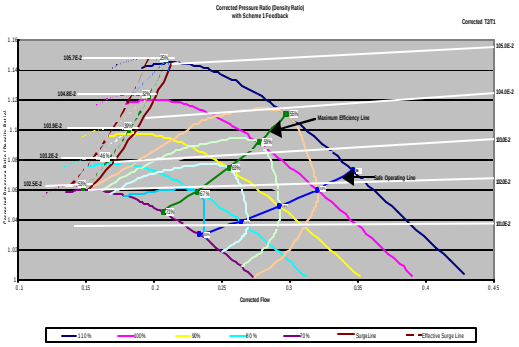

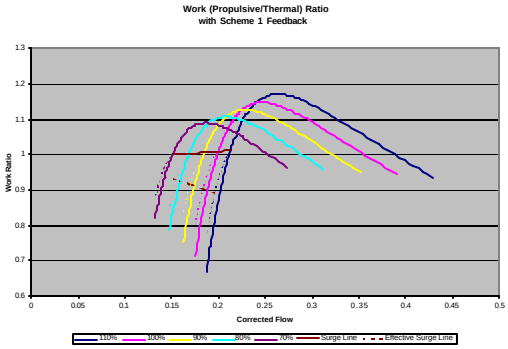

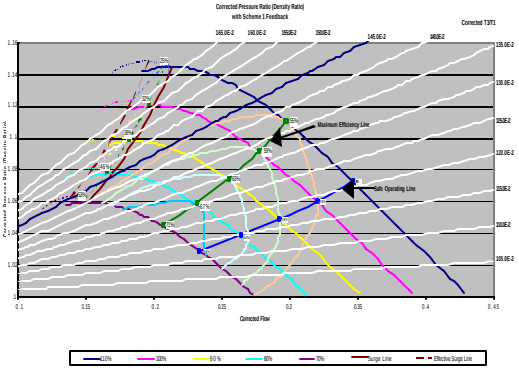

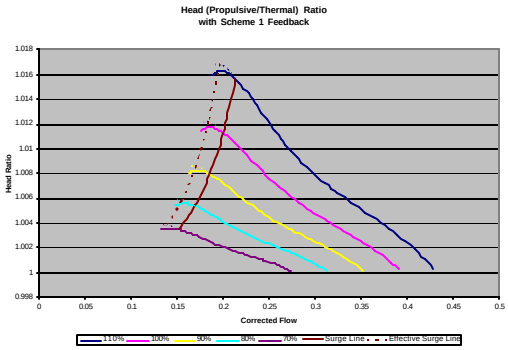

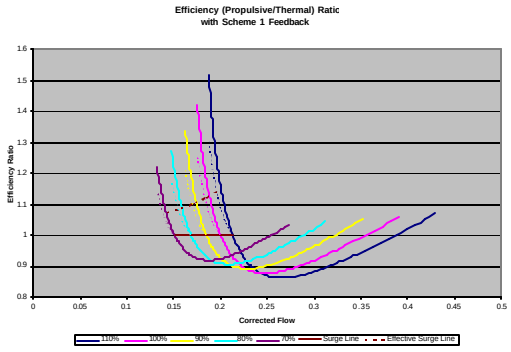

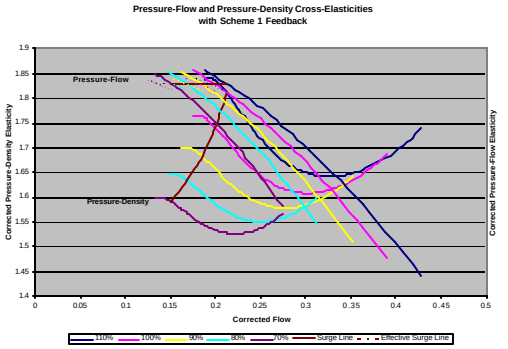

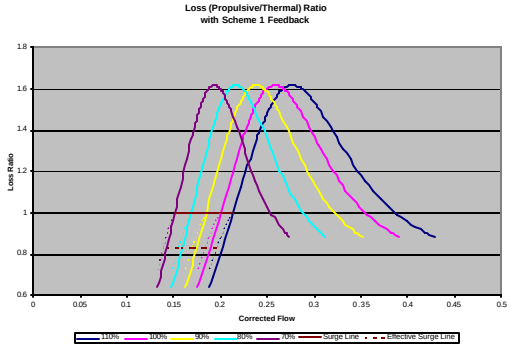

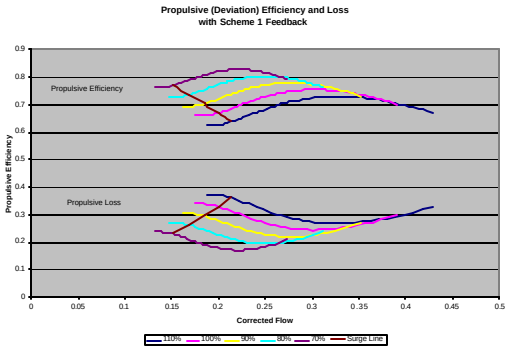

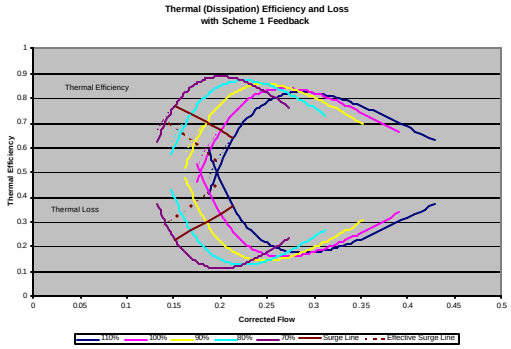
Thermal (Dissipation) Efficiency and Loss
with Scheme 1 Feedback
Thermal Efficiency
Thermal Loss
Thermal Efficiency
Corrected Flow
110%
100%
90%
80%
70%
Surge Line
Effective Surge Line

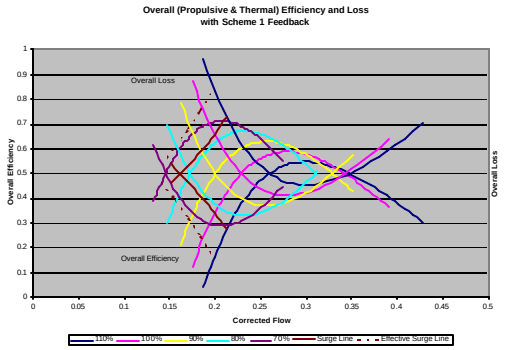
Overall (Propulsive & Thermal) Efficiency and Loss
with Scheme 1 Feedback
Overall Loss
Overall Efficiency
Overall Efficiency
Overall Loss
Corrected Flow
110%
100%
90%
80%
70%
Surge Line
Effective Surge Line

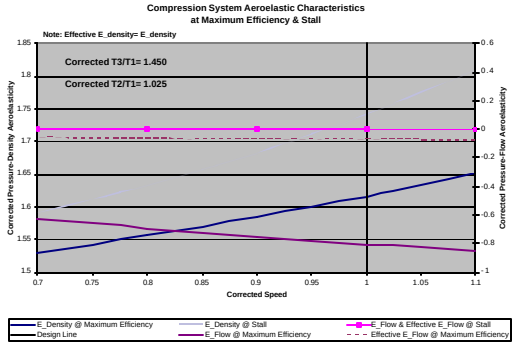
Compression System Aeroelastic Characteristics
at Maximum Efficiency & Stall
Note: Effective E_density= E_density
Corrected T3/T1= 1.450
Corrected T2/T1= 1.025
Corrected Pressure-Density Aeroelasticity
Corrected Pressure-Flow Aeroelasticity
Corrected Speed
E_Density @ Maximum Efficiency
E_Density @ Stall
E_Flow & Effective E_Flow @ Stall
Design Line
E_Flow @ Maximum Efficiency
Effective E_Flow @ Maximum Efficiency

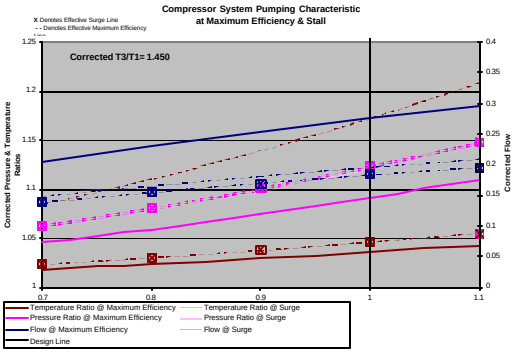
Compressor System Pumping Characteristic
at Maximum Efficiency & Stall
X Denotes Effective Surge Line
- - Denotes Effective Maximum Efficiency
Corrected T3/T1= 1.450
Corrected Pressure & Temperature Ratios
Corrected Flow
Temperature Ratio @ Maximum Efficiency
Temperature Ratio @ Surge
Pressure Ratio @ Maximum Efficiency
Pressure Ratio @ Surge
Flow @ Maximum Efficiency
Flow @ Surge
Design Line

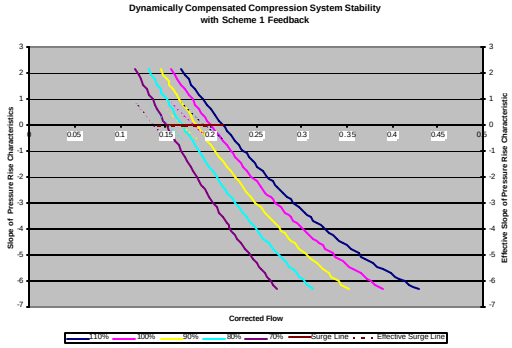
Dynamically Compensated Compression System Stability
with Scheme 1 Feedback
Slope of Pressure Rise Characteristics
Effective Slope of Pressure Rise Characteristic
Corrected Flow
110%
100%
90%
80%
70%
Surge Line
Effective Surge Line

MIT 3 Scheme 2

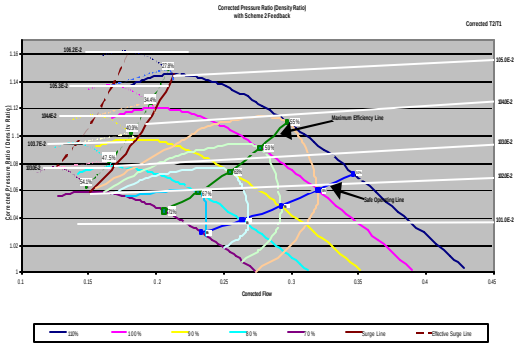

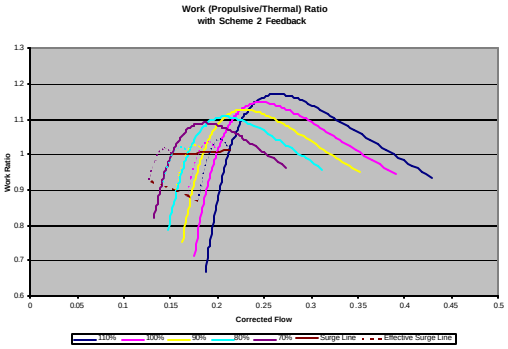

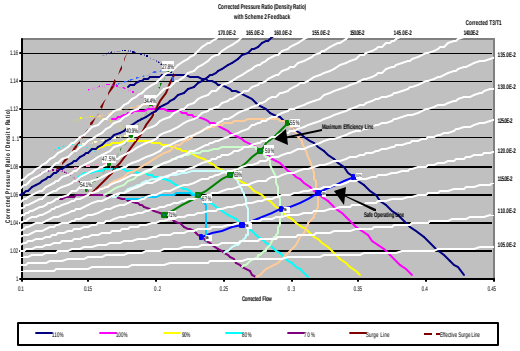

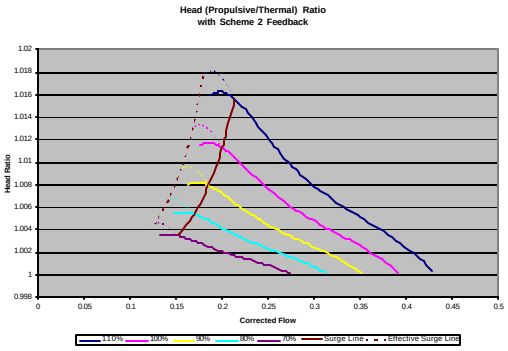

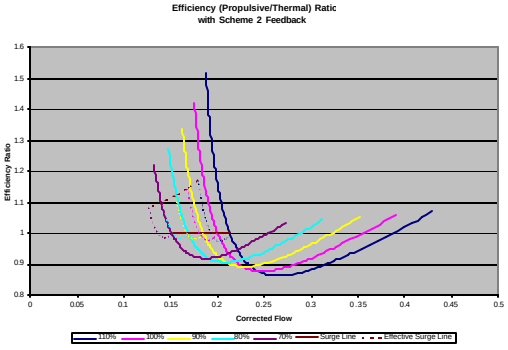

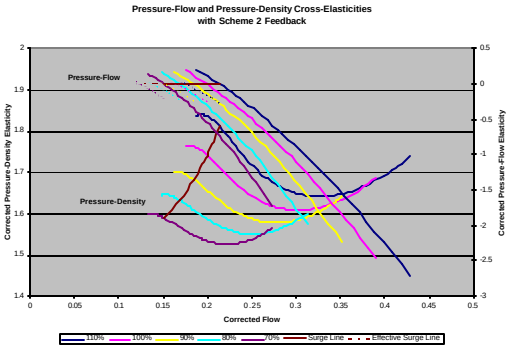

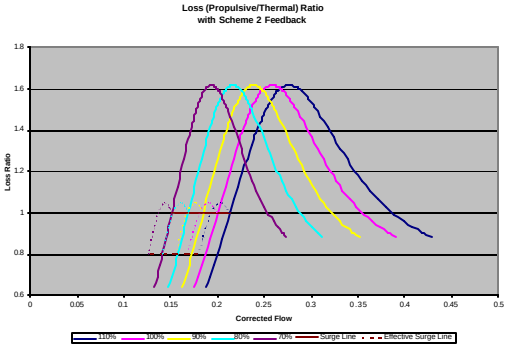

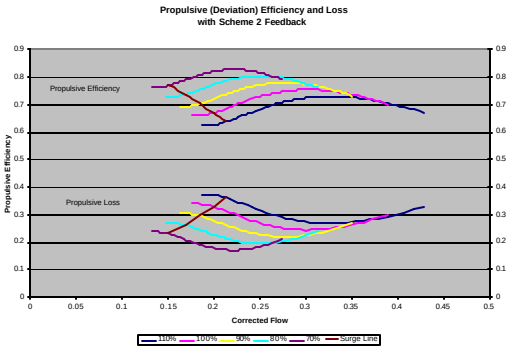

Thermal (Dissipation) Efficiency and Loss with Scheme 2 Feedback

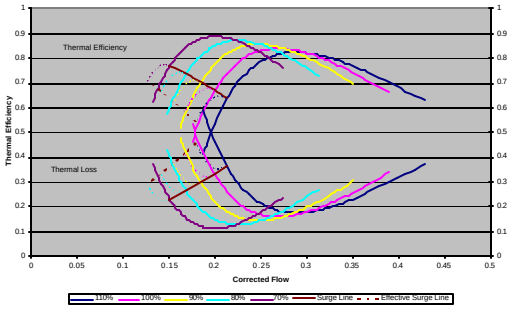

Overall (Propulsive & Thermal) Efficiency and Loss with Scheme 2 Feedback

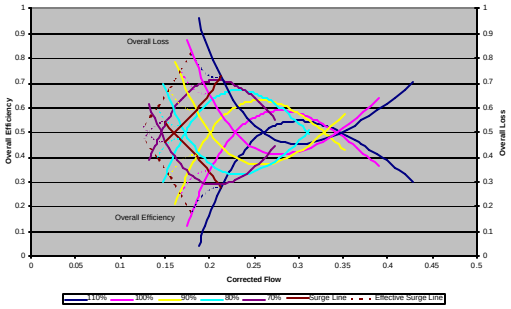

Compression System Aeroelastic Characteristics at Maximum Efficiency & Stall

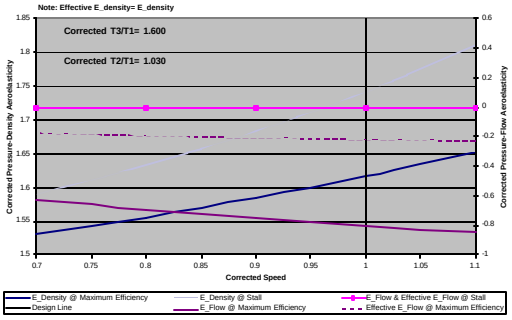

Compressor System Pumping Characteristic at Maximum Efficiency & Stall

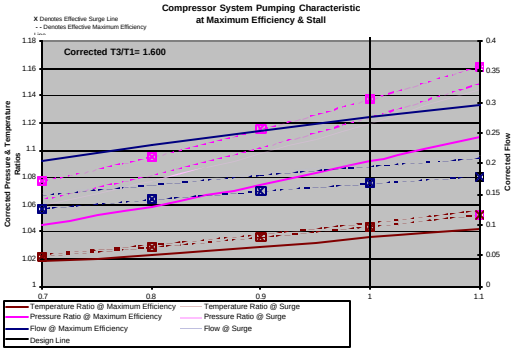

Dynamically Compensated Compression System Stability with Scheme 2 Feedback

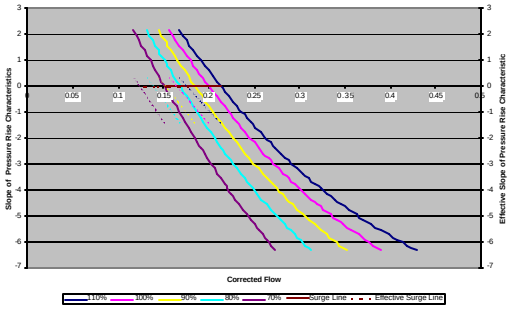

MIT 3 Scheme 3

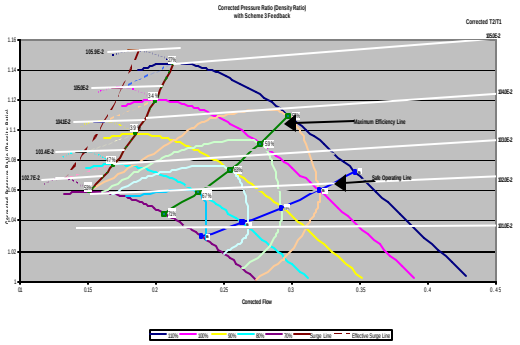

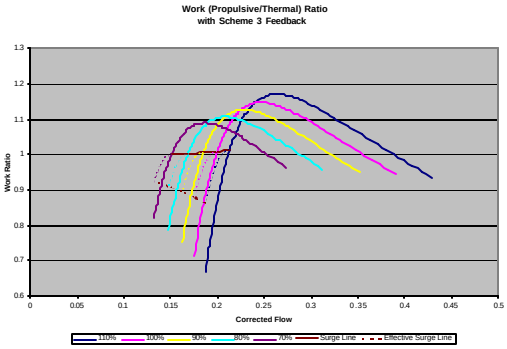

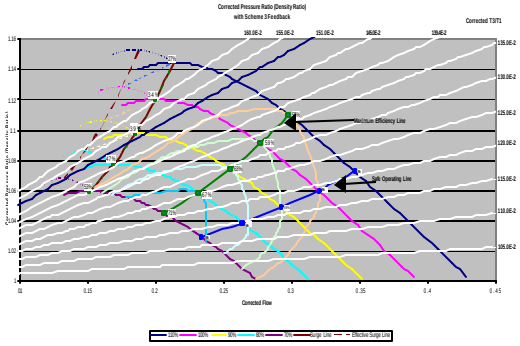

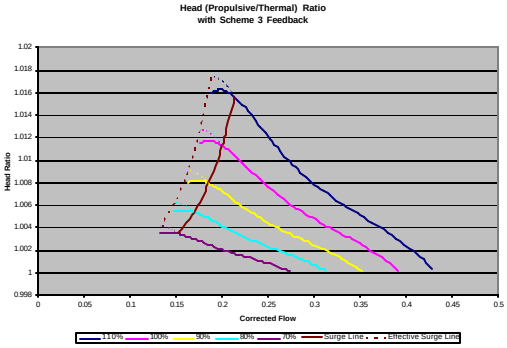

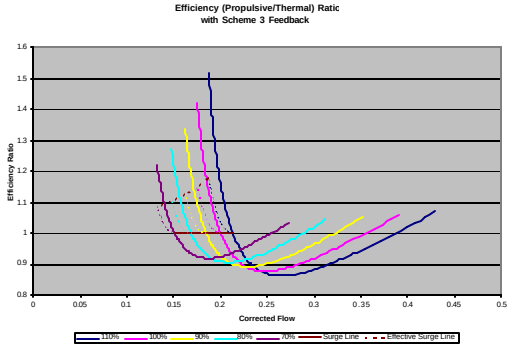

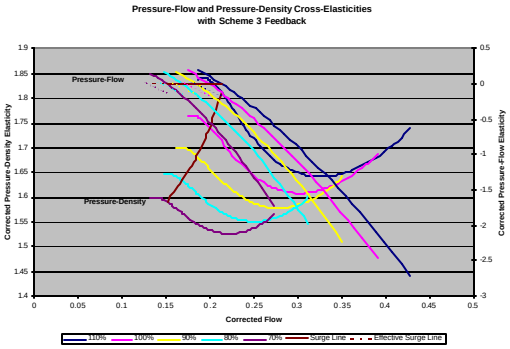

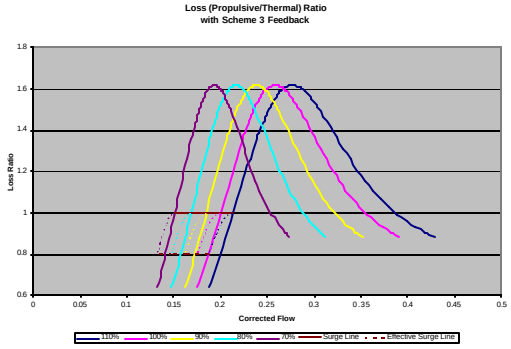

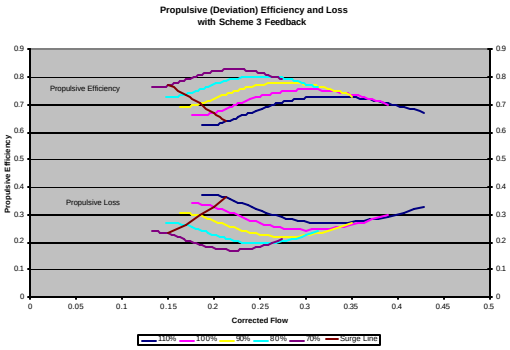

Thermal (Dissipation) Efficiency and Loss with Scheme 3 Feedback

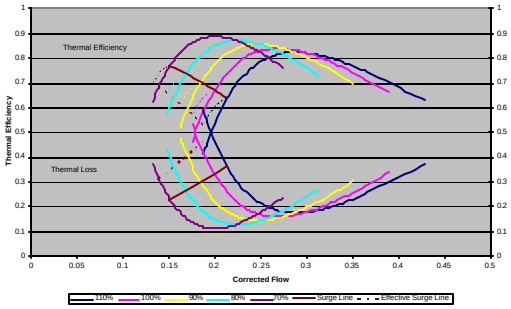

Overall (Propulsive & Thermal) Efficiency and Loss with Scheme 3 Feedback

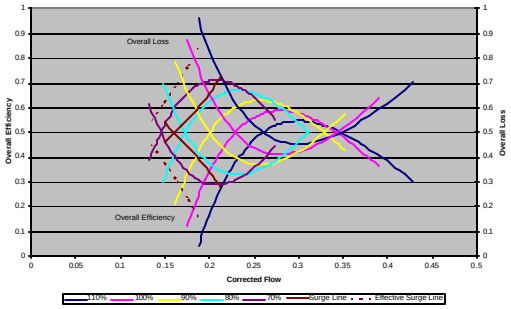

Compression System Aeroelastic Characteristics at Maximum Efficiency & Stall

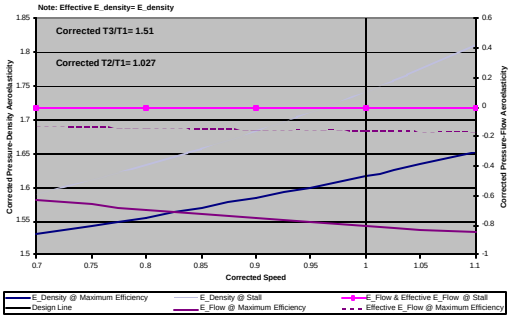

Compressor System Pumping Characteristic at Maximum Efficiency & Stall

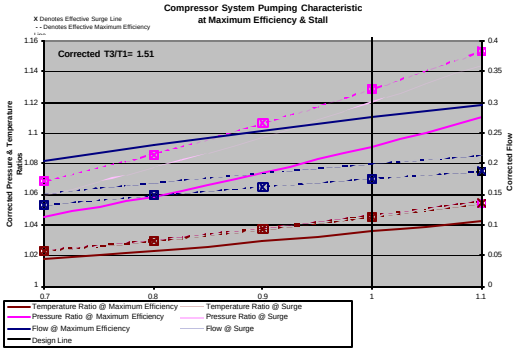

Dynamically Compensated Compression System Stability with Scheme 3 Feedback

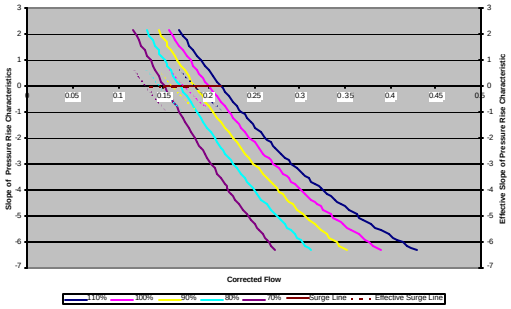

MIT 3 Scheme 4

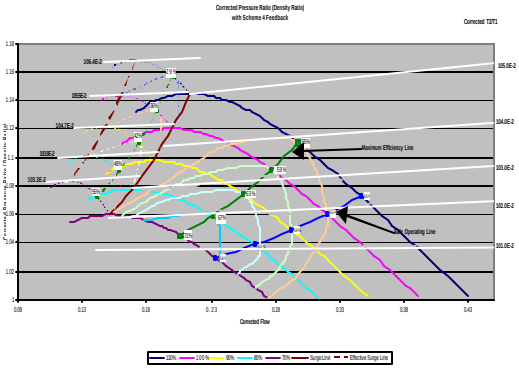

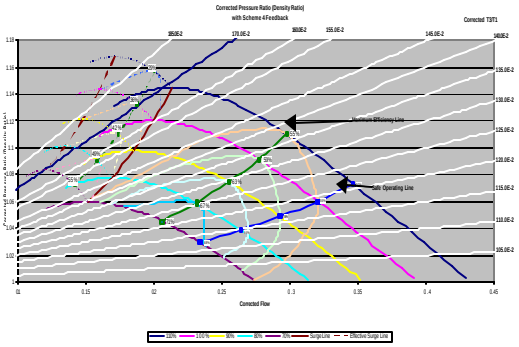

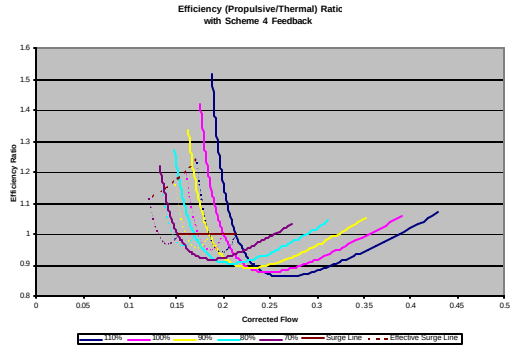

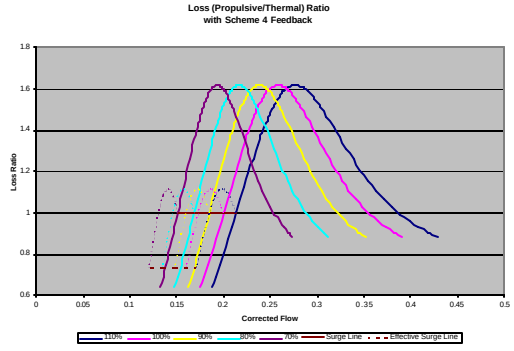

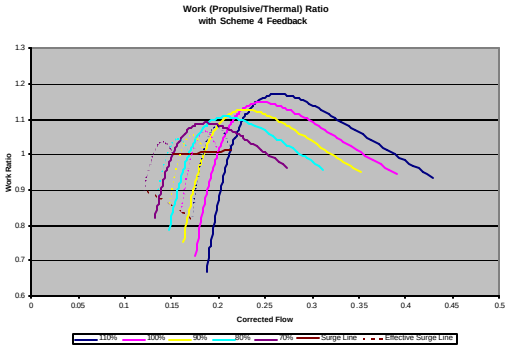

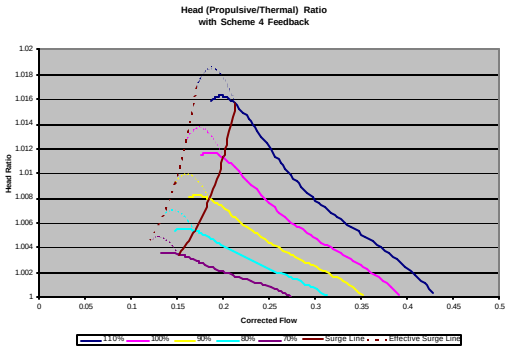

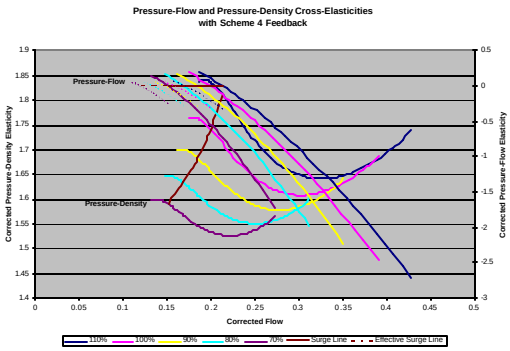

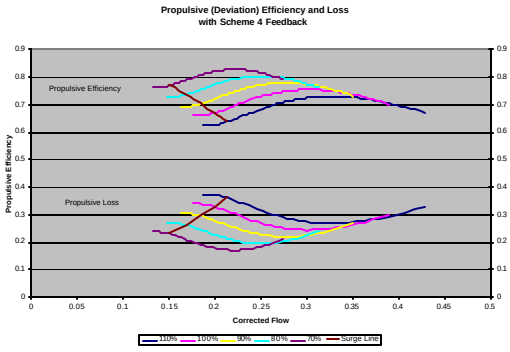

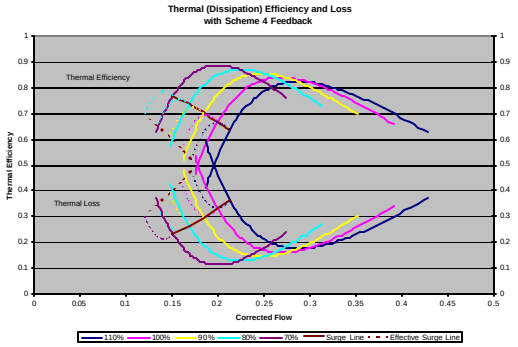
Thermal (Dissipation) Efficiency and Loss
with Scheme 4 Feedback
Thermal Efficiency
Thermal Loss
Thermal Efficiency
Corrected Flow
110%
100%
90%
80%
70%
Surge Line
Effective Surge Line

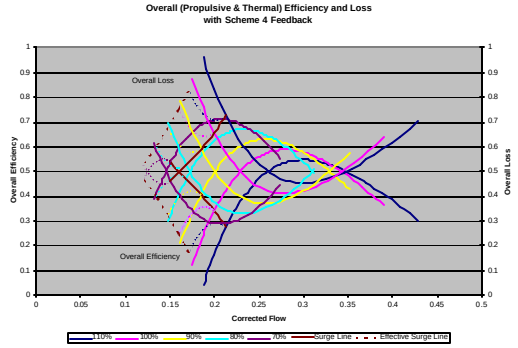
Overall (Propulsive & Thermal) Efficiency and Loss
with Scheme 4 Feedback
Overall Loss
Overall Efficiency
Overall Efficiency
Overall Loss
Corrected Flow
110%
100%
90%
80%
70%
Surge Line
Effective Surge Line

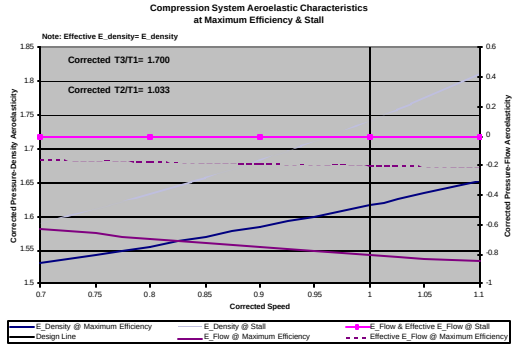
Compression System Aeroelastic Characteristics
at Maximum Efficiency & Stall
Note: Effective E_density= E_density
Corrected T3/T1= 1.700
Corrected T2/T1= 1.033
Corrected Pressure-Density Aeroelasticity
Corrected Pressure-Flow Aeroelasticity
Corrected Speed
E_Density @ Maximum Efficiency
E_Density @ Stall
E_Flow & Effective E_Flow @ Stall
Design Line
E_Flow @ Maximum Efficiency
Effective E_Flow @ Maximum Efficiency

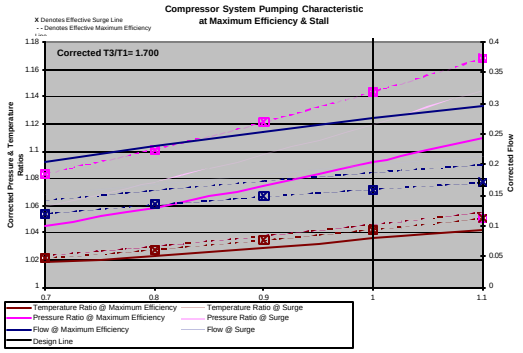
Compressor System Pumping Characteristic
at Maximum Efficiency & Stall
X Denotes Effective Surge Line
Denotes Effective Maximum Efficiency
Line
Corrected T3/T1= 1.700
Corrected Pressure & Temperature Ratios
Corrected Flow
Temperature Ratio @ Maximum Efficiency
Temperature Ratio @ Surge
Pressure Ratio @ Maximum Efficiency
Pressure Ratio @ Surge
Flow @ Maximum Efficiency
Flow @ Surge
Design Line

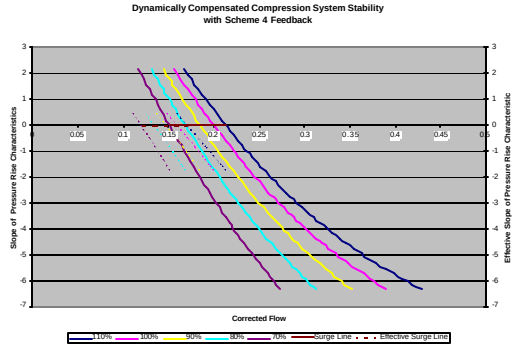
Dynamically Compensated Compression System Stability
with Scheme 4 Feedback
Slope of Pressure Rise Characteristics
Effective Slope of Pressure Rise Characteristic
Corrected Flow
110%
100%
90%
80%
70%
Surge Line
Effective Surge Line

MIT 3 Scheme 5

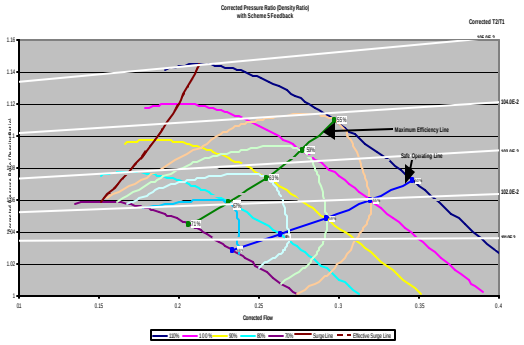

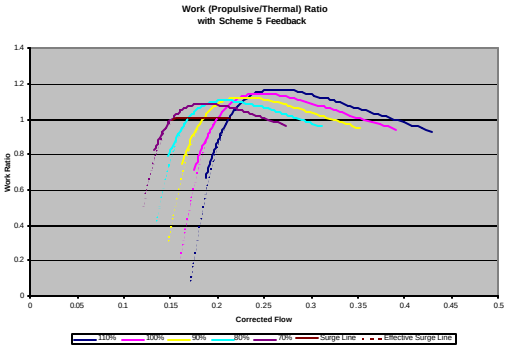

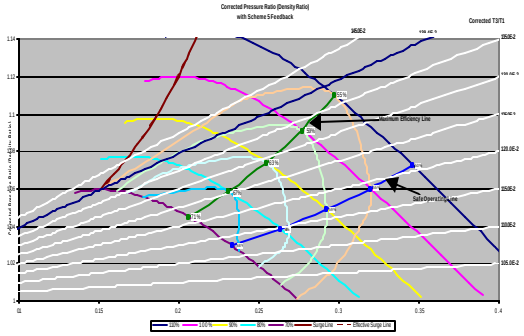

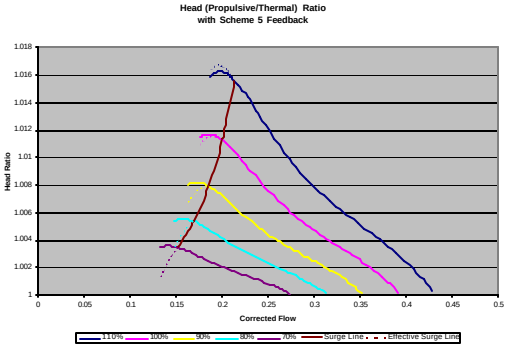

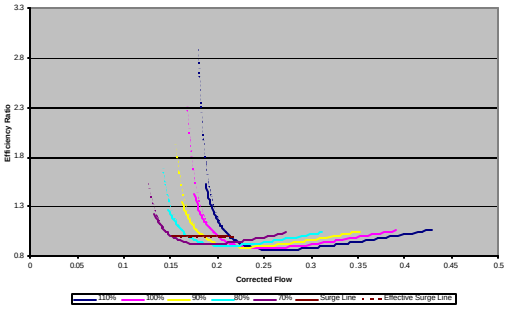

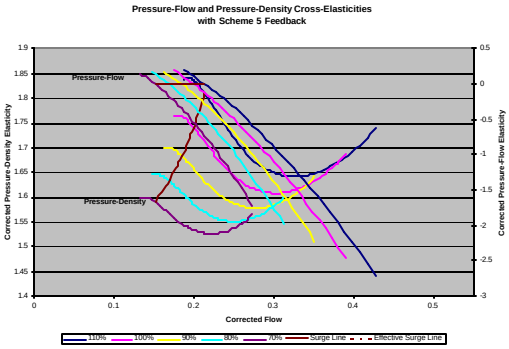

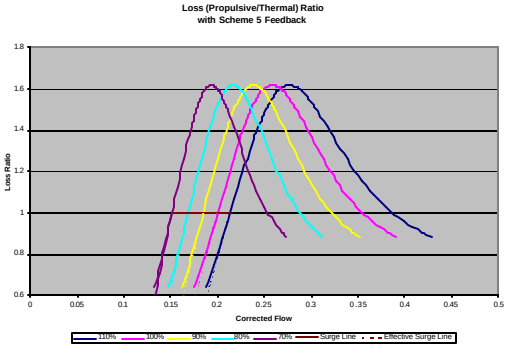

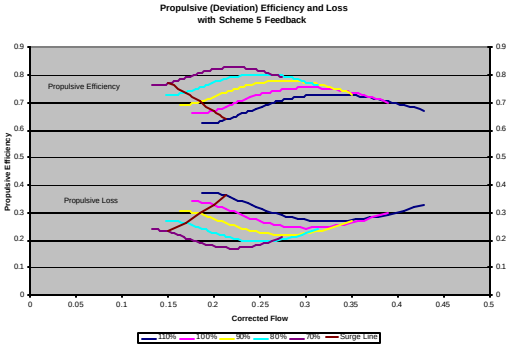

Thermal (Dissipation) Efficiency and Loss with Scheme 5 Feedback

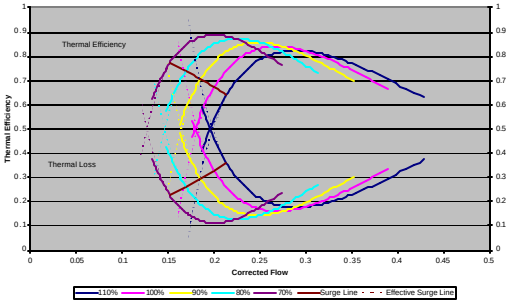

Overall (Propulsive & Thermal) Efficiency and Loss with Scheme 5 Feedback

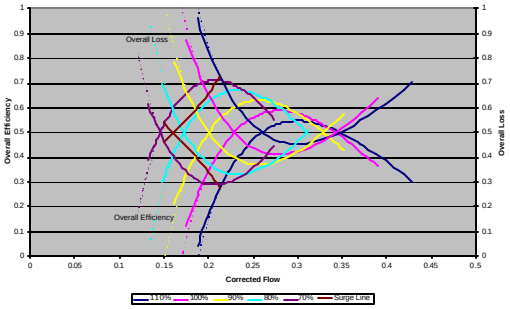

Compression System Aeroelastic Characteristics at Maximum Efficiency & Stall

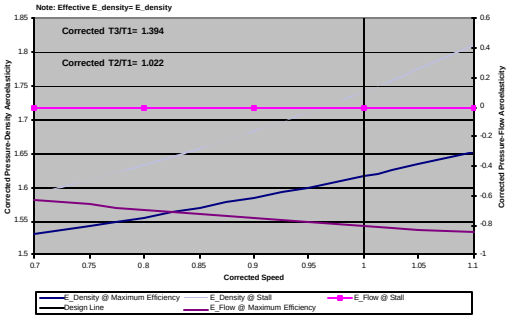

Compressor System Pumping Characteristic at Maximum Efficiency & Stall

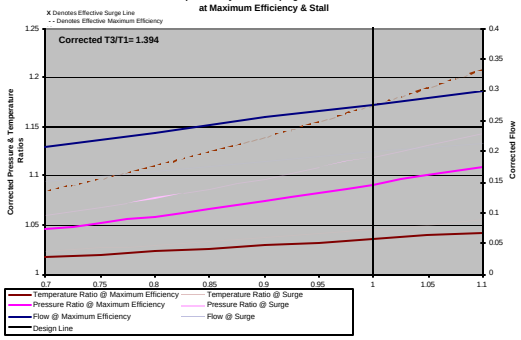

Dynamically Compensated Compression System Stability with Scheme 5 Feedback

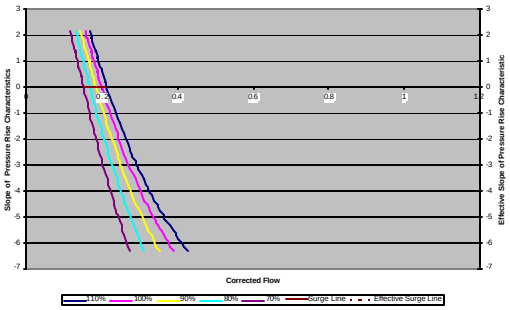

MIT 3 Scheme 6

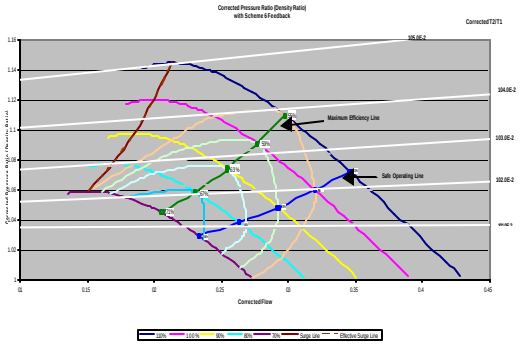

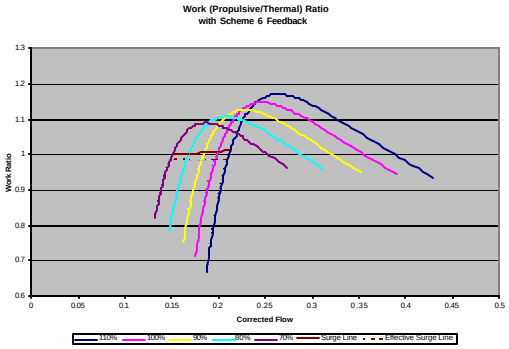

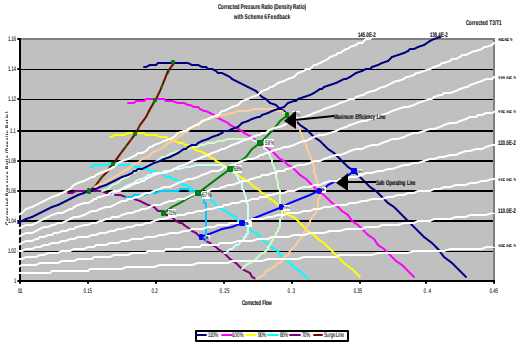

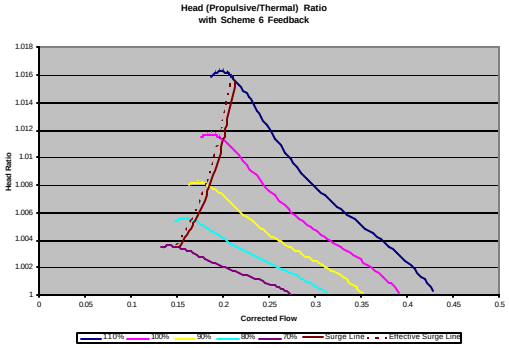

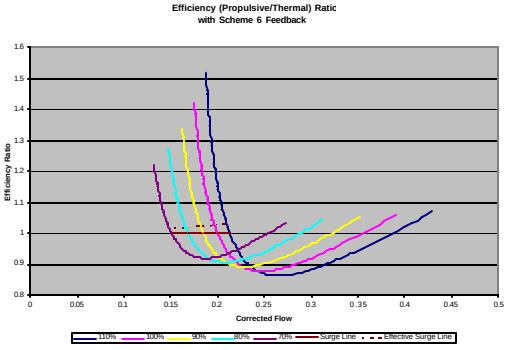

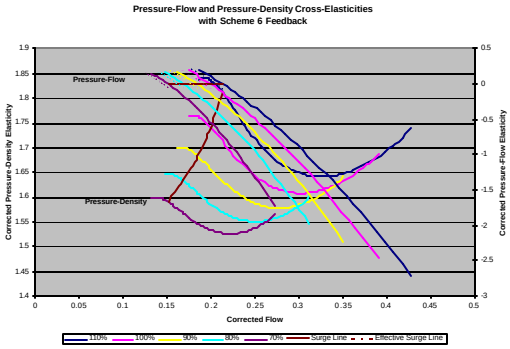

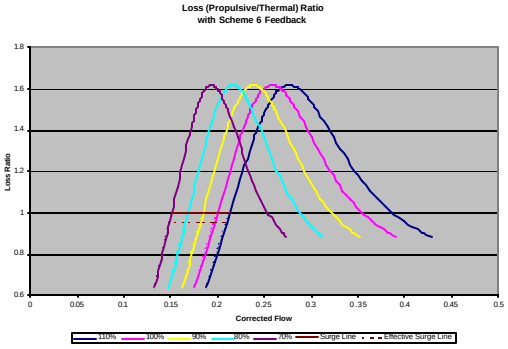

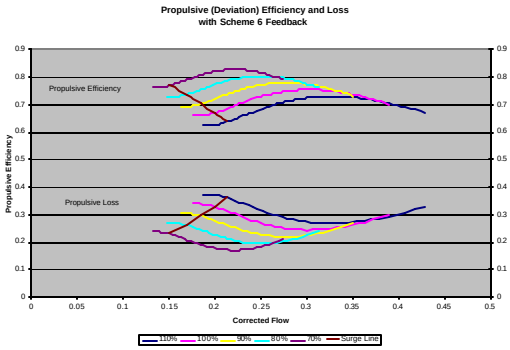

Thermal (Dissipation) Efficiency and Loss with Scheme 6 Feedback

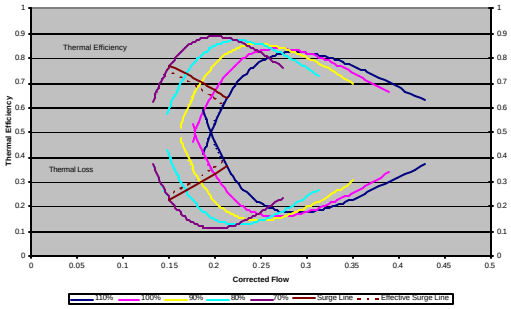

Overall (Propulsive & Thermal) Efficiency and Loss with Scheme 6 Feedback

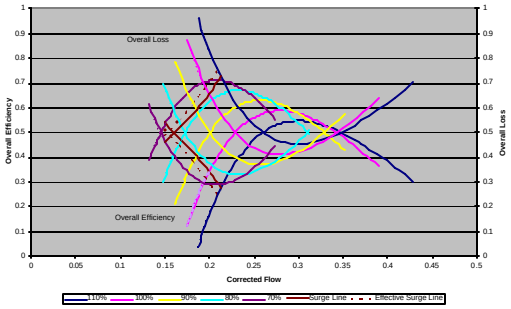

Compression System Aeroelastic Characteristics at Maximum Efficiency & Stall

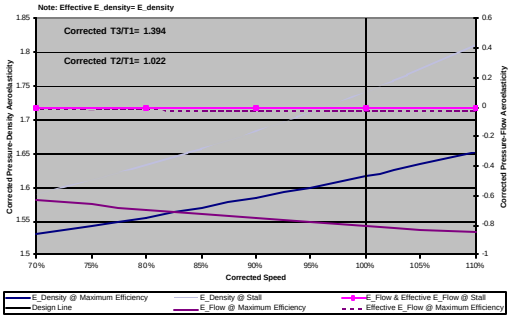

Compressor System Pumping Characteristic at Maximum Efficiency & Stall

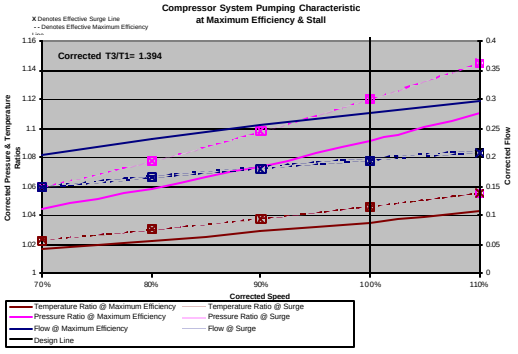

Dynamically Compensated Compression System Stability with Scheme 6 Feedback

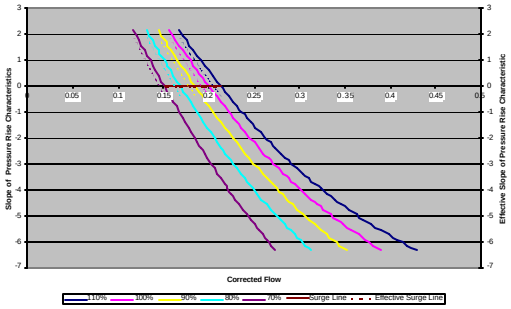

MIT 3 Scheme 7

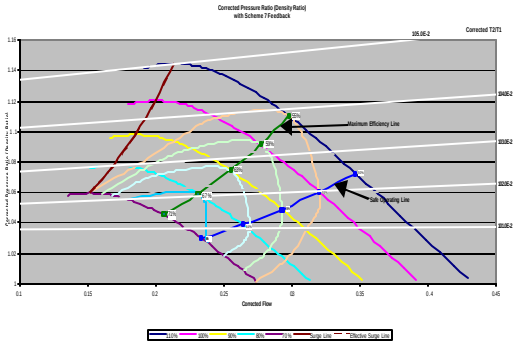

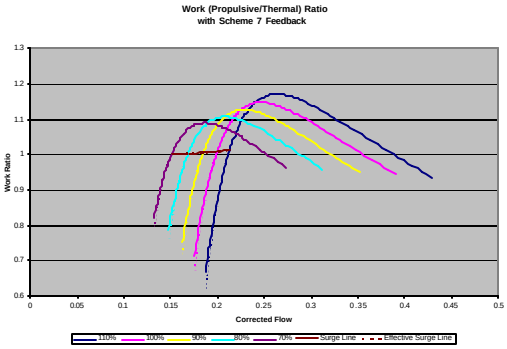

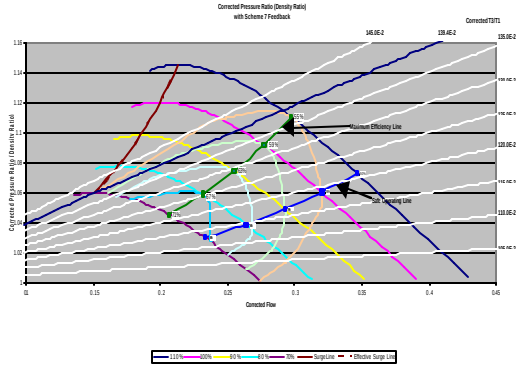

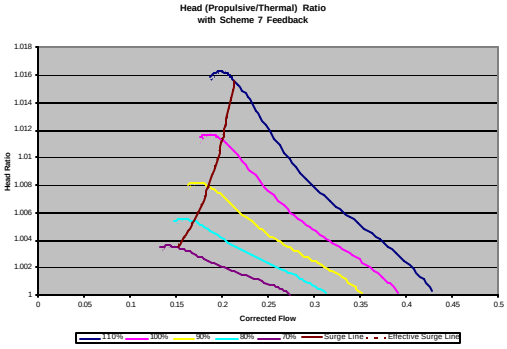

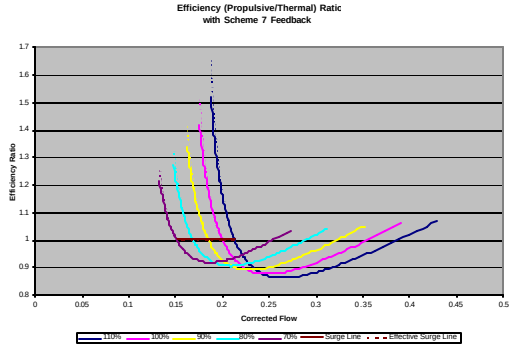

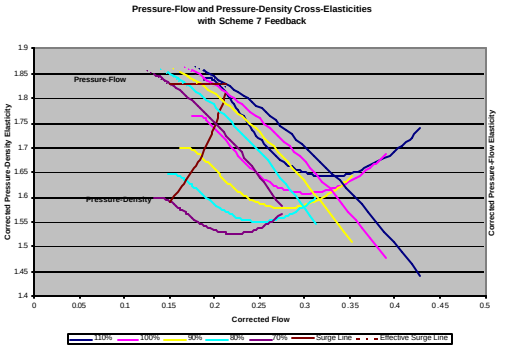

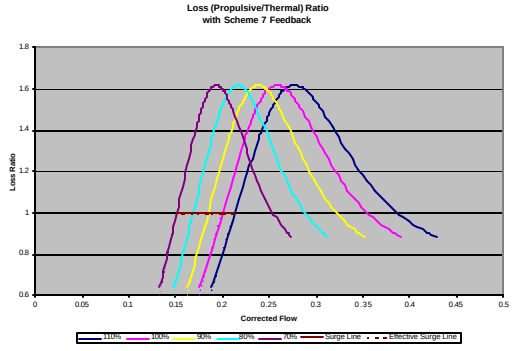

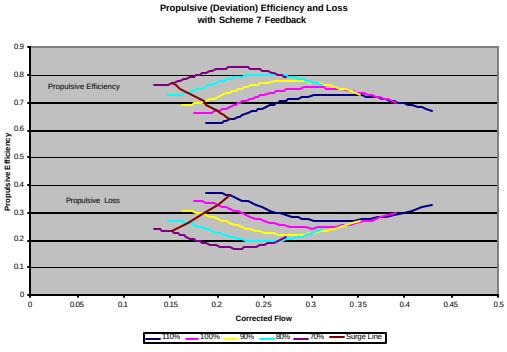

Thermal (Dissipation) Efficiency and Loss with Scheme 7 Feedback

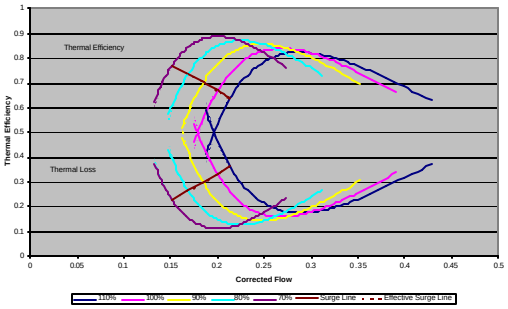

Overall (Propulsive & Thermal) Efficiency and Loss with Scheme 7 Feedback

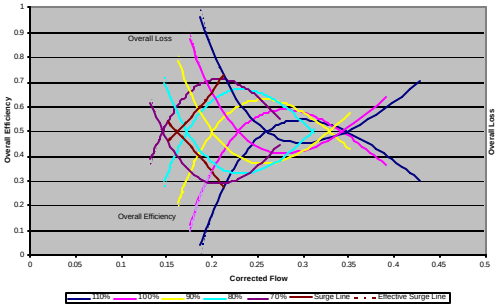

Compression System Aeroelastic Characteristics at Maximum Efficiency & Stall

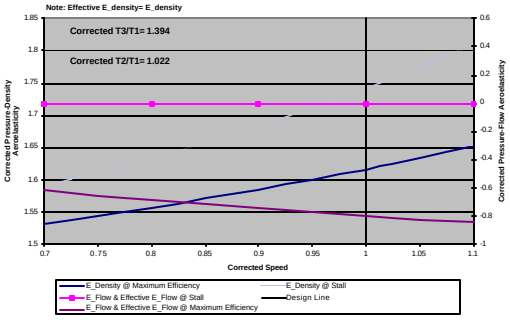

Compressor System Pumping Characteristic at Maximum Efficiency & Stall

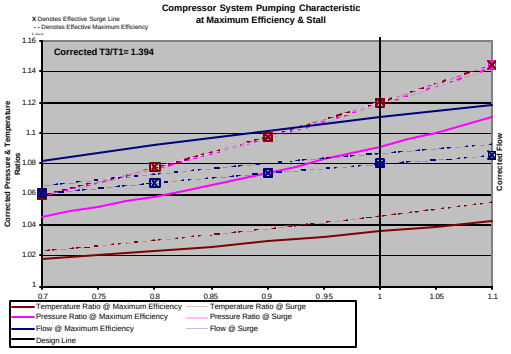

Dynamically Compensated Compression System Stability with Scheme 7 Feedback

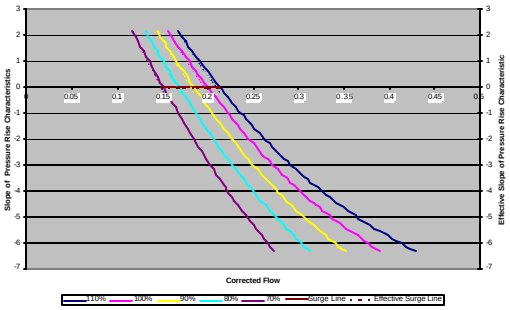

MIT 3 Scheme 8

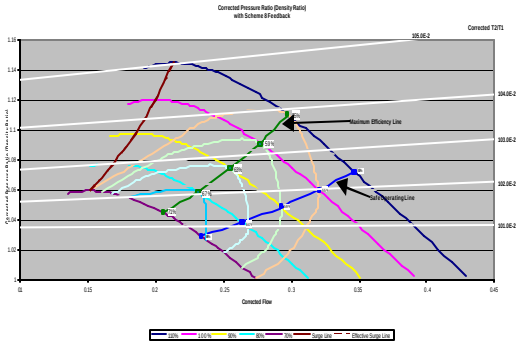

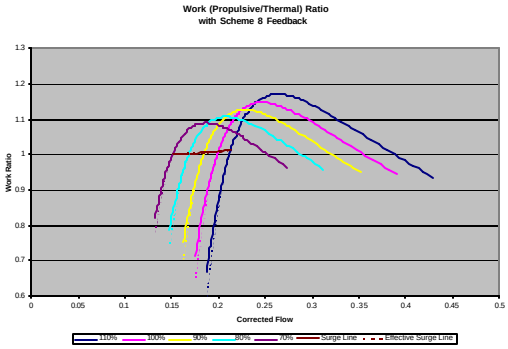

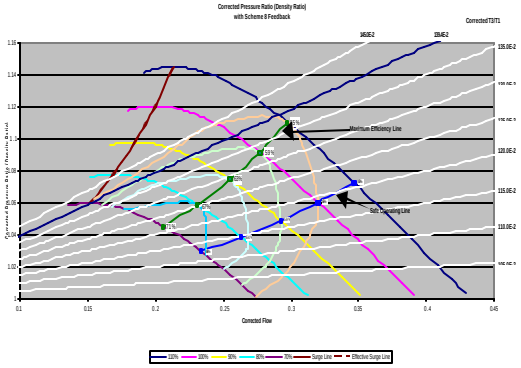

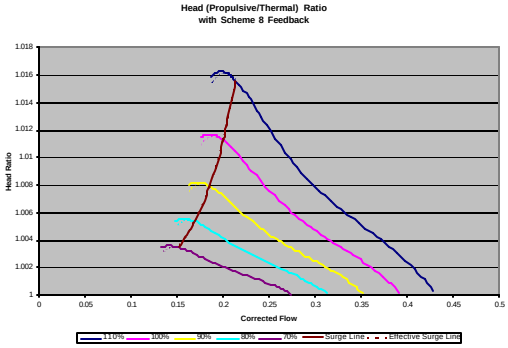

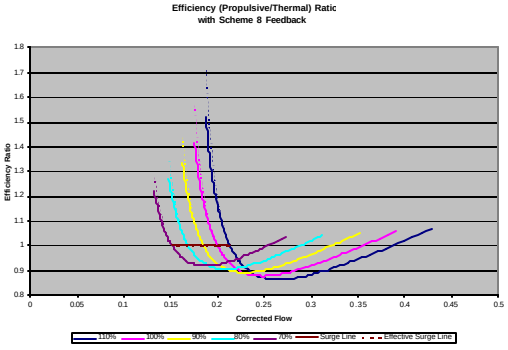

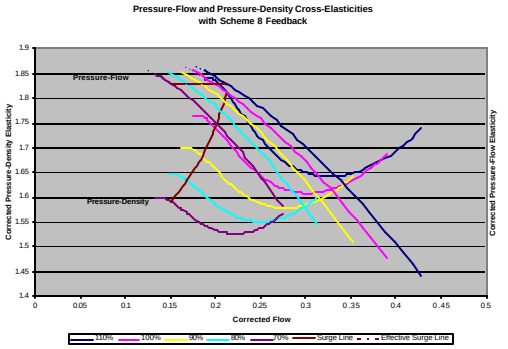

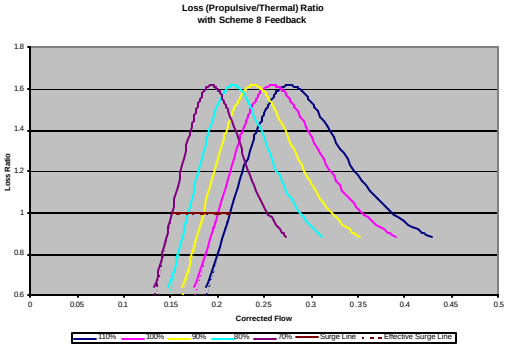

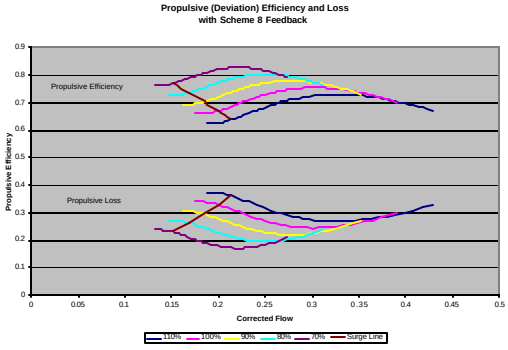

Thermal (Dissipation) Efficiency and Loss with Scheme 8 Feedback

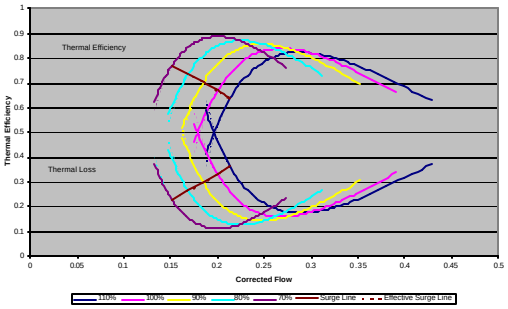

Overall (Propulsive & Thermal) Efficiency and Loss with Scheme 8 Feedback

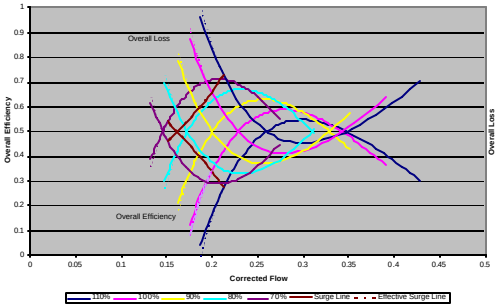

Compression System Aeroelastic Characteristics at Maximum Efficiency & Stall

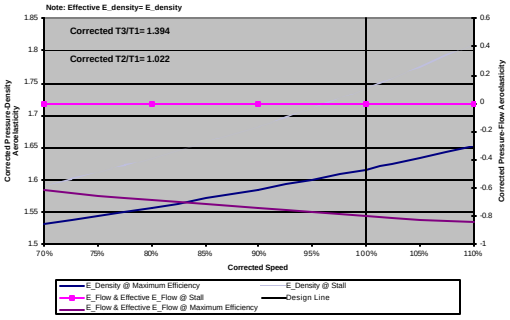

Compressor System Pumping Characteristic at Maximum Efficiency & Stall

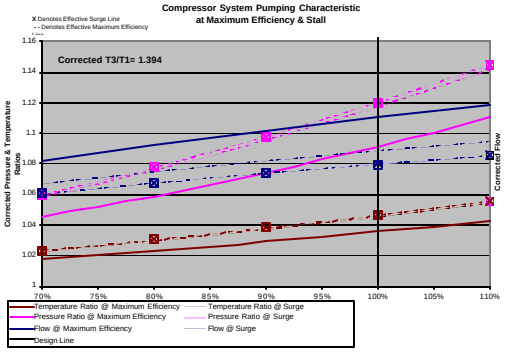

Dynamically Compensated Compression System Stability with Scheme 8 Feedback

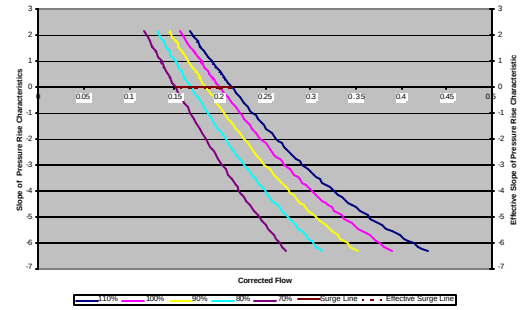

MIT 3 Scheme 9

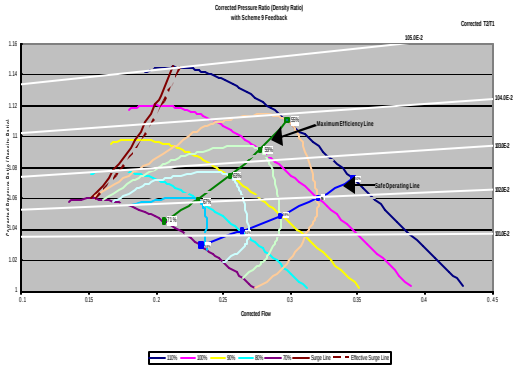

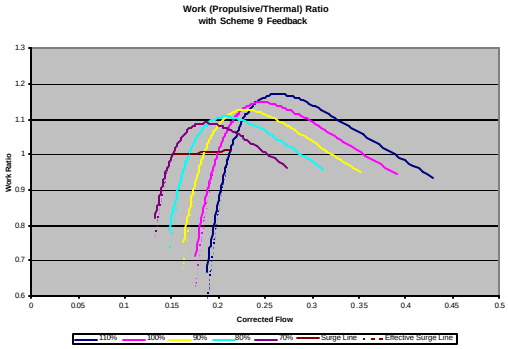

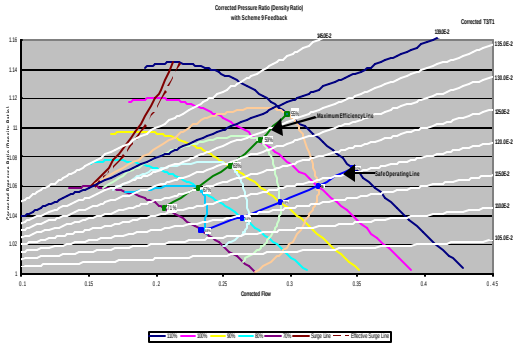

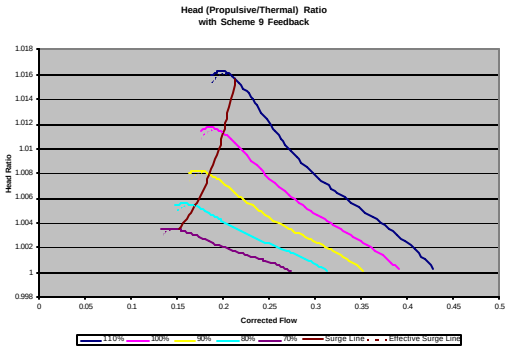

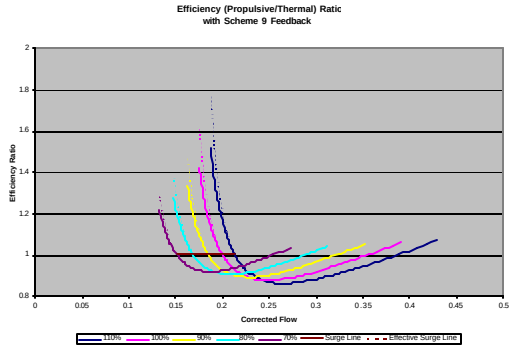

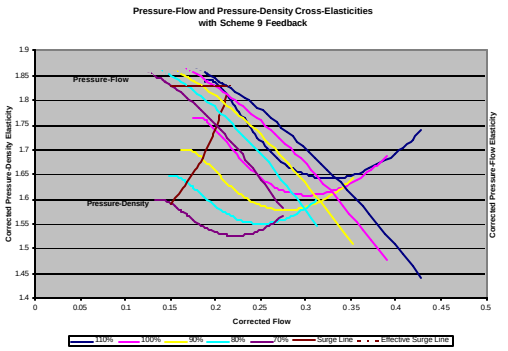

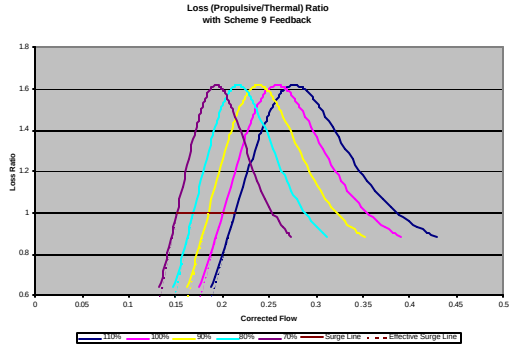

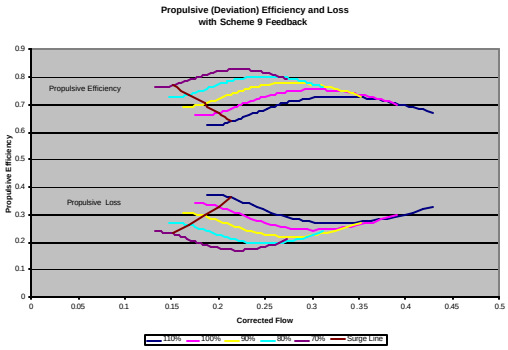

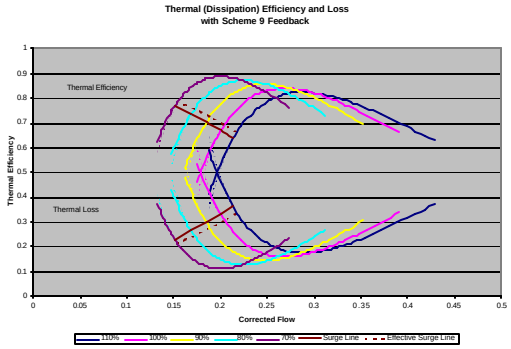
Thermal (Dissipation) Efficiency and Loss
with Scheme 9 Feedback
Thermal Efficiency
Thermal Loss
Thermal Efficiency
Corrected Flow
110%
100%
90%
80%
70%
Surge Line
Effective Surge Line

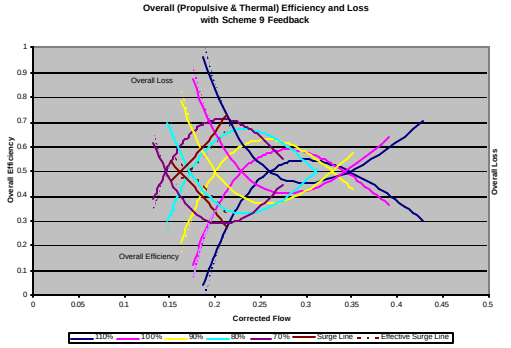
Overall (Propulsive & Thermal) Efficiency and Loss
with Scheme 9 Feedback
Overall Loss
Overall Efficiency
Overall Efficiency
Overall Loss
Corrected Flow
110%
100%
90%
80%
70%
Surge Line
Effective Surge Line

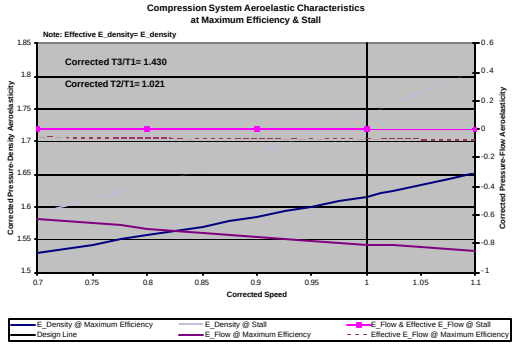
Compression System Aeroelastic Characteristics
at Maximum Efficiency & Stall
Note: Effective E_density= E_density
Corrected T3/T1= 1.430
Corrected T2/T1= 1.021
Corrected Pressure-Density Aeroelasticity
Corrected Pressure-Flow Aeroelasticity
Corrected Speed
E_Density @ Maximum Efficiency
E_Density @ Stall
E_Flow & Effective E_Flow @ Stall
Design Line
E_Flow @ Maximum Efficiency
Effective E_Flow @ Maximum Efficiency

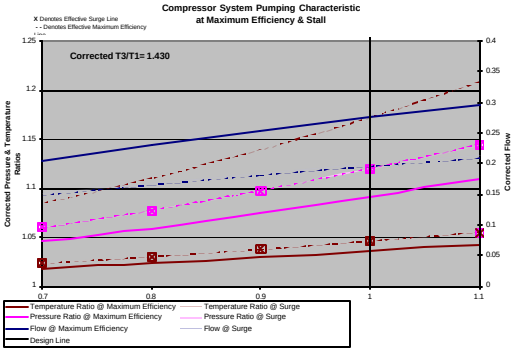
Compressor System Pumping Characteristic
at Maximum Efficiency & Stall
X Denotes Effective Surge Line
- - Denotes Effective Maximum Efficiency
Corrected T3/T1= 1.430
Corrected Pressure & Temperature Ratios
Corrected Flow
Temperature Ratio @ Maximum Efficiency
Temperature Ratio @ Surge
Pressure Ratio @ Maximum Efficiency
Pressure Ratio @ Surge
Flow @ Maximum Efficiency
Flow @ Surge
Design Line

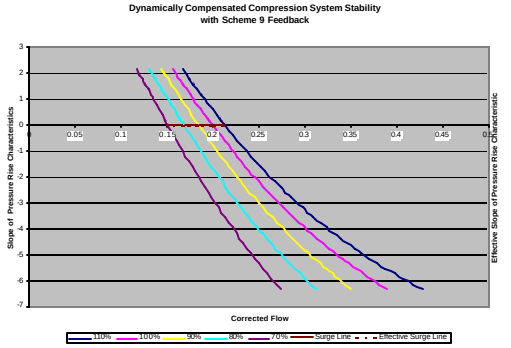
Dynamically Compensated Compression System Stability
with Scheme 9 Feedback
Slope of Pressure Rise Characteristics
Effective Slope of Pressure Rise Characteristic
Corrected Flow
110%
100%
90%
80%
70%
Surge Line
Effective Surge Line

MIT 3 Scheme 10

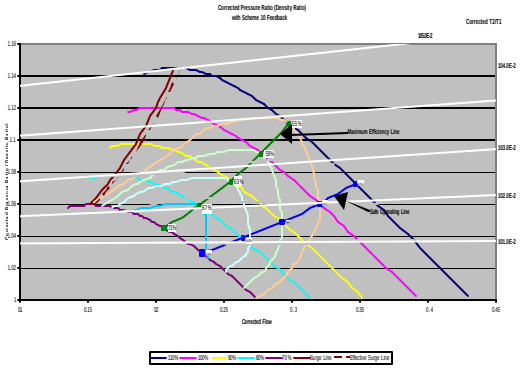

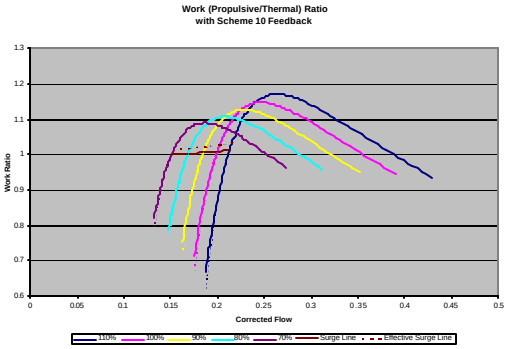

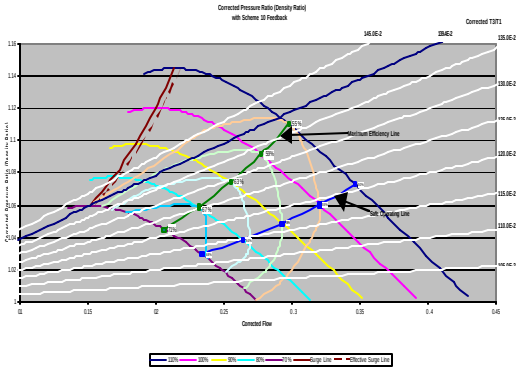

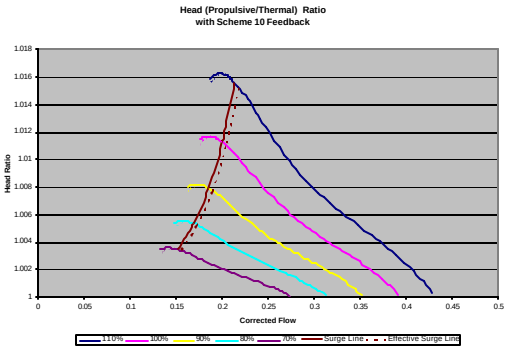

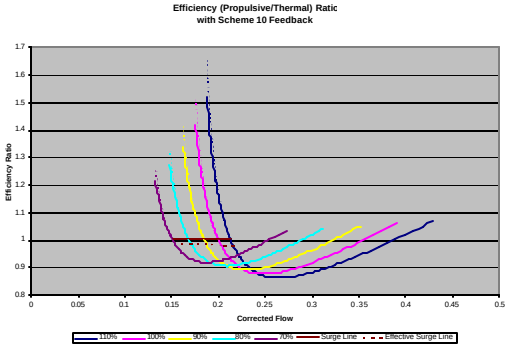

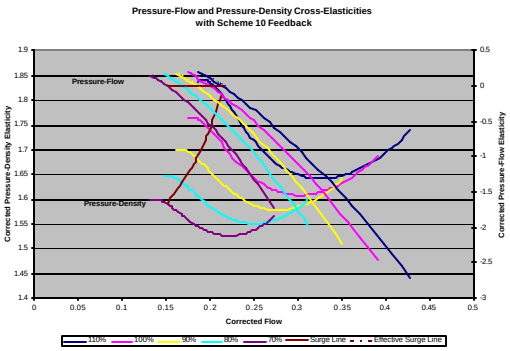

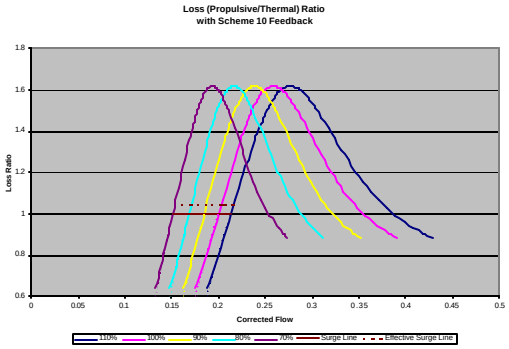

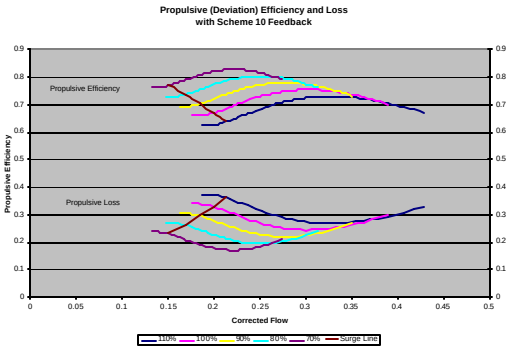

Thermal (Dissipation) Efficiency and Loss with Scheme 10 Feedback

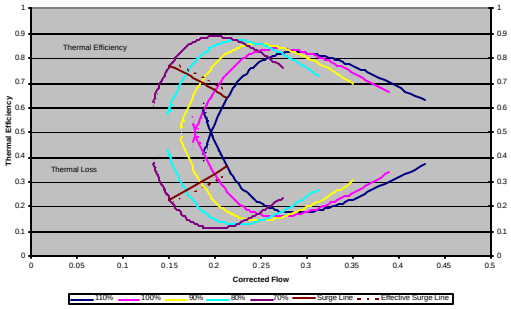

Overall (Propulsive & Thermal) Efficiency and Loss with Scheme 10 Feedback

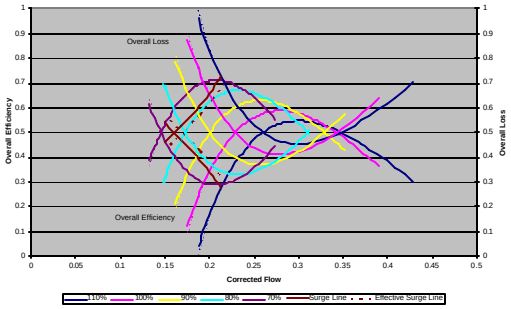

Compression System Aeroelastic Characteristics at Maximum Efficiency & Stall

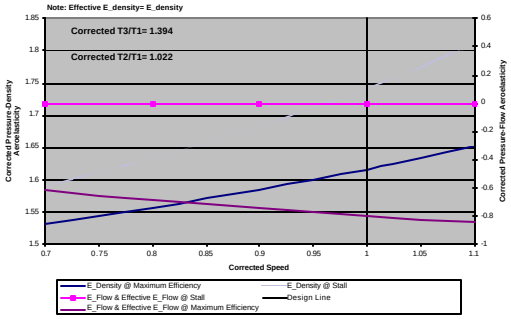

Compressor System Pumping Characteristic at Maximum Efficiency & Stall

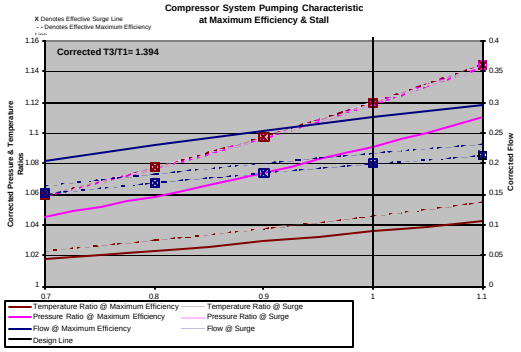

Dynamically Compensated Compression System Stability with Scheme 10 Feedback